EFFECT OF ORGANOCLAY SURFACE COVERAGE ON POLYMER CLAY NANOCOMPOSITES FORMATION

JUMPEI HOSHINO

**THESIS SUBMITTED IN PARTIAL FULFILLMENT
OF THE REQUIREMENTS FOR THE DEGREE OF
DOCTOR OF PHILOSOPHY
(MATERIALS SCIENCE AND ENGINEERING)
FACULTY OF GRADUATE STUDIES
MAHIDOL UNIVERSITY
2010**

Copyright by Mahidol University

COPYRIGHT OF MAHIDOL UNIVERSITY

Thesis

entitled

EFFECT OF ORGANOCLAY SURFACE COVERAGE ON POLYMER CLAY NANOCOMPOSITES FORMATION

Jumpei Hoshino

.....

Mr. Jumpei Hoshino

Candidate

.....

Asst. Prof. Toemsak Srikhirin, Ph.D.

Major-advosor

T. Amornsakchai

.....

Assoc. Prof. Taweechai Amornsakchai, Ph.D.

Co-advisor

T. Osotch

.....

Asst. Prof. Tanakorn Osotchan, Ph.D.

Co-advisor

B. Mahaisavariya

.....

Prof. Banchong Mahaisavariya, M.D., Dip Thai Board of Orthopedics

Dean

Faculty of Graduate Studies

Mahidol University

.....

Asst. Prof. Toemsak Srikhirin, Ph.D.

Program director

Doctor of Philosophy program in Materials Science and Engineering,

Faculty of Science, Mahidol University

Copyright by Mahidol University

Thesis

entitled

EFFECT OF ORGANOCLAY SURFACE COVERAGE ON POLYMER CLAY NANOCOMPOSITES FORMATION

was submitted to the faculty of Graduate Studies, Mahidol University
for the degree of Doctor of Philosophy
(Materials Science and Engineering)
on
September 2, 2010

Jumpei Hoshino
.....
Mr. Jumpei Hoshino
Candidate

T. Osotchan
.....
Asst. Prof. Tanakorn Osotchan, Ph.D.
Member

R. Traiphol
.....
Asst. Prof. Rakchart Traiphol, Ph.D.
Chair

T. Amornsakchai
.....
Assoc. Prof. Taweechai Amornsakchai, Ph.D.
Member

.....
Asst. Prof. Toemsak Srikhirin, Ph.D.
Member

B. Mahaisavariya
.....
Prof. Banchong Mahaisavariya, M.D., Dip Thai Board of Orthopedics
Dean
Faculty of Graduate Studies
Mahidol University

.....
Prof. Skorn Mongkolsuk, Ph.D.
Dean
Faculty of Science
Mahidol University

Copyright by Mahidol University

ACKNOWLEDGEMENTS

This thesis was accomplished by extensive support and assistance of my major advisor, Asst. Prof. Toemsak Srikhirin, and co-advisors, Asst. Prof. Tanakorn Osotchan and Assoc. Prof. Taweechai Amornsakchai. I am grateful to them for their valuable advice and guidance on this research.

I wish to thank Dr Sarintorn Limpanart and Khun Srichalai Khunthon, Material and Metallurgical Research Institute in Chulalongkorn University, for giving suggestions to my work.

I wish to thank Asst. Prof. Rakchart Traiphol, Department of Chemistry and Center for Innovation in Chemistry, Faculty of Science, Naresuan University, for supporting Differential Scanning Calorimetry (DSC) and suggesting to my work.

I would like to thank National Metal and Materials Technology Center (MTEC) and National Nanotechnology Center (NANOTEC), NATSDA for technical and financial support in my work.

I would like to thank all my colleagues at the Capability Building Unit in Nanoscience and Nanotechnology, for giving me such a nice environment that made my project possible.

Finally, I would like to appreciate that my family, especially my parents, gave me permission to study in Thailand.

Copyright by Mahidol University

Jumpei Hoshino

EFFECT OF ORGANOCLAY SURFACE COVERAGE ON POLYMER CLAY NANOCOMPOSITES FORMATION

JUMPEI HOSHINO 4836021 SCME/D

Ph.D. (MATERIALS SCIENCE AND ENGINEERING)

THESIS ADVISORY COMMITTEE: TOEMSAK SRIKHIRIN, Ph.D., TANAKORN OSOTCHAN, Ph.D., TAWEECHAI AMORNSAKCHAI, Ph.D.,

ABSTRACT

In polymer clay nanocomposite formations by a two-roll mill and twin screw extruder, the adsorption behaviors of surfactant onto clay surface, and the relationship between surface coverage of surfactant and clay dispersion in matrix polymer were investigated by differential thermogravimetry (DTG), contact angle measurement, thermogravimetric analysis (TGA), X-ray diffraction (XRD), scanning electron microscopy (SEM), transmission electron microscopy (TEM), and tensile test etc.

The first system was based on synthesized organoclay with various degrees of surfactant (S18) adsorption. The adsorption behaviors of surfactant (S18) onto clay platelets were divided into three distinct stages. At the third stage of adsorption of surfactant (15mM of S18 loading), the wettability of clay platelets was improved in polypethylene-clay nanocomposites compounded by a two-roll mill, although a submicronmeter size agglomerate was detected. The intercalate-exfoliated was found in the medium coverage organoclay, and a conventional composite was found in the high coverage organoclay. The highest ultimate tensile strength was exhibited by the addition of oxidized polyethylene wax (OWax), where the organoclay can achieve a higher degree of dispersion in the polymeric matrix.

Commercially available clay platelets with different degrees of surface coverage (low; LC, medium; MC, and high; HC) were prepared at polymer clay nanocomposite formations by a twin screw extruder with polypropylene and high density polyethylene with the co-intercalant. Critical surface energy (CSE) greatly depends on the degree of surface coverage of surfactant. Intercalation of compatibilizers and polymer into interlayer of LC and MC was observed on XRD. However, HC did not exhibit intercalation and exfoliation in pre-dispersed organoclay and nanocomposites.

KEY WORDS: BENTONITE / NANOCOMPOSITES / ORGANOCLAY / POLYETHYLENE / POLYPROPYLENE

Copyright by Mahidol University

114 pages

CONTENTS

	Page
ACKNOWLEDGEMENT	**iii**
ABSTRACT	**iv**
LIST OF TABLES	**xi**
LIST OF FIGURES	**xii**
CHAPTER	
Ⅰ INTRODUCTION	**1**
1.1 Polymer clay nanocomposites	1
1.2 Surface active agent	1
1.3 Compatibilizer	2
1.4 Nanocomposites formation	3
1.5 Objectives of study	4
1.5.1 The formation of the nanocomposites by two-roll mill	4
1.5.2 The formation of the PP-clay and PE-clay nanocomposites by twin screw extruder	4
1.6 Thesis outline	5
Ⅱ RELEVANT THEORY	**6**
2.1 Clay minerals	6

Copyright by Mahidol University

CONTENTS (cont.)

	Page
2.1.1 Structure of clay	6
2.1.2 Cation exchange capacity (CEC)	7
2.1.3 Organic surface active agent (surfactant)	7
2.2 Surface coverage of clay particles	8
2.2.1 d-spacing	8
2.2.2 Δ d-spacing	9
2.2.3 Thermogravimetric Analysis (TGA)	10
2.2.4 Critical surface energy (CSE) by Zisman plot	11
2.3 Nanocomposites formation	12
2.3.1 Compatibilizers	13
2.3.2 Methods of preparation	14
2.3.3 Equipment for compounding	15
2.4 Clay dispersion (X-ray diffraction technique)	16
2.5 Mechanical properties	17
2.5.1 Tensile strength / strain measurement	17
2.5.2 Strain measurement	18
2.6 Differential scanning calorimetry (DSC)	19
2.7 Gas barrier properties	20
2.8 Electron microscopy	22
2.8.1 Scanning electron microscopy	22

Copyright by Mahidol University

CONTENTS (cont.)

page

2.8.2 Transmission electron microscopy 22

Ⅲ HIGH-DENSITY POLYETHYLENE (HDPE)-CLAY NANOCOMPOSITES FORMATION BY TWO-ROLL MILL 24

3.1 Introduction 24

3.2 Experimental procedure 26

3.2.1 Materials 26

3.2.2 Organoclay preparation 26

3.2.3 X-ray diffraction (XRD) 27

3.2.4 Thermal gravimetric analysis (TGA) 27

3.2.5 Contact angle measurement 28

3.2.6 Surface energy 28

3.2.7 Critical surface energy (CSE) 29

3.2.8 High-density polyethylene (HDPE)-clay nanocomposite preparation using a two-roll mill 30

3.2.9 Tensile Test 30

3.2.10 Transmission electron microscopy (TEM) 31

3.2.11 Scanning electron microscopy (SEM) 31

3.3 Results and Discussion 31

3.3.1 Organoclay preparation 31

Copyright by Mahidol University

CONTENTS (cont.)

Page

3.3.2 The first state (monolayer formation) 34

3.3.3 The second state (intermediate state of double layer formation) 37

3.3.4 The third state (double layer formation with excess surfactant) 38

3.3.5 Contact angle measurement and critical surface energy (CSE) 40

3.3.6 Pre-dispersed organoclay 43

3.3.7 Nanocomposite Formation 45

3.4 Conclusion 51

Ⅳ HIGH-DENSITY POLYPROPYLENE (PP) CLAY NANOCOMPOSITES FORMATION BY TWIN SCREW EXTRUDER 53

4.1 Introduction 53

4.2 Experimental Procedure 54

4.2.1 Materials 55

4.2.2 Contact angle measurement 55

4.2.3 Surface energy 56

4.2.4 Critical surface energy (CSE) 56

4.2.5 Thermogravimetric analysis (TGA) 57

4.2.6 Formation of pre-dispersed organoclay 57

4.2.7 Formation of PP-clay nanocomposites 58

4.2.8 X-ray diffractometry (XRD) 59

Copyright by Mahidol University

CONTENTS (cont.)

Page

4.2.9 Tensile test 60

4.2.10 Differential scanning calorimetry (DSC) 60

4.2.11 Scanning electron microscopy (SEM) 61

4.2.12 Gas barrier property 61

4.3 Results and Discussion 61

4.3.1 Thermogravimetric analysis (TGA) 61

4.3.2 Contact angle measurement and critical surface energy (CSE) 62

4.3.3 Organoclay and pre-dispersed organoclay 64

4.3.4 Nanocomposites formation 67

4.3.5 Tensile test 69

4.3.6 DSC (differential scanning calorimetry) 71

4.3.7 SEM (scanning electron microscopy) 74

4.3.8 Gas barrier property 76

4.4 Conclusion 77

V HIGH-DENSITY POLYETHYLENE (HDPE) CLAY NANOCOMPOSITES FORMATION BY TWIN SCREW EXTRUDER 79

5.1 Introduction 79

5.2 Experiments 80

5.2.1 Materials 80

Copyright by Mahidol University

CONTENTS (cont.)

	Page
5.2.2 Formation of pre-dispersed organoclay	81
5.2.3 Formation of HDPE-clay nanocomposites	82
5.2.4 X-ray diffractometry (XRD)	83
5.2.5 Tensile test	83
5.2.6 Differential scanning calorimetry (DSC)	84
5.2.7 Scanning electron microscopy (SEM)	84
5.3 Results and discussion	85
5.3.1 X-ray diffractometry (XRD)	85
5.3.1.1 Formation of pre-dispersed organoclay	85
5.3.1.2 Nanocomposites formation	88
5.3.2 Differential Scanning Calorimetry (DSC)	92
5.3.3 Tensile test	96
5.3.4 Scanning electron microscopy (SEM)	98
5.4 Conclusion	100
VI CONCLUSIONS	**102**
REFERENCES	**105**
BIOGRAPHY	**114**

Copyright by Mahidol University

LIST OF TABLES

Table		Page
2.1	Comparison of molecular weight between common polymers and compatibilizers.	14
3.1	Dispersive components (γ^d_L), polar components (γ^p_L), and surface tension of solvents.	29
3.2	Calculated weight loss, total area occupied, and spacing for S18.	32, 33
3.3	Dispersive component, polar component, overall surface energy (γ_S), ratio between the polar to dispersive component and the critical surface tension of S18 organoclay derived from water, glycerol and diiomethane.	41
3.4	Mechanical properties (tensile test)	50
4.1	Formulation of the prepared nanocomposites.	59
4.2	Dispersive component, polar component, overall surface energy (γ_S), ratio between the polar to dispersive component, and the critical surface tension of LC, MC, and HC.	63
5.1	Formulation of the prepared nanocomposites.	82

Copyright by Mahidol University

LIST OF FIGURES

Figure		Page
2.1	Structure of 2:1 phyllosilicates.	6
2.2	Organic cations (surfactant) aggregation in layered silicates.	9
2.3	TG curves of PE and PE/clay nanocomposites in nitrogen atmosphere.	10
2.4	Zisman plots.	11
2.5	Scheme of different types of composites arising from the intercalation of layered silicates and polymers.	12
2.6	X-ray diffractram of (a) phase separated microcomposite.	16
2.7	Effect of clay loading on tensile strength of PP-clay nanocomposite.	18
2.8	DSC curves of PE/clay nanocomposites for various contents.	19
2.9	DSC curves of crystallization on PP-clay nanocomposites.	20
2.10	Tortuous diffusion path of conventional composites (A) and polymer clay nanocomposites (B).	21
2.11	Gas permeability of the nanocomposites for various clay contents.	21
2.12	SEM micrograph of PP clay nanocomposites.	22
2.13	TEM micrograph of PHDE clay nanocomposites.	23
3.1	The plot of d-spacing of organoclay at different S18 loadinngs.	35
3.2	The plot of DTG of S18 organoclay at different loadings.	39
3.3	The possible arrangement of S18 in the interlayer.	39
3.4	Zisman plots of S18-loaded and unloaded clay.	42

Copyright by Mahidol University

LIST OF FIGURES (cont.)

Figure		Page
3.5	The dispersion of organoclay at various S18 loading in OWax by melt mixing.	44
3.6	X-ray diffractgram of nanocomposites with OWax.	46
3.7	X-ray diffractgram of nanocomposites with Wax.	47
3.8	SEM image of fracture surface after chemical etching. (a) 15mM/OWax/HDPE represents a dispersion of the organoclay and (b) 15mM/Wax/HDPE represents the agglomerate of the organoclay	48
3.9	TEM image 15mM/OWax/HDPE shows the presence of the primary particle at (a) medium and (b) high magnification. The stack of the organoclay can be clearly seen at the high magnification.	49
4.1	TGA curves of organoclays (LC, MC, and HC).	62
4.2	Critical surface energy of LC, MC, and HC.	64
4.3	X-ray diffractgram of organoclays, pre-dispersed organclays and nanocomposites with 2wt% loading of organoclay loading.	65
4.4	Possible structures/surface coverage of LC, MC, and HC.	68
4.5(a)	Tensile strength of polymer-clay nanocomposites and pure PP.	70
4.5 (b)	Elongation of polymer-clay nanocomposites and pure PP.	71
4.6(a)	DSC curves of two-component composites in heating process.	72
4.6(b)	DSC curves of PP clay nanocomposites in cooling process.	73
4.6(c)	Crystallinity of PP-clay nanocomposites.	74

Copyright by Mahidol University

LIST OF FIGURES (cont.)

Figure		Page
4.7	SEM micrgraphs of PP clay nanocomposites.	75
4.8	Relative oxygen permeability of nanocomposites with 10 wt% of organoclay loading.	77
5.1	X-ray diffractgram of LC, MC, and HC and pre-dispersed organoclay.	86
5.2	X-ray diffractograms of nanocomposites with HC .	88
5.3	X-ray diffractogram of nanoposites with LC.	89
5.4	X-ray diffractogram of nanocomposites with MC.	90
5.5	Possible structures/surface coverage of LC, MC, and HC.	92
5.6	DSC curves of melting process on two-component OWax-HDPE composites.	93
5.7	DSC curves of cooling process on HDPE-clay nanocomposites	94
5.8	Crystallinity of HDPE-clay nanocomposites.	96
5.9	Tensile strength of pure HDPE, HDPEclay composites, and two-component OWax-HDPE composites.	97
5.10	Elongation at break of pure HDPE, HDPEclay composites, and two-component OWax-HDPE composites.	98
5.11	SEM micrographs of HDPE clay nanocomposites.	99

Copyright by Mahidol University

CHAPTER I

INTRODUCTION

1.1 Polymer clay nanocomposites

Polymer-clay nanocomposites based on thermoplastic polymers such as polyethylene (PE) [1], polypropylene (PP) [2], polystyrene (PS), nylon(N-6, N-6,6) [3] have been emerged as a new kind of composite material during the past decade. Applications, such as food packaging films, wires, fibers and cable jacketing, automotives, and agriculture films, of the matrix polymer have been realized. It was reported that an average annual growth rate of global consumption of nanocomposites would be 24% [4].

Polymer clay nanocomposites possess several unique properties, such as strength and permeation, which can be achieved by adding a small amount of the clay into the polymeric matrix. It was found that the properties of polymer-clay nanocomposites are controlled by clay dispersion and delamination of individual clay layer [1, 2, 14]. The addition of clay into polymeric matrices can improve mechanical, physical (thermal and barrier) and chemical properties of matrices and reduces cost in some cases compared to other additives.

Copyright by Mahidol University

1.2 Surface active agent

Surface energy on the clay particles is considered as high, or polar surface,

due to the presence of oxygen on the surface of the clay and is often referred as hydrophilic in nature. Most of the commoidity polymers, such as polypropylene (PP) and polyethylene (PE), are hydrophobic in nature. In order to accomplish a homogeneous dispersion of clay platelets in polymer matrix, surface treatment with a surface active agent, surfactant, is required. This results in reduction of surface energy, which leads to the promotion of the interaction between clay surface and the polymer molecules. This can be viewed as the promotion of the enthalpy of mixing in the clay's surface treatment, surfactants such as groups of trimethyl ammonium and octadecyl ammonium with halide ions are often used [1]. The additional factors play a fundamental role in controlling the dispersion and wetting of a clay platelet with polymer or monomer [5, 6].

1. type of surfactant functional group
2. degree of surfactant coverage on the clay surface

1.3 Compatibilizer

It is difficult to achieve perfectly dispersed clay particles, complete delamination of clay platelet or exfoliation, in nanocomposites by using only organically modified clay and matrix polymer, because exfoliation as well as intercalation of clay particles can not be made solely by polymer and/or monomer. In most systems, the aggregation of organoclay particles or incomplete delamination often occurs, even if clay particle are treated with surfactant. In order to solve this problem for the system of PE and PP-clay nanocomposites, compatibilizers such as low molecular weight oxidized wax [7, 8], polyethylene-grafted maleic anhydride

Copyright by Mahidol University

(PE-g-MA) [9] or polypropylene-grafted maleic anhydride (PP-g-MA) [2], are often compounded with organoclay to promote the dispersion of the organoclay through an increase of the polymer due to the presence of polar group in the polymeric structure. It is believed that intercalation of organoclay platelets is initiated by both of following factors.

1. wetting between organically modified clay particles and matrix polymer
2. use of compatibilizer to pre-disperse the organoclay

1.4 Nanocomposites formation

It was reported that the processing also has an influence on the nanocomposites formation [10]. The exfoliation and delamination of clay particles are enhanced by shear stress during compounding. The equipment for extrusion process in polymer-clay nanocompsites formation is categorized into two types, single and twin screw extruders. It is well -known that higher shear force can be exerted by twin screw extruder which promotes the dispersion of nanocmposites [11]. Recycles plastic also needs improvement of mechanical property, which leads to the introduction of organoclay in order to improve its property. In some cases such as the recycled polymer, the metallic debris may be presence and can result in considerable damage to the screw extruders, therefore, two-roll mills are preferred. In this study, the effect of the procession method will be investigated by comparing a two-roll mill and twin screw extruder for the preparation of polymer-clay nanocomposites.

Copyright by Mahidol University

The optimization of surfactant loading into clay for synthesis of polymer-clay nanocomposites with well-dispersed organoclay particles in the polymer matrix was used for both investigations. The enhancement of intercalation and delamination of clay particles, compatibilizers such as low molecular weight oxidized wax, PE-g-MA, and PP-g-MA were applied as a co-intercalant.

1.5 Objectives of study

In order to make polymer-clay nanocomposites promising material, we have to find the optimum condition in order to achieve desirable properties such as high mechanical properties, high heat resistance and improved gas barrier property. It is well-known that these properties greatly depend on degree of dispersion of organoclay [6]. In this work, the effect of the surfatant surface coverage on the polymer-clay nanocomposites formation will be investigated which include

1.5.1 The formation of the nanocomposites by two-roll mill

It was reported that the organoclay dispersion is influenced by extent of surface coverage on clay platelets by surface active agents [6]. An investigation of the organoclay surface coverage on polymer clay nanocomposites formation by two rollers mill will be investigated.

1.5.2 The formation of the PP-clay and PE-clay nanocomposites by twin screw extruder

Copyright by Mahidol University

The formation of the PP and PE-clay nanocomposites by using twin-screw

extruder, with and without the compatabilizer, will be investigated.

1.6 Thesis outline

This thesis is organized as followed.

Chapter II introduces the required low materials, theories, and characterizations for synthesizing polymer-clay nanocomposites.

Chapter III mentions the adsorption mechanism of surface active agents on clay platelets and organoclay dispersion on polymer-clay nanocomposites formation.

Chapter IV and V presents the degree of surfactant surface coverage on the formation of polymer-clay nanocompsoites formation.

Chapter VI is the conclusions.

Copyright by Mahidol University

CHAPTER II
RELEVANT THEORY

2.1 Clay minerals

2.1.1 Structure of clay

The clay particles commonly used in nanocomposites belong to the structural known as the 2:1 phyllosilicates as shown in figure 2.1.

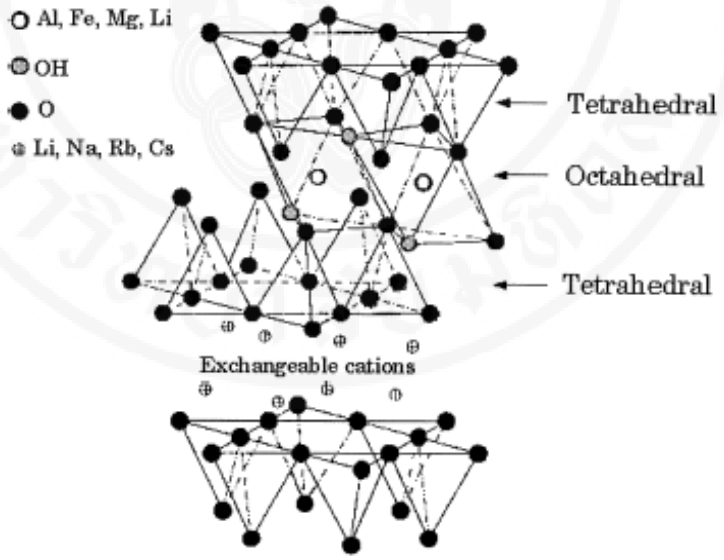

Figure 2.1 Structure of 2:1 phyllosilicates [12].

Their structure consists of two-dimensional layers of aluminosilicate where a central octahedral sheet of alumina or magnesium sandwiched by two silica tetrahedron sheets. The layer thickness is around 1.0 nm and the lateral dimensions of these layers may vary from 300 A^o to several microns. Aspect ratio of commonly used clay particles

Copyright by Mahidol University

often ranges from 100 to 1000, depending on the degree of delamination. Due to such aspect ratios, polymer clay nanocomposites with well dispersed clay platelets exhibit excellent gas barrier property.

2.1.2 Cation exchange capacity (CEC))

Clays are 2:1 phyllosilicates in which some of the aluminum and silicon ions have been replaced by elements with low valence. For example, aluminum (Al^{3+} may be replaced by iron (Fe^{2+}) or magnesium (Mg^{2+}), leading to an unbalance or a net negative charge on its surface as illustrated in figure2.1. This charge attracts cations when the clay is immersed in solutions of surface active agents such as quaternary alkylammonium salts. Different source of 2:1 phyllosilicates clay possess the different cation exchange capacity (CEC), which is defined as the amount of exchange cation accommodated in their interlayer structures. The quantity of exchangeable positively charged ions, cations, that a clay mineral or similar materials can keep on its negatively charged surface is expressed as milliequivalent per 100g, or more commonly as milliequivalent (meq) per 100 g of clay or cmol/kg. The quantity reflects the amount of organic surfactants that the clay can hold in the interlayer.

2.1.3 Organic surface active agents (surfactant)

Surface treatment of clay platelets with organic surface active agents, surfactant, is required in order to promote the compatibility between polymer and the clay. Surfactants reduce the surface energy on clay platelets and make them more compatible with polymeric matrix.

Copyright by Mahidol University

Organic compounds used to prepare organoclays can be categorized into

three types, a group of alkylammonium salts, nonionic surfactant (linear alcohol ethoxylate with low toxicity and potential for biodegradation), and biomolecules (protein, enzymes, and amino acids etc.) [13]. Quaternary alkylammonium salts are often used to prepare organoclays due to its price and availability in the commercial scale. Several kinds of quaternary alkyl ammonium salts (bromides or chlorides) were used for modification of clay minerals. Quaternary alkyl ammonium salts ions are preferred over the primary alkyl ammonium ions because it is free from hydrolysis and desorption of free alkyl amine is strongly reduced. The different kind of quaternary alkyl ammonium salt is known to influences the affinity between the clay mineral and the polymer.

2.2 Surface coverage of clay particles

2.2.1 d-spacing

Organic cations, surfactant, incorporated into clay particles shows different types of interlayer arrangement, depending on amount of loading, length of molecules, and the numbers of tail groups etc. From the X-ray diffraction (XRD), the organic chains have long been thought to lie either parallel to the silicate layer, forming mono- or double-layers or, depending on the packing density or as a tilted layer interdigitates where the chain is radiated away from the surface, forming mono or even bimolecular tilted ‘paraffinic’ arrangement as shown in figure 2.2.

Copyright by Mahidol University

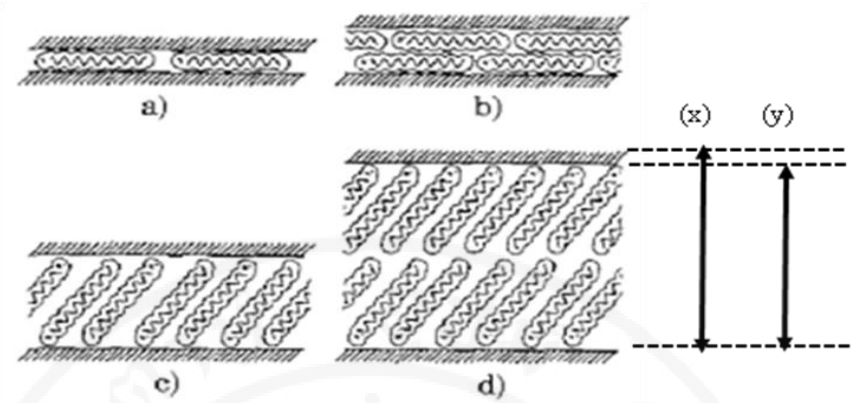

Figure 2.2 Organic cations (surfactant) aggregation in layered silicates [14]: (a) lateral monolayer; (b) lateral double layer; (c) paraffin-type monolayer, and (d) paraffin-type double layer.

The d-spacing, the distance between nearby clay particles indicated by (x), is the parameter that reflects the degree of delamination or the dispersion of individual clay platelet. It is also varied depending upon the arrangement of the interlayer cation. Intercalation of polymer chains into clay interlayer in the compounding process is resulting in an increase of the d-spacing. Removing of the surfactant molecules may result in collapse of layered structure of clay platelets. Calculation of d-spacing is presented in the section **2.4**.

2.2.2 Δ d-spacing

Δd-spacing indicated by "y" in figure 2.2 is also one of the most important parameters which is related to an arrangement of organic surfactant in the interlayer. Net thickness of each clay platelet can be estimated at 9.5 A°, so that Δ d-spacing can be calculated by subtract it from the observed d-spacing.

Copyright by Mahidol University

When the nominal length and diameter of surfactant molecules are known, conformation of organic surfactant can be predicted. When Δ d-spacing is almost equal to diameter of organic surfactant molecules, it is normally assumed that the surfactant molecules possess a flat-lying monolayer in the interlayer. When Δ d-spacing is almost equal to twice of diameter of organic surfactant molecules, it can be assumed that the surfactant molecules keep a flat-lying double-layer in the interlayer.

2.2.3 Thermogravimetric Analysis (TGA)

Thermogravimetric analysis (TGA) is used to determine the weight loss as a function of the temperature. This technique can be used for analysis of the organic content in an organoclay as well as flame retardancy of polymer clay nanocomposites.

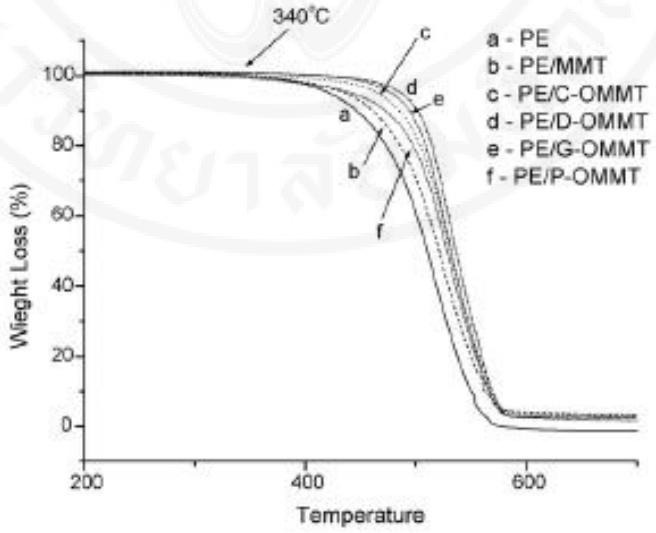

Figure 2.3 TG curves of PE and PE/clay nanocomposites in nitrogen atmosphere [15]. PE: high density polyethylene, MMT: Na-montmorilonite, C, D, G, P: abbreviation of surface active agents.

Copyright by Mahidol University

With increasing temperature of sample at a constant rate, the weight loss occurs because of vaporization or thermal decomposition of organic components. This is often expressed in weight loss curves as a function of temperature as illustrated in figure 2.3. Various thermal information such as the starting temperature for pyrolysis and net weight of clay in organoclay can be obtained.

2.2.4 Critical surface energy (CSE) by Zisman plot

Critical surface energy (CSE) is a parameter which reflects wettability of organically modified clay, organoclay, platelets. CSE of organoclay is calculated according to the Zisman plot as illustrated in figure 2.4.

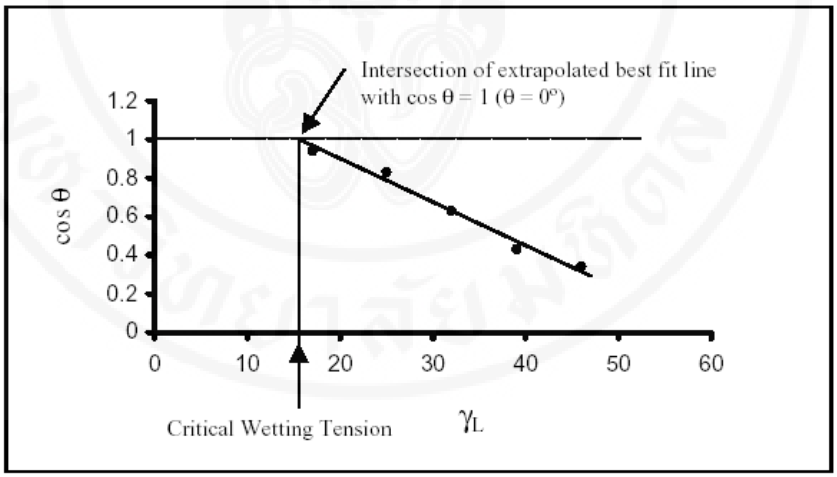

Figure 2.4 Zisman plots [16].

When the cosine of the contact angles (θ) is plotted against the surface tensions, a straight line can be obtained. This line is extrapolated to the point of θ=0, which is where $\cos\theta = 1$. The full wettability surface is determined on the intersection between the straight line and $\cos\theta = 1$. Therefore, as organoclays

Copyright by Mahidol University

indicating higher CSEs, they may show higher wettability against polymer and compatibilizers which have lower CSEs than the organoclays.

2.3 Nanocomposites formation

Depending on the nature of the component used and methods of preparation as follows, three main types of composites may be obtained when clays are associated with a polymer as shown in figure 2.5.

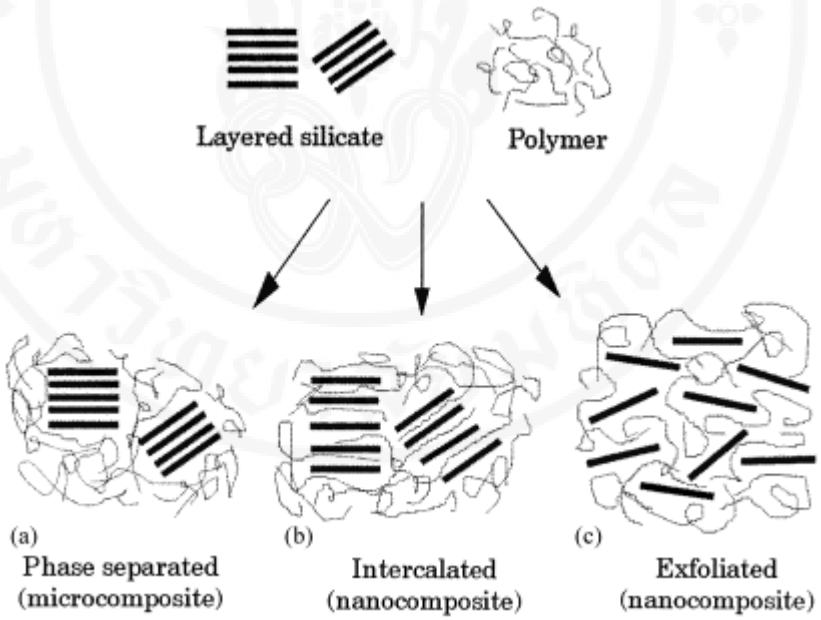

Figure 2.5 Scheme of different types of composites arising from the intercalation of layered silicates and polymers [17]:
(a) phase separated microcomposite,
(b) intercalated nanocomposite, and
(c) exfoliated / delaminated nanocomposite

Copyright by Mahidol University

When intercalation of polymer does not occur, a phase separated composite (figure 2.5(a)) is obtained, it is referred to as conventional composites. Intercalation of polymer chains into silicate layers results in intercalated nanocomposites (figure2.5 (b)), while the clay platelets are still well ordered. A crystallographic register along the clay thinkness dimension often preserves. When the clay platelets are completely and uniformly dispersed in polymer matrix, an exfoliated and delaminated structure is obtained (figure 2.5 (c)).

2.3.1 Compatibilizers

The compatibilizers such as low molecular weight paraffin wax, oxidized paraffin wax, polypropylene-grafted maleic anhydride (PP-g-MA), Polyethylene-grafted maleic anhydride (PE-g-MA) are used to improve the clay dispersion [19]. There are two major reasons why compatibilizers are required to synthesize polymer clay nanocomposites.

The first is the size factor. There is a large difference in molecular weight between polymer and compatibilizers as shown in table 2.1. Due to larger molecular weight of polymers, it is very difficult for clay particles and platelets to be directly intercalated by polymer molecules. Molecules of compatibilizers can intercalate into the galleries of clay platelets and play a role of initiation of delamination of clay platelets.

The second is the polarity factors. The compatibilizers commonly used such as PP-g-MA, HDPE-g-MA, and oxidized paraffin wax have polar components in their structures. Attractive force between polar components of compatibilizers and clay platelets of surfactants is the driving force for intercalation. A representative

Copyright by Mahidol University

polar component is carboxylic acid or maleic anhydride group. The acid number, or acid value, is the amount of carboxylic acid groups in a chemical compound, such as a fatty acid, or in a mixture of compounds. Acid number reflects the polarity of compatibilizers. Acid numbers are defined as the mass of potassium hydroxide (KOH) in milligrams that is required to neutralize one gram of chemical substance as shown in table1 [2, 8, 18, 19].

Table 2.1 Comparison of molecular weight between common polymers and compatibilizers.

Polymer	Mw [g/mol]	Compatibilizers	Mw [g/mol]	Acid number [mgKOH/g]
PP	330000 [2]	PP-g-MA (Epolene E43)	9100 [2]	45 [2]
LLDPE	50000 [18]	PP-g-MA	1010 [19]	52 [19]
LDPE	96000 [8]	PE-g-MA	2950 [19]	27 [19]

2.3.2 Methods of preparation

Preparation of polymer clay nanocomposites can be categorized into four main processes which are 1) exfoliation adsorption, 2) in-situ intercalative polymerization, 3) melt intercalation, and 4) template synthesis. Due to a cost issue and efficiency in synthesis, the melt processing is the most investigated. No solvent is required, and organoclay platelets are directly compounded with polymer in molten

Copyright by Mahidol University

state. Sufficient compatibility between clay surface and polymer can lead to intercalation of polymer into clay interlayer through the enthalpy of mixing. In order to use this method, the clay particles need to be previously treated with surface active agents as mentioned in section 2.1.3.

2.3.3 Equipment for compounding

Two-roll mill, single or twin screw extruder are common equipment for compounding polymer clay nanocomposites. Each of them has both of advantages and disadvantages.

Two-roll mills are preferred for compounding polymer composites made from recycle plastics. Debris in recycle plastics can not be serious damages to the equipment. Moreover, operations and maintenance are not difficult. It is difficult to achieve mass production because of low throughput. Shear stress can be changed by increasing and decreasing a gap between the two rolls, but it is difficult to obtain parameters for quantifying shear stress.

Single and twin screw extruders are the most widely used technique for the preparation of polymer clay nanocomposites because of high throughput. The rotation of screws in the barrel can generates higher shear stress, which can enhance delamination of clay particles. However, contaminations such metallic debris and grains of sand can be serious damage to the screws in the barrel. It is difficult to remove contaminations in order to keep the barrel clean after use. The method has drawn an interest from the recycle plastic community as an approach in improving the polymer property.

Copyright by Mahidol University

2.4 Clay dispersion (X-ray diffraction technique)

X-ray diffractgram on some types of composites is illustrated in figure 2.6. D-spacing (the distance between nearby clay particles indicated by "x" in figure 2.2) can be calculated by Bragg's law.

$$2d \times \sin\theta = n \times \lambda \qquad (1)$$

where d is d-spacing (A°), θ is diffraction peaks at 2θ, λ is wavelength of X-ray source. X-ray diffraction is used for characterized the d-spacing of clay platelets. The intercalation of polymer chains leads to the shift of diffraction peak toward lower angle values. For exfoliated structure, no more diffraction peaks are observed from the X-ray diffractgram .

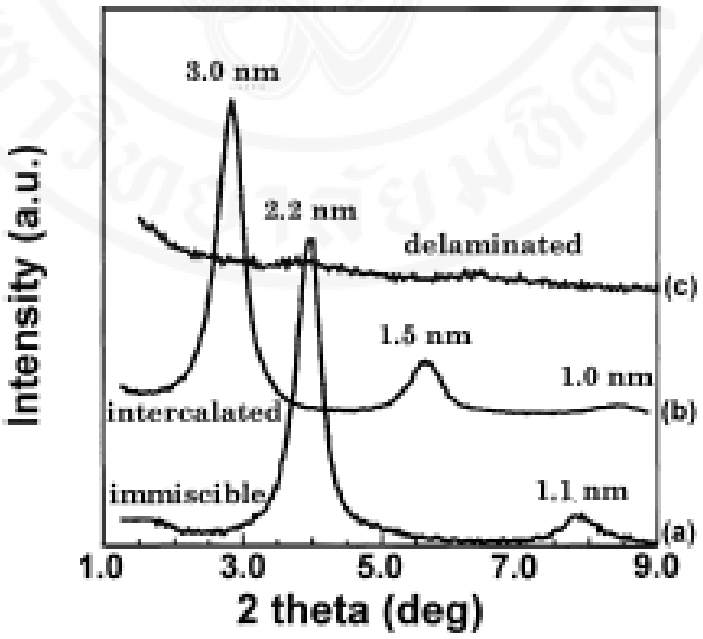

Figure 2.6 X-ray diffractram of (a) phase separated microcomposite (organomodified fluorohectrite in a HDPE matrix);

Copyright by Mahidol University

(b) intercalated nanocomposite (same organomodified fluorohectrite in PS matrix), and (c) exfoliated nanocomposite (the same organo-modified fluorohectrite in a rubber matrix) [12]

2. 5 Mechanical properties

2.5.1 Tensile strength / strain measurement

Tensile strength is determined by dividing the highest load experienced by the specimen before rupture by the original cross section of the test specimen as shown in the equation (2). The average of five rectangular or dumb-bell shaped specimens at a constant cross-head speed is taken as the value for each compound. As illustrated in figure 2.7, polymer clay nanocomposites with higher loading of well-dispersed clay platelets leads to higher tensile strength.

$$\sigma = F/A \qquad (2)$$

, where σ, F(u), and A represent tensile strength, ultimate tensile force, and the original cross section of the test specimen.

Copyright by Mahidol University

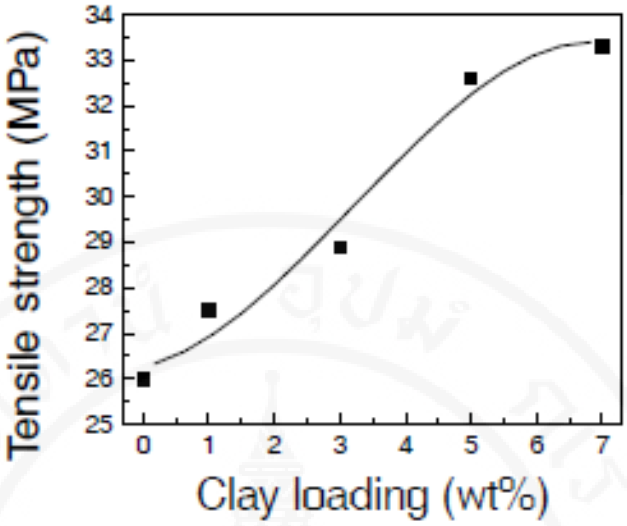

Figure 2.7 Effect of clay loading on tensile strength of PP-clay Nanocomposite [20].

2.5.2 Strain measurement

The relative deformation for materials is defined by strain such as engineering strain, strain ratio, normal strain, or shear strain. Engineering strain is the most common definition applied to polymer clay nanocomposites. This could be applied by elongation and original length of materials.

Engineering strain, so called strain, of materials is expressed as the ratio of total deformation to the original length, or gage length, of specimen along the direction where the forces are being applied. Strain is a dimensionless quality, which can be expressed as a decimal fraction, a percentage or in parts-per notation.as shown in the equation (3)

$$e = \Delta L/Lo = (L - Lo)/Lo \quad (3)$$

where e is the strain, ΔL is total deformation, L is the length of material under being loaded, and Lo is the original length, so called gage length.

Copyright by Mahidol University

2. 6 Differential scanning calorimetry (DSC)

DSC is a very useful technique for investigating thermal properties, melting and crystallization temperature, of polymer clay nanocomposites.

Melting temperature can be determined by the temperature at a minimum heat flow in heating process at a constant rate. Figure 2.8 shows DSC curves of PE clay nanocomposites for various clay contents in heating process. Temperatures at minimum heat flow indicate melting temperatures. In figure 2.7, it is found that melting temperature gradually increases with increasing clay content.

Crystallization temperature is determined by the temperature at maximum heat flow in cooling process at a constant rate. Typical DSC curves on cooling process are illustrated on figure 2.9. Polymer clay nanocomposites with higher-dispersed clay platelets show higher crystallization temperature due to the presence of the spherulite, a spherical semi-carstalline regions inside non-branched lineaer polymers. In formation of the spherulites, clay particles can play a role of nucleation.

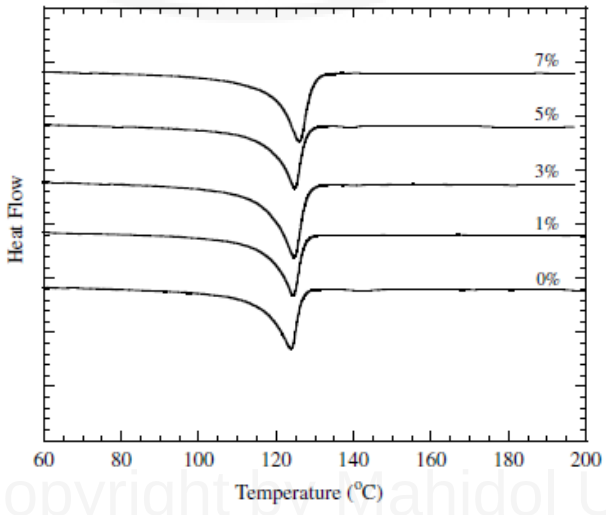

Copyright by Mahidol University

Figure 2.8 DSC curves of PE/clay nanocomposites for various contents [19].

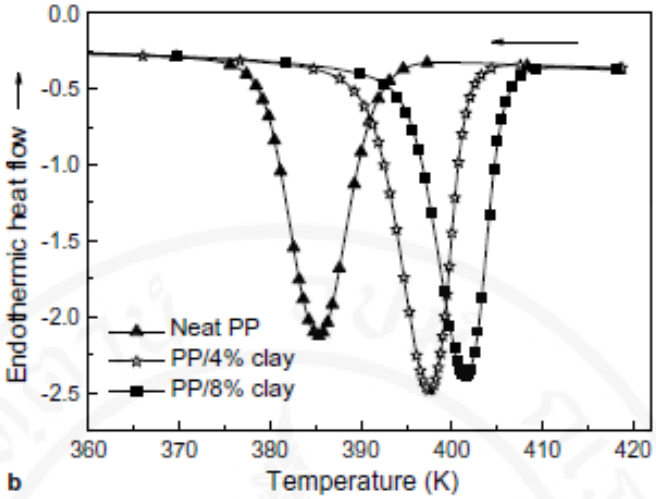

Figure 2.9 DSC curves of crystallization on PP-clay nanocomposites [21].

2. 7 Gas barrier properties

One of essential properties of polymer clay nanocomposites is a gas barrier property. It shows a very promising application in the field of food packaging. Polymer clay nanocomposites are suitable for manufacturing packaging films, because of their nanodispersed structure as compared to conventional composites as shown in figure 2.10. Clay platelets dispersed in polymer clay nanocomposites act as an obstacle for permeation of gas molecules and atoms. Moreover, in general the higher clay loading is in nanocomposites, the lower permeability of gas molecules as shown in figure 2.11.

Copyright by Mahidol University

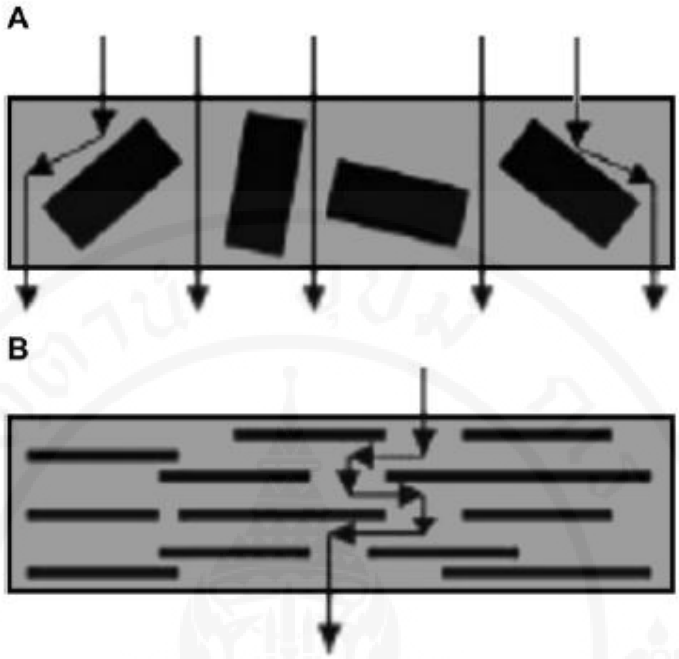

Figure 2.10 Tortuous diffusion path of conventional composites (A) [22] and polymer clay nanocomposites (B) [23].

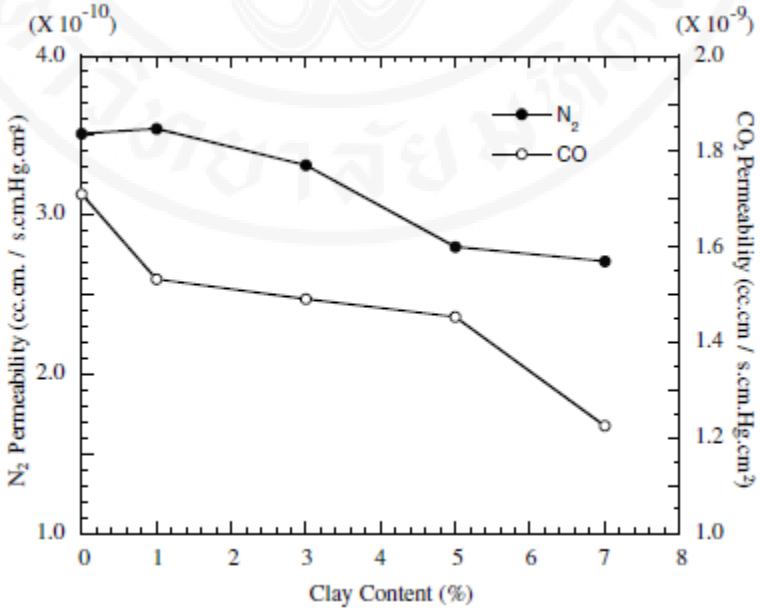

Figure 2.11 Gas permeability of the nanocomposites for various clay contents [19].

Copyright by Mahidol University

2.8 Electron microscopy

2. 8. 1 Scanning electron microscopy (SEM)

SEM is one of the most reliable procedures for observation of the dispersion of clay particles in matrix polymers in a micrometer scale. Therefore, the dispersion of clay aggregations in polymer matrix can be observed as shown figure 2.12. It is necessary to chemically treat the surface of specimens before being coated with conductive metals.

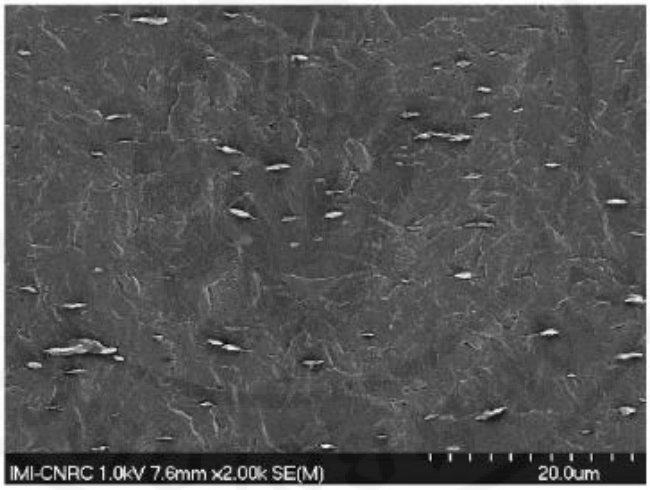

Figure 2.12 SEM micrograph of PP clay nanocomposites [2].

2. 8. 2 Transmission electron microscopy (TEM)

TEM is normally used for observation of the dispersion of clay platelets in matrix polymers in a ranging from a submicron to nanometer scale. The dispersion of individual clay platelet in polymer matrix can be observed as shown in figure 2.13. One of the difficulties for the TEM technique is the fact that the samples have to be cut, microtomed, into less thin section with less than 100nm in the thickness.

Copyright by Mahidol University

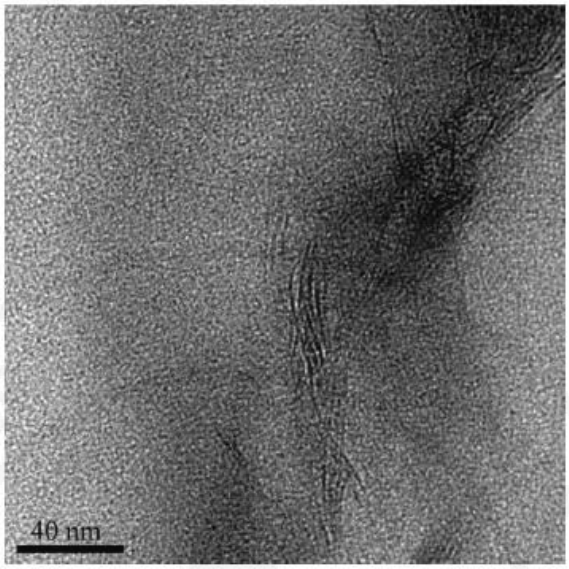

Figure 2.13 TEM micrograph of PHDE clay nanocomposites [1].

Copyright by Mahidol University

CHAPTER III
HIGH-DENSITY POLYETHYLENE (HDPE)-CLAY NANOCOMPOSITESFORMATION BY TWO-ROLL MILL

3.1. Introduction

Polymer-clay nanocomposite is an emerging class of advanced engineering materials. Several key properties, such as strength and permeation, can be improved by adding a small amount of clay into the polymeric matrix [24, 25]. The properties of polymer-clay nanocomposites depend on the degree of clay dispersion or on the extent of delamination of the individual clay layers in the polymeric matrix [26]. The clay layer is hydrophilic in nature and can be converted to organoclay to promote the wetting of the polymer molecule onto the clay surface [27, 28]. By properly controlling the surface properties of the organoclay, various degrees of organoclay dispersion can be achieved includes: (a) conventional composites, (b) intercalated nanocomposites, (c) intercalated-exfoliated nanocomposites and (d) exfoliated nanocomposites [28]. The clay's surface properties can be modified in various ways. One can use clay with a different layer charge density, control the surfactant surface coverage or vary the type of intercalated surfactant [29-31].

The main objective of this work was to find the proper surface treatment condition for the 2:1 layer type aluminosilicate or bentonite from the Lopburi province in Thailand in order to optimize the organoclay dispersibility in high density

Copyright by Mahidol University

polyethylene (HDPE). Because the source of the clay was fixed, the organoclay surface property was controlled varying the amount of the adsorbed surfactant. The organoclay with different degrees of surface polarity were produced and quantified in terms of surface energy. The relationship between the organoclay dispersion in the polymer-clay nanocomposites and its surface energy was investigated to gain a better understanding of the interaction between the polymer and organoclay. A higher degree of organoclay dispersion was achieved through the use of co-intercalants, such as PP-maleic anhydride and olefin wax, which act as the predispersing agent for the organoclay [32-34]. Organoclay was mixed with the co-intercalants prior to the mixing with the polymeric matrix by the twin screw extruder prior to the let down process. The degree of organoclay dispersion was higher when two-step mixing was utilized [34].

The incorporation of organoclay into polymeric material for large-scale production is often carried out by either in situ intercalative polymerization, where the organoclay is dispersed in a monomer which is subsequently polymerized, or by melt intercalation, where the organoclay is melt-mixed with the polymer [35]. The processing of the commodity polymer is often carried out by the melt mixing process. In recycled plastic, impurities such as metallic debris result in considerable damage to the screws in the extruders; a two-roll mill is sometimes preferred for the preparation of clay nanocomposites. Organoclay can improve the mechanical properties of recycled plastic; having an effective way for dispersing the organoclay is thus in great need. In this study, we investigated the adsorption mechanism of octadecyltrimethyl ammonium chloride (S18) onto the organoclay and the properties of the resulting polymer-clay nanocomposites. We compared the results from using a low molecular

Copyright by Mahidol University

weight oxidized polyethylene wax as a dispersing agent, with that from using co-intercalants as the dispersing agent.

3.2. Experimental procedure

3.2.1 Materials

Na-clay was provided by Thai Nippon Chemical in Thailand. It is a bentonite clay from the Lopburi province in Thailand, with a cation exchange capacity of 0.98 meq/ g of clay (provided by the supplier). Octadecyl trimethyl ammonium chloride (S18), produced by Akzo Noble Surface Chemistry in the USA, was supplied by Thai Specialty Chemical Co. Ltd in Thailand. S18 is a mixture of long chain alkyl ammonium consisting of 64% C18, 31% C16 and 4% C14. It was used without any further purification.

The solvents used for contact angle measurement were distilled water (W, surface tension: 72.8 mN m^{-1}), glycerol (G, 63.4 mN m^{-1}, VWR International Ltd), diiodomethane (D, 50.8 mN m^{-1}, Merck Schuchardt OHG), and benzyl alcohol (B, 39 mN m^{-1}, Ajax Finechem).

3.2.2 Organoclay preparation

Purified clay mineral (1.0 g) was dispersed in 50 ml of distilled water. In separate beakers, solutions of 0.25, 0.50, 0.75, 1.0, 1.5, 2.0 and 2.5 mmol tallow alkylammonium ion, with octadecyl trimethyl ammonium chloride (S18) as a major component, were prepared in 50 ml of distilled water. Both the clay and the

Copyright by Mahidol University

alkylammonium solution, at a total volume of 100 ml, were heated to 70 ^{o}C for 30 minutes. The solution of alkylammonium was slowly poured into the clay suspension under rigorous stirring. The total concentration of the S18 will be stated as 2.5, 5.0, 7.5, 10.0, 15.0, 20.0 or 25.0 milli-molar (mM) per 10 g of clay while the organoclay will be referred to by the concentration of the S18 loading, for example, 2.5 mM. The mixture was stirred rigorously for an hour after which it stood, unstirred, overnight. The supernatant was carefully discarded. The precipitate was separated by filtration. The organoclay precipitate was washed, successively, with three 100-ml portions of warm deionized water. The sample was dried at 110 ^{o}C, ground with a mortar, and passed through a sieve mesh No. 200. The sample S18 organoclay was kept for further characterization.

3.2.3 X-ray diffraction (XRD)

The X-ray diffractometer, Bruker model D8 ADVANCE with CuKα radiation (1.5406 Å), is used in this study. The voltage and the current of X-ray tubes were 40 kV and 30 mA, respectively. The measurement was done by step scanning with a step size of 0.05 degree 2 theta and integration time of 5 seconds. The measurement of the pre-dispersed organoclay and nanocomposites was scanned in a range from 1.5° to 10.0° with the same conditions as those for organoclay. The interlayer of distance was determined by the diffraction peak.

3.2.4 Thermal gravimetric analysis (TGA)

Copyright by Mahidol University

Thermal gravimetric analysis was obtained using a Netzsch STA 409 C. The measurement was determined at a temperature range of 25-1000 ^{o}C under N_2

atmosphere. The heating rate was 10 ^{o}C/min. An alumina crucible was used as a reference material.

3.2.5 Contact angle measurement

Contact angle measurement of sessile drops on organoclay tablets was conducted in order to quantify its degree of hydrophobicity. The sample was made from 1.0 g of organoclay hydraulic-pressed into tablets of 1.5 cm diameter and thickness around 5.0 mm. The volume of each drop was 5.0 microliters. Average value of ten droplets at each solvent on each sample was adopted as contact angle.

3.2.6 Surface energy

The calculation of the surface energy was performed using Owedt's method [35, 36]. The solvents possess different dispersive and polar components.

$$\gamma_L(1+\cos\theta) = 2\sqrt{(\gamma_S^d.\gamma_L^d)} + 2\sqrt{(\gamma_S^p.\gamma_L^p)} \quad (1)$$

$$\gamma_S = \gamma_S^d + \gamma_S^p \quad (2)$$

In the equations (1) and (2), γ_S, γ_S^d, and γ_S^p represent the surface energy of the substrate and the dispersive and polar components of the solvent, respectively [36]. The values for both the polar and dispersive components of the solvent are reported in Table 3.1. The surface energy was obtained by plotting $\left[(\gamma_L(1+\cos\theta))/2\sqrt{\gamma_L^d}\right]$ against (γ_L^p/γ_L^d), which yielded a linear relationship. The dispersive component, γ_S^d, was obtained from the y-intercept and the polar

Copyright by Mahidol University

component, γ_S^p from the slope. The sum of the dispersive and polar components gave the surface energy.

Table 3.1 Dispersive components (γ^d_L), polar components (γ^p_L), and surface tension of solvents.

Solvents	γ^d_L (mN m^{-1})	γ^p_L (mN m^{-1})	γ_L (mN m^{-1})
DI-water	21.8	51.0	72.8
Glycerol	33.9	29.8	63.7
Di-iodomethane	49.5	1.3	50.8
Benzyl alcohol	30.3	8.7	39.0

3.2.7 Critical surface energy (CSE)

The critical surface energy (CSE) of organoclay was calculated using the Zisman plot [37]. The following equation was used for determining the CSE.

$$\cos\theta = 1 - b(\gamma_L - \gamma_C) \quad (3)$$

A CSE on the organoclay surface is defined as the surface tension of the reference liquid that fully wets the surface when $\gamma_L = \gamma_C$. If the experimental plots of the reference liquids fall on a straight line, the surface wettability is determined from the intersection of the straight line and $\cos\theta = 1$. The same contact angle data was used to generate a Zisman's plot for our organoclay sample to calculate its CSE. A pure solvent was used rather than one of mixed solutions due to a possible contamination from specific and selective adsorption of the components constituting the solution [38].

Copyright by Mahidol University

3.2.8 High-density polyethylene (HDPE)-clay nanocomposite preparation using a two-roll mill

Organoclays with different degrees of surface coverage were used to make various polymer-clay nanocomposites. Oxidized polyethylene wax (OWax) with an acid number of 25mg KOH/g (available under the product name EO-42, will be referred to here as OWax) was obtained from Q-compound Co., Ltd in Nonthaburi, Thailand. The low molecular weight polyethylene wax (Wax) was used for comparison. High-density polyethylene (HDPE), from Thai-Zex (7000 F), was used as the matrix. S18 organoclay (10 g) was pre-dispersed in 20 g of OWax by melting in a silicone oil bath at 120 °C with a homogenizer (IKA, Germany). The pre-dispersed organoclay was ground to around 5 mm in size before mixing with the polymer matrix. The time during which OWax and organoclay were compounding was kept under 10 minutes in order to avoid chemical degradation. The interlayer spacing of organoclay was studied by X-ray diffraction.

The pre-dispersed S18 organoclay (4.5 g) was mixed with 30g of HDPE by a two-roll mill (En Mach Co Ltd., Bangkok, Thailand) at 140 °C. As a reference, 30g of HDPE was directly compounded with 1.5g of S18-unloaded clay at 140 °C. The rotating speed was kept constant during the processing. Nanocomposites were compressed into a sheet that was 1.0 mm thick and characterized.

3.2.9 Tensile test

Tensile test was conducted using Tensometer 10, Monsanto Instruments & Equipment, USA) following ASTM D638. Each compressed sample was die-cut into

Copyright by Mahidol University

type-4 specimens. Five specimens per sample were taken to obtain the reported data. Crosshead speed of 500 mm/min was applied.

3.2.10 Transmission electron microscopy (TEM)

The microscopic investigation of the clay microstructure was performed using JEOL 2010 TEM at an acceleration voltage of 200 kV. All the samples were cut by ultramicrotome with a diamond knife. The thickness was set at 100 nm.

3.2.11 Scanning electron microscopy (SEM)

The micrometer scale distribution of the nanocomposites was investigated with a scanning electron microscope (SEM, Hitachi SEM S-2500) with an operating voltage of 15 kV. Fractured surface was prepared by breaking a notched specimen in liquid nitrogen. The specimens were etched by solution of 0.7 wt% $KMnO_4$ in a 2:1 mixture of H_2SO_4 and 85% H_3PO_4 for 30 min. The sample was exposed to 30% H_2O_2 aqueous solution and distilled water, and then dried in a nitrogen stream.

3.3 Results and discussion

3.3.1 Organoclay preparation

The clay used in this study had a cation exchange capacity of 0.98 meq/g. The S18 organoclay exhibited a weight loss below 100 ^oC due to the evaporation of free water absorbed on the external surface of the clay [31]. The amount of water varied inversely with the S18 surface coverage. The organoclay with the lowest surface coverage (2.5 mM S18 loading) had the highest amount of free water. As the

Copyright by Mahidol University

surface coverage of S18 increased, the amount of free water absorbed leveled off due to the organoclay surface becoming more organophillic. The amount of free water released was subtracted from the total weight obtained from TGA. The remaining weight of the clay and intercalated S18 was normalized to 100%. The percentages of intercalated S18 and of clay are listed in columns 2 and 3 in Table 3.2.

Table 3.2 Calculated weight loss, total area occupied, and spacing for S18.

1	2	3	4	5	6	7
S18 loading (mM/10g of clay)	**Percent weight loss of S18 obtained from TGA (%)**	**Percent clay content (%)**	**S18 in inter-layer (mmol)**	**S18 in inter-layer per gram of clay (mmol)**	**Ad-sorption efficiency (%)**	**d-spacing (A^o)**
2.5	5.1	94.9	19.6	0.21	82.6	13.58
5.0	9.9	90.1	38.1	0.42	84.6	13.96
10.0	15.0	85	57.7	0.68	67.9	15.42
15.0	19.7	80.3	75.8	0.94	62.9	19.42
20.0	23.2	76.8	89.2	1.16	58.1	20.17
25.0	25.5	74.5	98.1	1.32	52.7	20.17

Copyright by Mahidol University

Table 3.2 Calculated weight loss, total area occupied, and spacing for S18 (cont.).

1	8	9	10	11	12	13
S18 loading (mM/10g of clay)	**Δd-spacing (A^o)**	**Estimated number of the S18 N (molecules)**	**Total available area of the bentonite (A^{o2})**	**Area occupied per S18 molecule (A^{o2})**	**Area occupied per molecule per one sheet of clay (A^{o2})**	**Predicted length of the S18 molecule on the surface L (A^o)**
2.5	4.08	$1.18x10^{22}$	$6.64 x10^{24}$	562.6	281.3	62.5
5.0	4.46	$2.29 x10^{22}$	$6.30 x10^{24}$	275.1	137.6	30.6
10.0	5.92	$3.47 x10^{22}$	$5.95 x10^{24}$	171.3	85.7	19.0
15.0	9.92	$4.56 x10^{22}$	$5.62 x10^{24}$	123.2	61.6	13.7
20.0	10.67	$5.37 x10^{22}$	$5.38 x10^{24}$	100.1	50.0	11.1
25.0	10.67	$5.90 x10^{22}$	$5.22 x10^{24}$	88.3	44.2	9.8

Hydrated water, found in the clay interlayers, is strongly associated with the exchangeable sodium ion. It evolved between 100 ^oC and 300 ^oC and was very difficult to identify due to an overlapping of its peak with the loss of surfactant.

The adsorption of S18 onto the bentonite interlayer can be divided into three states depending on the coverage of the interlayer surfactant: an initial state where there is monolayer formation, an intermediate state of double layer formation,

Copyright by Mahidol University

and a final state where there is double layer formation. Each state was characterized by documenting changes in the interlayer spacing, its characteristic weight loss profile, and its surface energy and nanocomposite formation.

3.3.2 The first state (monolayer formation)

In this state, a flat-lying monolayer of S18 molecules forms on the clay surface. The amount of intercalated S18 was calculated from the weight loss observed from TGA between 150 and 500 ^{o}C (columns 2 and 3, Table 3.2). The weight loss at temperatures below 150^{o}C originated from evaporation of free water or of physisorbed water, which exists between clay particles and is adsorbed on the external surface of the clay [29, 31]. Physisorbed water was not considered in the calculation; therefore, just the free water was subtracted from the total weight loss to give the weight of intercalated S18. The weight loss temperatures higher than 500 ^{o}C originated from the dehydroxylation of aluminosilicate and the release of residual organic carboneous residue product; these processes also were not considered in the calculation [29, 39]. Around 300 ^{o}C water tightly bound to the interlayer evaporates. This was difficult to identify [29] due to an overlapping of the peaks and may have caused an error of less than 1% in the interpretation of the total weight loss.

At the loading at 2.5 mM, the d_{001} was 13.6 Å. The weight of the intercalated surfactant and clay, after subtracting the amount of free water, was 5.1 % from the decomposition of the S18 molecules, (column 2, Table 3.2) and 94.9 % from the clay, (column 3, Table 3.2). The weight loss from S18 was equal to the amount of intercalated S18. This amount was converted into milli-molar (mmol) by dividing the average molecular weight of S18 at 260 g/mol (column 4 Table 3.2) and normalizing

Copyright by Mahidol University

to the loss in mmol per 1 g of clay (column 5, Table 3.2). We estimated the amount of intercalated S18 to be 19.6 mmol or 0.21 mmol/ g of clay, below the cation exchange capacity of 0.98 meq/ g of clay. The chloride counter anion of the S18 was not accounted in the calculation because S18 underwent cation exchange reaction, releasing its counter anion to the solution. The adsorption efficiency (in percent), (column 6, Table 3.2) was obtained by taking the ratio of the intercalated S18 / 1 gram of clay and the amount of S18 loading in mmol/g of clay and multiplying it by 100. The adsorption efficiency was used to properly load S18 in the reactor.

The change in d-spacing (figure 3.1, column 7 Table 3.2) was obtained by subtracting the thickness of the bentonite, 9.5 Å, from the observed d_{001} spacing (column 8 Table 3.2). The Δd-spacing of the S18 molecules was estimated to be 4.1 Å, which is about the cross-section of one S18 molecule [29, 40]. This suggests that there is a flat layer of S18 molecules on the bentonite surface [41].

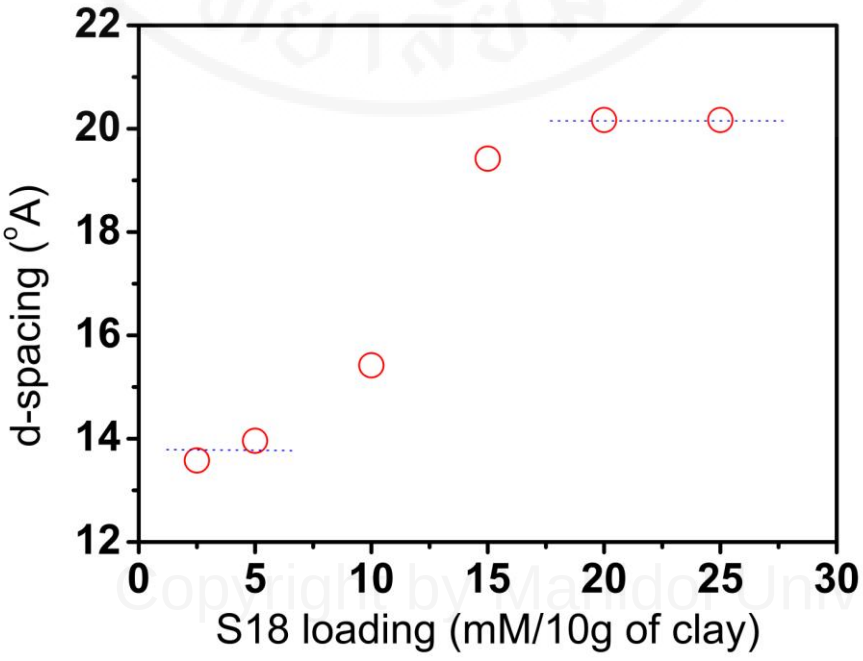

Copyright by Mahidol University

Figure 3.1 The plot of d-spacing of organoclay at different S18 loadinngs.

The arrangement of S18 in the interlayer was obtained from the total amount of weight loss from TGA, under the assumption that the S18 in the interlayer undergoes a cation exchange reaction [42]. The intercalate S18 was washed thoroughly to insure that only exchanged S18 molecules were present in the bentonite. The arrangement of S18 on the clay surface was deduced from the area occupied per molecule in the interlayer. N represents the total number of S18 molecules in the interlayer calculated from the cation-exchanged intercalated S18, i.e. with the counter anions for the interlayer S18 molecules on the bentonite surface and no chloride counter anions. However, at high surfactant loading or higher surface coverage, physisorption can occur, causing chloride ions to be present. The total number of S18 molecules in the interlayer (column 9, Table 3.2) was obtained by multiplying Avogadro's number with the amount of intercalate S18 in mmol (column 4 Table 3.2), i.e. 19.6 mmol for 0.25 mM loading. The total surface area, excluding the edge contribution, of clay was about 700 m^2 /gram of clay [43], which with 94.9 g of total clay, gave a total area of 6.64×10^{24} A^{o2} (column 10 Table 3.2). Factoring in the total number of S18 molecules in the interlayer calculated above, the total area occupied by S18 was estimated to be 562.6 A^{o2}/molecule for the layer covering the clay surface. Dividing this number by 2 yielded the area occupied per plate of clay, or 281.3 A^{o2}/molecule per plate of the clay surface (column 11 Table 3.2). To get the length $\mathcal{L}$ of S18 on the surface, the area occupied per plate of the clay calculated above (281.3 A^{o2}/molecule) was then divided by the width of S18 (4.5 A^{o}).

$\mathcal{L}$ = (calculated area occupied per 1 plate of the clay)/ 4.5 Å

Copyright by Mahidol University

The calculated length $\mathcal{L}$ was compared to the actual length of the S18 molecule, which is 21.0 A^{o}. If $\mathcal{L}$ was larger than the actual length, then there was

enough area on the surface for S18 to pack as a monolayer. If $\mathcal{L}$ was less than the actual length, then there was not enough area for S18 to be packed as a monolayer and the formation of S18 would be in an intermediate state of double layer formation or in double layer formation. Our calculated arrangement of S18 was consistent with the observed result for 2.5 mM loading where the interlayer spacing was 4.5 Å. The S18 molecule was most likely anchored to the available negative site on the bentonite surface due to strong ionic interactions between the S18 head group and the charge-deficient site on the clay surface. This is different from monolayer formation at the gas-water interface where the surfactant molecule is often packed as an island [44].

The total weight loss increased to 9.9 % and the Δd-spacing to 4.46 Å at 5.0 mM loading. The XRD peak at 5.0 mM loading was better defined and the arrangement of S18 in the interlayer was more uniform than at 2.5 mM loading. The calculated amount of intercalated S18 was 0.42 mmol/ g of clay, corresponding to 84.6 % adsorption efficiency. The calculated $\mathcal{L}$ is at 30.6 Å, longer than the actual length of S18 at 21.0 Å. Thus, at 5.0 mM loading, we predict a flat-lying monolayer formation. This was consistent with the observed XRD results. A derivative of the weight loss peak, DTG, for 2.5 mM S18 loading showed a peak at 400 ^{o}C. The 5.0 mM showed a similar peak but with a higher weight loss, suggesting that the interlayers for 2.5 mM and 5.0 mM loading have similar environments. At 5.0 mM loading, the amount of intercalated S18 was well within the bentonite's capacity to hold the cation.

Copyright by Mahidol University

3.3.3 The second state (intermediate state of double layer formation)

In this state, the interlayer packing is transitioned from a monolayer to a double layer. At a surfactant loading of 10.0 mM, the observed Δd-spacing increased to 5.92 Å and the weight loss to 15.0 %, or 0.68 mmol/g of clay. These values are in between the values for the monolayer and double layer formation states, suggesting that the S18 molecules are arranged in an intermediate state of double layer formation. The adsorption efficiency was 67.9 % lower than the valued obtained in the monolayer state. This decrease in adsorption efficiency may be related to a change in the adsorption mechanism and the arrangement of the intercalated S18. A change in the DTG peak around 300 ^{o}C is most likely associated with the change in S18 arrangement in the interlayer as well. The calculated $\mathcal{L}$ is 19.0 Å which is slightly shorter than the actual length of the S18 molecules, but comparable to the length of S18 molecules arranged in an intermediate state of double layer formation.

3.3.4 The third state (double layer formation with excess surfactant)

In this state, the adsorbed S18 molecules are arranged in a flat-lying double layer. The total amount of intercalated S18 was almost equal to the cation exchange capacity. As the loading increased to 15.0 mM, the Δd-spacing increased to 9.9 Å and the amount of adsorbed alkylammonium to 0.94 mmol/ g of clay. The adsorption efficiency was 62.9%. The DTG peak at 300 ^{o}C was clearer and there was a new peak at 250 ^{o}C (Figure 3.2). This suggested that this phase of packing was the least stable. The weight loss mechanism for the different state of material differed depending upon the packing of the surfactant molecule within the clay layer and the interaction between surfactant and clay [30]. At this concentration, some S18 molecules arranged themselves into flat-lying double layers (model c, Figure 3.3)

Copyright by Mahidol University

while others remained as a flat-lying monolayer on top of the clay surface. It should be noted that the total amount of S18 in the interlayer at 0.94 mmol/g of clay was comparable to the clay's cation exchange capacity at 0.90 meq/g of clay. The $\mathcal{L}$ was calculated to be 13.7 Å, more than half the theoretical length of S18 (21.0 Å), confirming that the S18 molecules have completely formed a flat-lying double layer. This result was also consistent with the observed Δd-spacing from the XRD data.

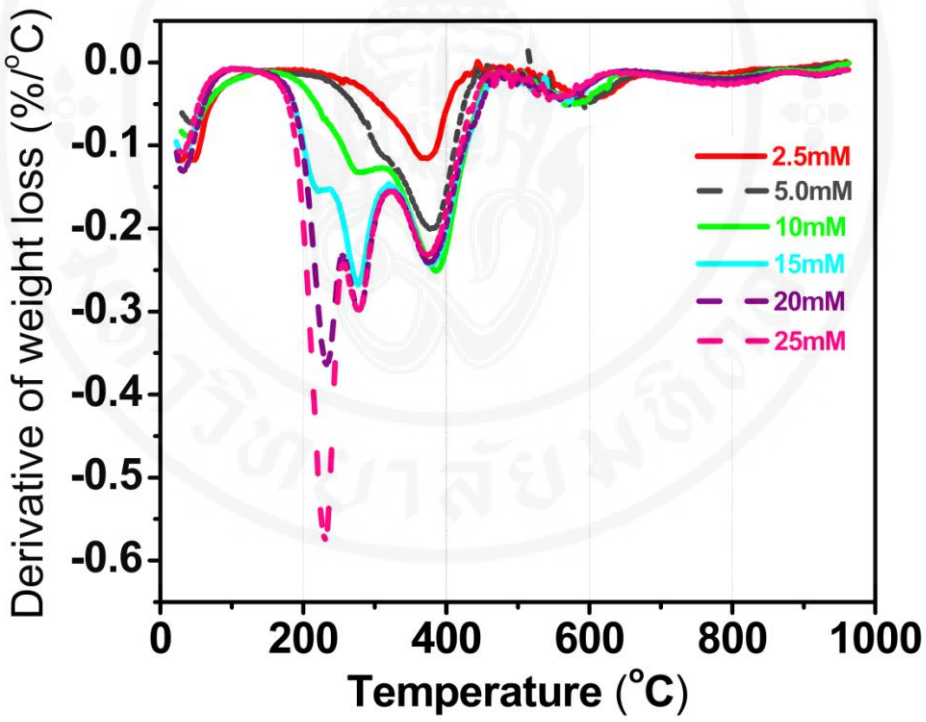

Figure 3.2 The plot of DTG of S18 organoclay at different loadings.

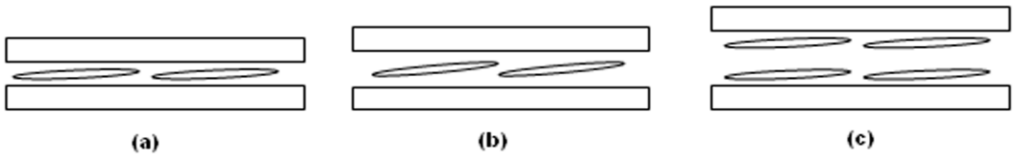

Copyright by Mahidol University

Figure 3.3 The possible arrangement of S18 in the interlayer.

The Δd-spacing remained at 10.7 Å for both 20.0 mM and 25.0 mM loading. The total weight loss, however, increased from 1.16 mmol/g of clay to 1.32 mmol/g of clay with adsorption efficiencies of 58.1 % and 52.7 %, respectively. At these loading concentrations, the amount of intercalated S18 exceeded the cation exchange capacity of the clay. Some of the intercalated S18 may have physisorbed in the interlayer and hence, did not undergo cation exchange. The $\mathcal{L}$ values were 11.1 and 9.8 Å, respectively, for the two loading concentrations, roughly half the theoretical length of S18 (21.0 Å). This suggested that the intercalated S18 had, more or less, a uniform distribution in the interlayer. The DTG peak at 250 ^{o}C was even more prominent, supporting the idea that a new arrangement of interlayer packing had developed.

It has been shown that the mechanism behind the S18 adsorption process can be altered if a different type of clay or a different surfactant were used [24, 25], or if a supramolecular structure [45] formed. Unfortunately, we could not load S18 at a concentration higher than 25.0 mM due to the limited solubility of the S18 molecules.

3.3.5 Contact angle measurement and critical surface energy (CSE)

Contact angles from distilled water (W), di-iodomethane (I), and glycerol (G) were measured and the surface energy (SE, γ_S) of the organoclay was calculated using Owedt's method [35, 36]. The surface energy of the organoclay is reported in Table 3.3 as three separate values: the dispersive component, polar component and surface energy. As expected, the surface energy decreased when both the dispersive and polar components decreased. This occurred as the amount of S18 coverage increased, resulting in the presence of a larger proportion of hydrocarbon coverage on

Copyright by Mahidol University

the bentonite instead of the polar group being directly exposed on the clay surface. The surface energy of the bentonite could not be obtained due to the complete adsorption of the water by the clay. The value of the surface energy was consistent with the three states of adsorption mentioned earlier. The first and second states were characterized by surface tension values higher than 33.1 mN m^{-1}. The values dropped to around 31.0 mN m^{-1} once the double layer was formed.

Table 3.3 Dispersive component, polar component, overall surface energy (γ_S), ratio between the polar to dispersive component and the critical surface tension of S18 organoclay derived from water, glycerol and diiomethane.

(mM / 10g of clay)	**Dispersive component (mN m^{-1})**	**Polar component (mN m^{-1})**	**Total surface energy (mN m^{-1})**	**Ratio P/D**	**Critical surface tension (mN m^{-1})**	**Number of solvents**
2.5	25.6	20.4	46.0	0.79	29.3	4
5.0	24.2	16.5	40.7	0.68	25.7	4
7.5	24.6	14.1	38.7	0.57	26.5	4
10.0	24.4	8.7	33.1	0.36	20.9	3
15.0	19.7	11.9	31.6	0.61	13.8	4
20.0	22.1	14.8	36.9	0.67		3

Another interesting term was the ratio of the polar to dispersive components. This value indicates the contribution from van der Waals interactions and other polar interactions. It was shown [36] that a low ratio of 0.01 to 0.05, is preferred in order to promote the mixing of organoclay with polypropylene and

Copyright by Mahidol University

polyethylene. The values obtained in this study, however, were in the range of 0.5 to 0.7.

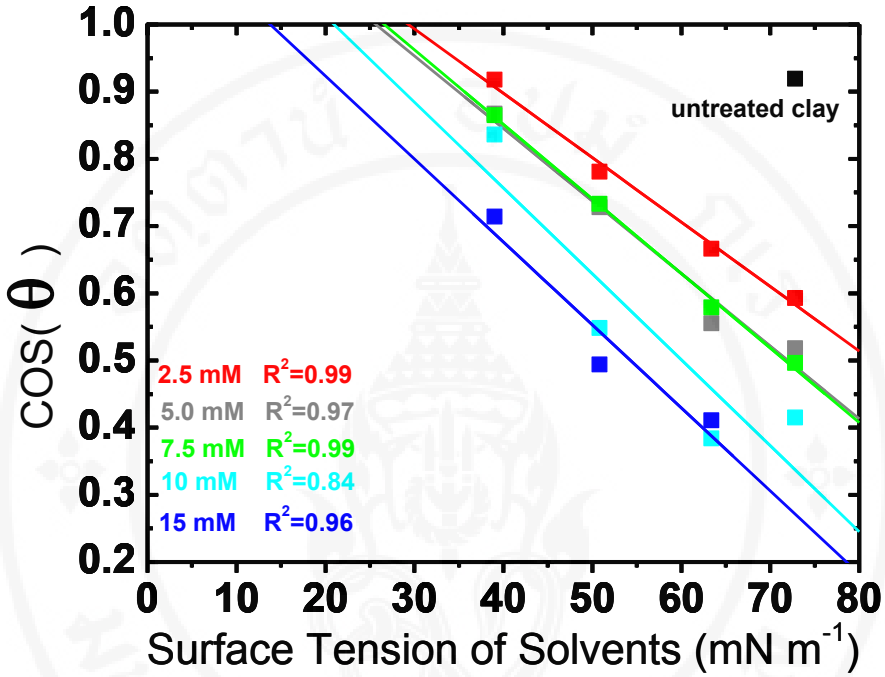

Figure 3.4 Zisman plots of S18-loaded and unloaded clay.

Zisman's plots of the S18-loaded clays and the correlation coefficients from each plot are shown in Figure 3.4. The critical surface energies (CSE) of the S18 loaded clays are listed in Table 3.3. The CSE of each S18 loaded clay was determined by calculating γ_L at the intersection of the plot and $\cos\theta = 1$. The CSE of organoclay decreased as S18 surface coverage increased on the clay. The observed CSE values were divided into three ranges, which were consistent with the three states of adsorption. The observed CSE values that corresponded with the first state at S18 concentrations of 2.5, 5.0 and 7.5 mM were 29.3, 25.7 and 26.5 mN m^{-1}, respectively. The CSE of the intermediate state of double layer formation, the second state, was

Copyright by Mahidol University

20.9 mN m^{-1}. It dropped further to 13.8 mN·m^{-1} for the third state, when the double layer completely formed.

3.3.6 Pre-dispersed organoclay

In this section, we report the results from our experiments on the formation of nanocomposites using high-density polyethylene (HDPE). The use of the co-intercalant polyethylene-co-maleic acid, has been shown to improve the dispersion of the organoclay in HDPE-clay nanocomposites [34]. However, a different co-intercalant, based on oxidized polyethylene wax (OWax), was used in this study. We used OWax in two ways: one involving direct mixing and the other involving low molecular weight non-polar dispersant, Wax. The intercalation of the OWax dispersing agent into the organoclay with different surface coverages was shown in figure 3.5. It was found that the organoclay surface coverage plays an important role in the intercalation of OWax. The first state of the surfactant at 2.5, 5.0 and 7.5 mM of the loading, occurring at low surface coverage, showed no evidence of intercalation of the OWax into the interlayer. The surface coverage did not provide enough organophilicity to promote the wetting of melted OWax on the organoclay surface. The peak at 19.7 A^{o} represented the d-spacing of the non-dispersed organoclay. Predicting the complete wetting of the polyethylene and polypropylene on the organoclay [36] depends on two parameters: (a) how well matched the surface energy of the organoclay is with the surface tension of the polymer and (b) the ratio of the polar component to the dispersive component in the low value range of 0.20. The surface tension of the OWax could not be obtained; the value of its surface energy at 36.0 mN m^{-1} was used [46]. There was a mismatch between the organoclay's surface

Copyright by Mahidol University

energy and the Owax's surface tension; dispersion was thus not favored at low surface coverage for the organoclay in OWax.

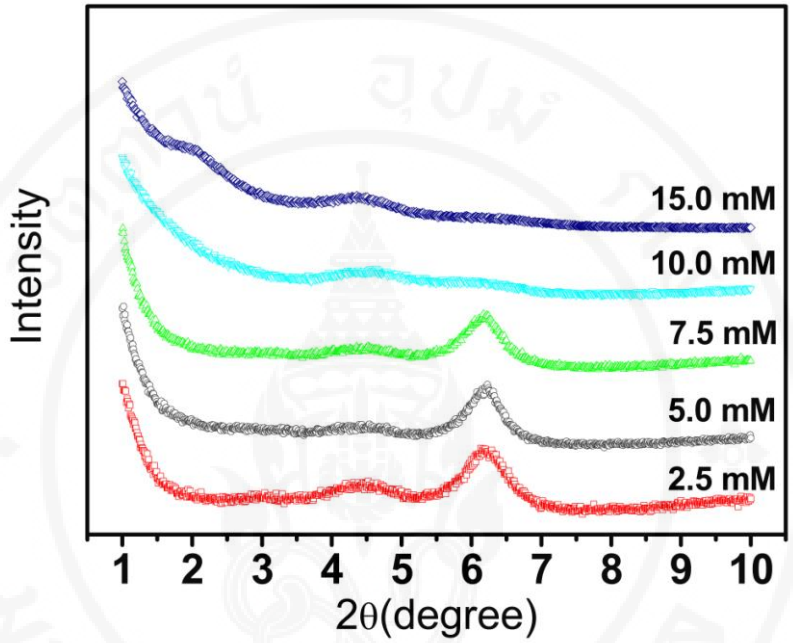

Figure 3.5 The dispersion of organoclay at various S18 loading in OWax by melt mixing.

Once the amount of S18 loading increased to 10.0 mM, the organoclay was in the second state, or the intermediate state, where both the monolayer and double layer S18 were formed on the clay surface. The peak of the organoclay in OWax started to change due to the intercalation of the OWax into the double layer S18 on the organoclay surface. This intercalation of the dispersant was believed to be packed in between the S18 molecules and caused the S18 molecules to form a tilted packing.

As the S18 loading increased to 15.0 mM, the S18 molecules had complete surface coverage on the clay surface. The observed XRD indicated that the OWax intercalated into the organoclay; the peaks at 42.3 Å and 20.6 Å correspond to the d_{001}

Copyright by Mahidol University

and d_{002} of the intercalated organoclay. It should be noted that the surface tension of the polyethylene, around 31.0 mN m^{-1}, was used [46]. The OWax could not wet the organoclay during the first state of formation because of an excess contribution from the polar portion of the clay [36]. This was the case for second state, but only in the region that had bilayer coverage. The surface energy of the organoclay that is in the third state matched very well with the surface tension of the OWax and the intercalate-exfoliate of the organoclay was observed [47].

Preparing organoclay at surfactant loading higher than 15.0 mM was not practical because the intercalation exceeded the optimum condition and too much S18 would have been lost during the intercalation process. In summary, we found that controlling the surface properties of the organoclay through the amount of surfactant molecules adsorbed was not effective towards preparing polymer clay nanocomposites. At low surfactant loading, too much of the area within the clay was left uncovered, disfavoring the wetting by the hydrophobic polymer. Controlling the surface properties of the organoclay through the functional group of the surfactant molecule was more suitable.

3.3.7 Nanocomposite Formation

The organoclay with OWax (Figure 3.6) was mixed with HDPE to form polymer-clay nanocomposites.

Copyright by Mahidol University

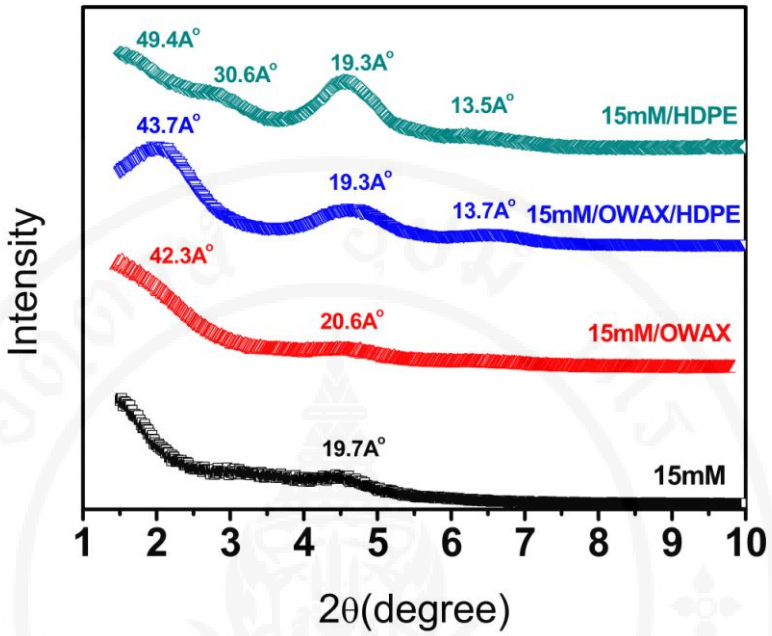

Figure 3.6 X-ray diffractgram of nanocomposites with OWax.

The 15.0mM organoclay (hereby known as 15mM) was directly compounded with HDPE to give 15mM/HDPE. The 15mM/HDPE showed diffraction peaks at 49.4 Å, 30.6 Å, 19.3 Å and 13.5 Å; the peaks at 49.4 Å and 30.6 Å were shoulders and not as strong as the other two. The peak at 19.7 Å represents the d-spacing of the 15.0mM organoclay. Its presence meant that the HDPE did not intercalate into the organoclay interlayer. A partial intercalation was observed, as evidenced by the large d-spacing. A similar result was observed when the 15.0mM organoclay was mixed with Wax (Figure 3.7).

Copyright by Mahidol University

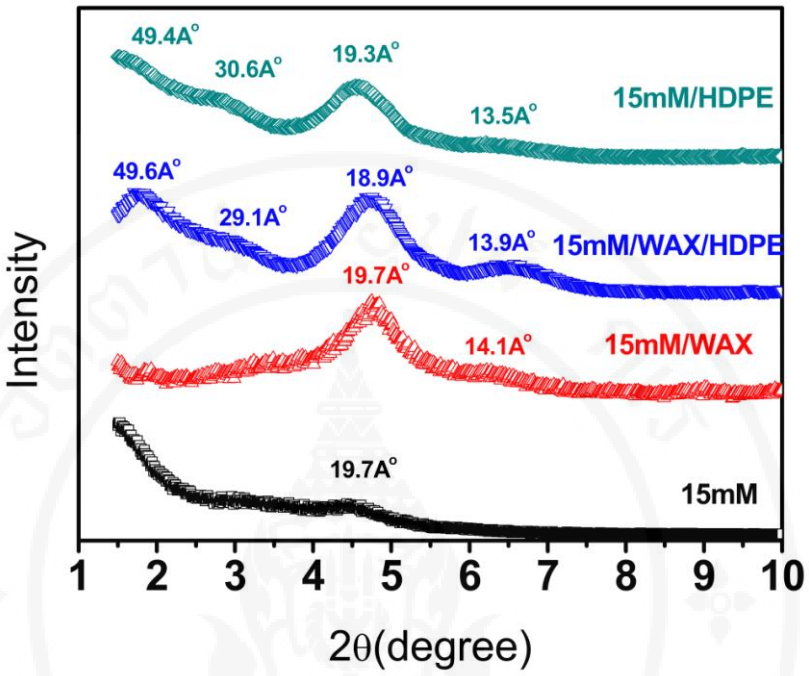

Figure 3.7 X-ray diffractgram of nanocomposites with Wax.

A clear intercalation without any trace of the organoclay peak was observed in the case of OWax. This implied that the intercalation of the HDPE into the organoclay layer was promoted by the OWax. The 15mM/OWax/HDPE compound showed three diffraction peaks at 43.74 Å, 19.25 Å and 13.73 Å and were assigned d_{001}, d_{002} and d_{003}, respectively. Its X-ray patterns suggested that the formation of the nanocomposites was influenced by the presence of OWax. OWax was more effective at dispersing the organoclay. The -OH functional group in OWax may play a role in enhancing the interaction between the OWax molecules and the organoclay surface, leading to better intercalation. The observed TEM and SEM images were in good agreement with the XRD data, all showing that greater dispersion was achieved when the OWax was used. However, we detected a submicrometer size agglomerate originating from the primary

Copyright by Mahidol University

particle of the organoclay (Figure 3.9). The size of this agglomerate was less than a micrometer for the case of OWax, but for 15mM/Wax, a large non-dispersed 15.0mM organoclay was observed (Figure 3.8(b)).

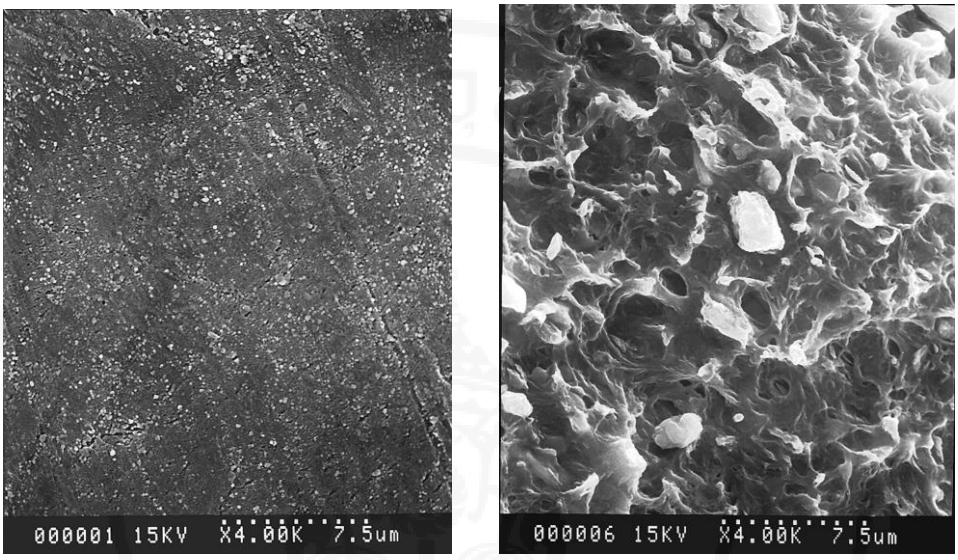

(a) (b)

Figure 3.8 SEM image of fracture surface after chemical etching.
(a) 15mM/OWax/HDPE represents a dispersion of the organoclay and
(b) 15mM/Wax/HDPE represents the agglomerate of the organoclay

This latter agglomerate was a few micrometers and we observed the organoclay stacked with a smaller size of the primary particle. This was in good agreement with the peak at 19.3 Å of the 15.0mM organoclay and thus, further supports that the OWax promoted the delamination process of the organoclay. The TEM images showed the size of the primary particle to be around a few hundred nanometers. To further improve the dispersion of the organoclay in the OWax, a more efficient dispersing agent is needed. The 15mM/Wax was intentionally loaded into the low molecular weight polyethylene wax, where the organoclay was not dispersed and the SEM image

Copyright by Mahidol University

was taken to show the non-dispersed organoclay, as seen in the XRD in Figure 3.7. The large organoclay agglomerate was present in the sample, compared to the smaller particle present when OWax and HDPE were used.

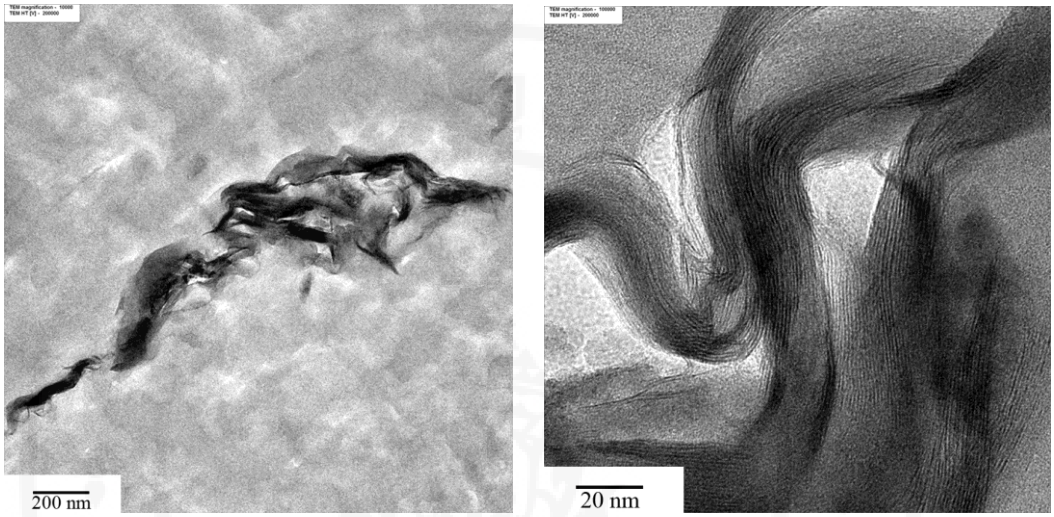

(a) (b)

Figure 3.9 TEM image 15mM/OWax/HDPE shows the presence of the primary particle at (a) medium and (b) high magnification. The stack of the organoclay can be clearly seen at the high magnification.

Tensile testing of dumbbell-shaped specimens (type-4) was carried out at an elongation rate of 500 mm/min. The ultimate strengths and fractured strengths are listed in Table 3.4. The ultimate strength of pure HDPE was 33.56+/-2.01 MPa. When pure HDPE was mixed with OWax (OWax/HDPE), the ultimate strength slightly decreased to 30.99+/-1.16 MPa. The same result was reported in [45], where the reduction in the mechanical property was observed in the presence of OWax. This implies that the presence of 10% of a low molecular co-intercalant such as OWax, softens HDPE and impairs the ultimate strength.

Copyright by Mahidol University

Table 3.4 Mechanical properties (tensile test)

	HDPE	**Wax /HDPE**	**15mM/ Wax/ HDPE**	**OWax /HDPE**	**15mM/ OWax/ HDPE**	**15mM/ HDPE**
Ultimate strength (MPa)	33.56 +/- 2.01	31.28 +/- 1.62	41.47 +/- 3.03	30.99 +/- 1.16	42.84 +/- 2.14	41.45 +/- 7.45
Fracture strength (MPa)	31.41 +/- 2.01	25.57 +/- 9.63	38.52 +/- 2.35	27.1 +/- 6.76	38.74 +/- 1.81	40.50 +/- 7.02

On the other hand, compounding HDPE with pre-dispersed 15.0mM/Owax, increased the ultimate strength of the composites to 42.48+/-2.141MP. This indicates that 15.0mM clay particles improve the ultimate strength of the HDPE-clay composites. The OWax used in this study is polar, and has a higher acid number, allowing it to promote interaction between the polymer and the organoclay.

The directly compounded 15.0mM loaded clay with HDPE (15mM/HDPE), had an ultimate strength of 41.45+/-7.45 MPa. These results were unexpected and may be due to the fact that the surface energy of the 15.0mM at 31.6 mN m^{-1} was too closely matched with the surface tension of HDPE at 31.0 mN m^{-1}.

The fracture strength of pure HDPE was 31.41+/-2.01 MPa. By directly mixing pure HDPE with OWax (OWax/HDPE), the fracture strength decreased to 27.1+/-6.76 MPa. Adding pre-dispersed organoclay (15mM/OWax) into HDPE

Copyright by Mahidol University

improved the fracture strength to 38.52+/-2.35 for 15mM/Wax/HDPE and 38.74+/-1.81 MPa.

When 15.0mM loaded clay was directly compounded with pure HDPE (15mM/HDPE) to form composites, the fracture strength was 40.50+/-7.02 MPa. This value was higher than that of pure HDPE, but lower than that of composites formed by using co-intercalants. It was found that co-intercalants were essential to improve the fractured strength.

3.4. Conclusion

The adsorption process for S18 molecules involved three states. The first state, where S18 forms a flat-lying monolayer, occurred at low loading concentrations. This state showed high adsorption efficiency, above 80%, with the surface energy in the range 40.7 – 46.0 mN m^{-1}. OWax did not mix with the organoclays due to a mismatch between the surface of the organoclay and the melted OWax. The second state, which was the intermediate state, was where the monolayer changed to a double layer formation. OWax interacted only with the portion of the organoclay that was in double layer formation. The third state, which is the complete double layer formation, involved the formation of the flat-lying double layer and occurred with high surface coverage. OWax intercalated with the double layer organoclay and dispersed the organoclay platelets into smaller particles. These results demonstrated that incomplete intercalation resulting from changes in surface coverage caused heterogeneity in the organoclay and created a non-uniform polymer-clay nanocomposite. OWax encouraged the delamination of the organoclay into smaller

Copyright by Mahidol University

platelets because the surface energy of the melted OWax matched that of the organoclay. An unexpected match in the surface energy of 15mM organoclay and HDPE showed intercalation and delamination. We found that both the ultimate strength and toughness of the nanocomposites improved when organoclay was present.

Copyright by Mahidol University

CHAPTER IV
POLYPROPYLENE (PP) CLAY NANOCOMPOSITES FORMATION BY TWIN SCREW EXTRUDER

4.1 Introduction

Polypropylene (PP) is one of the most widely used thermoplastic polymers in various applications due to its versatility, toughness, inertness and attractive property-cost ratios. In order to make improvement of the properties, composites made with fillers such as $CaCO_3$ or layered aluminosilicates were investigated [48, 49]. The layered aluminosilicates homogeneously dispersed in PP matrix, PP-clay nanocomposites, leads to a remarkably improvement in term of mechanical properties, flammability resistance and barrier properties with a slight additional cost. This had led to a lot of research on PP-clay nanocomposites in both academic and industry. [49-51]. It is difficult to get exfoliated and fully-dispersed clay particles in a PP matrix because the lack of polar group on PP molecules. Moreover, clay particle is hydrophilic in nature. The surface must be treated with surface active agents, surfactant, to adjust the surface property of the clay before compounding with the polymer. The arrnagement of the surfactant molecule on the surface had been shown to have a profound effect in controlling the organoclay dispersibility. Therefore the parameter such as length of molecules, the number of tail groups and degree of surface coverage on clay surface are important parameters in controlling the compatibility

Copyright by Mahidol University

between organoclay and the polymer [5]. It is reported that the extent of surface coverage of clay particles, low, middle or high coverage, is very important in the treatment with surfactant [6]. It is expected that low surface coverage on clay particles allow a better intercalation of molecules of matrix polymer.

The compounding approach was reported to have an effect on the clay dispersion where two kind of processes, master batch and single-pass process, were generally employed [52, 53, 57]. The master batch process showed higher dispersion of organoclay particles in polymer matrix more than single pass process [53]. The compatibilizers, such as maleic anhydride-grafted PP (MA-g-PP), was reported to improve the dispersion of the organoclay in composite by adding adequate amount of MA-g-PP into PP-clay nanocomposites [2, 49, 52, 53, 61]. Exfoliated or intercalated-exfoliated typed of dispersion had led to an improvement in term of gas barrier property, mechanical properties, and flame retardency.

The objective of this study is to investigate effects of commercially available organoclay surface coverage, with low (LC), medium (MC) and high surface coverage (HC), on the formation of polypropylene (PP)-clay nanocomposites formation through master batch process with MA-g-PP as a compatibilizer. The MA-g-PP is used in order to promote the intercalation into clay intergallery. The organoclay is the grade used in the paint industry which is being marketed at lower cost.

4.2 Experimental Procedure

Copyright by Mahidol University

4.2.1 Materials

Three different types of organoclay used in this study were trialkylaryl ammonium hectorite (Bentone 27, referred as to LC, because of low surface coverage on clay particles), tetra-alkyl ammonium bentonite (Bengel 434, referred as to MC, because of medium surface coverage on clay particles), and organic derivative of montmorillonite clay (Bentone SD-1, referred as to HC, because of high surface coverage on clay particles). All the clays were manufactured by Elementis Specialties Inc and were used without any further purification. Maleic anhydride grafted polypropylene (MA-g-PP) with acid number of 45mg KOH/g (molecular weight of 9100 g/mol and MA content of 3.8%, available under the product name Epolene E-43, Eastman Co., Ltd.) was used as the co-intercalant. Polypropylene (PP), (Basell 500N produced by HMC polymers Company Limited, MFI: 7.5g/10g) was used as a matrix polymer.

The solvents used for contact angle measurement were distilled water (W, surface tension 72.8 mN/m), glycerol (G, 63.4 mN/m, VWR International Ltd.), di-iodomethaine (D, 50.8mN/m, Merk Schuchardt OHG), and benzyl ahcohol (B, 39.mN/m, Ajax Finechem).

4.2.2 Contact angle measurement

Contact angle measurement of sessile drops on organoclay tablets was conducted in order to quantify the degree of hydrophobicity. The sample was made from 1.0 g of organoclay hydraulic-pressed into tablets of 1.5 cm diameter and thickness around 5.0 mm. The volume of each drop was 5.0 microliters. Average value of ten droplets at each solvent on each sample was adopted as contact angle.

Copyright by Mahidol University

4.2.3 Surface energy

The calculation of the surface energy was performed using Owedt's method [35, 36]. The solvents possess different dispersive and polar components were used.

$$\gamma_L(1+\cos\theta) = 2\sqrt{(\gamma_S^d.\gamma_L^d)} + 2\sqrt{(\gamma_S^p.\gamma_L^p)} \quad (1)$$

$$\gamma_S = \gamma_S^d + \gamma_S^p \quad (2)$$

In the equations (1) and (2), γ_S, γ_S^d, and γ_S^p represent the surface energy of the substrate and the dispersive and polar components of the solvent, respectively [37]. The values for both the polar and dispersive components of the solvent are reported in our previous work [54]. The surface energy was obtained by plotting $\left[(\gamma_L(1+\cos\theta))/2\sqrt{\gamma_L^d}\right]$ against (γ_L^p/γ_L^d), which yielded a linear relationship. The dispersive component, γ_S^d, was obtained from the y-intercept and the polar component, γ_S^p from the slope. The sum of the dispersive and polar components gave the surface energy.

4.2.4 Critical surface energy (CSE)

The critical surface energy (CSE) of organoclay was calculated using the Zisman plot [37]. The following equation was used for determining the CSE.

$$\cos\theta = 1 - b(\gamma_L - \gamma_C) \quad (3)$$

Copyright by Mahidol University

A CSE on the organoclay surface is defined as the surface tension of the reference liquid that fully wets the surface when $\gamma_L = \gamma_C$. If the experimental plots

of the reference liquids fall on a straight line, the surface wettability is determined from the intersection of the straight line and $\cos\theta = 1$. The same contact angle data was used to generate a Zisman's plot for our organoclay sample to calculate its CSE. A pure solvent was used rather than one of mixed solutions due to a possible contamination from specific and selective adsorption of the components constituting the solution [38].

4.2.5 Thermogravimetric analysis (TGA)

The thermogravimetric analysis (TGA) of LC, MC, and HC was carried out using SDT 2960 Simultaneous DSC-TGA (TA Instruments). The organoclays were heated from room temperature to 900^{o}C at a heating rate of 10^{o}C min^{-1} under nitrogen atmosphere (50cm^{3} min^{-1}) in order to evaluate the amount of physically adsorbed and intercalated surfactants, and their decomposition temperature.

4.2.6 Formation of pre-dispersed organoclay

The organoclay was pre-dispersed in co-intercalant by mixing MA-g-PP and organoclay at weight ratio of 1:1. Compounding was carried out by using a co-rotating twin screw extruder (produced by En Mach Co., Ltd in Thailand L/D=40:1). The temperature was set at 100°C in the 1st zone and at 190 °C from the 2nd to the 9th zone in the barrel of the extruder with the screw speed of 180 rpm. The same processing conditions were applied throughout this work except for the screw speed. Pre-dispersed organoclay composed of 50wt% of organocaly and 50wt%MA-g-PP, which is referred as to such as LC50MA50 and LC50MA50. The notation first 2 letters represent the type of the organoclay used which are LC, MC and

Copyright by Mahidol University

HC. The following number indicates the amount of the organoclay in the polymer matrix. The next two letters represent the type of the compatibilizer while the number indicates the amount of the compatibilizer in the composition.

4.2.7 Formation of PP-clay nanocomposites

The master batch having 20wt% organoclay content was prepared by adding pure PP into the pre-dispersed organoclay. The preparation was conducted by using a co-rotating twin screw extruder (produced by En Mach Co., Ltd in Thailand L/D=40:1). The processing temperature was set at 100 ^{o}C in the 1st zone and at 190 ^{o}C from the 2nd to 9th zone in the barrel of extruder with the screw speed of 600 rpm. In this paper, master batch having 20wt% of LC is described as LC20MA20PP.

The master batch was diluted with PP into 2, 5, and 10wt% organoclay content. In compounding master batch and PP-clay nanocomposites, the same twin screw extruder as in the preparation of pre-dispersed organoclay was used. In this paper, nanocomposites with 2wt% of LC and 2wt% of MA-g-PP are described as LC2MA2PP.

Two-component MA-g-PP/PP composites were prepared by directly compounding MA-g-PP with pure PP. In order to investigate the effect of MA-g-PP on Differential Scanning Calarimetery, 2, 5, and 10wt% of MA-g-PP were loaded on pure PP. Two-component MA-g-PP composites with 2wt% of MA-g-PP are also referred as to MA2PP. All formulation prepared were described in Table 4.1.

Copyright by Mahidol University

Table 4.1 Formulation of the prepared nanocomposites.

	Organoclay			MA-g-PP (wt%)	PP (wt%)
	LC (wt%)	MC (wt%)	HC (wt%)		
LC2MA2PP	2	-	-	2	96
LC5MA5PP	5	-	-	5	90
LC10MA10PP	10	-	-	10	80
MC2MA2PP	-	2	-	2	96
MC5MA5PP	-	5	-	5	90
MC10MA10PP	-	10	-	10	80
HC2MA2PP	-	-	2	2	96
HC5MA5PP	-	-	5	5	90
HC10MA10PP	-	-	10	10	80
MA2PP	-	-	-	2	98
MA5PP	-	-	-	5	95
MA10PP	-	-	-	10	90
pure PP	-	-	-	-	100

4.2.8 X-ray diffractometry (XRD)

The X-ray diffractometer in this study was Bruker model D8 ADVANCE with CuKα radiation (1.5406 Å). The voltage and the current of X-ray tubes were 40kV and 30mA, respectively. The scanning was done by step scanning with a step size of 0.05 degree at 2θ and integration time of 10 seconds. The measurement of the pre-dispersed organoclay and nanocomposites was scanned in a range from 1.0° to 10.0° with the same conditions as those for organoclay. The pre-dispersed organoclay was grounded with a mortal, and the composites extruded were compressed into a stab and cut into a 2.5 cm-diameter disc.

Copyright by Mahidol University

4.2.9 Tensile test

Tensile test of the PP-clay nanocomposites and pure PP was carried out by using the Series IX Automated Materials Testing System (INSTRON Corporation) with 50mm/min of crosshead speed according to ASTM D638.

After PP-clay nanocomposites were compressed by using a hydraulic pressing (K. V. S Engineering Co., LTD. Patumwan, Thailand), they were die-cut into the shape of type-4. Tensile strength and elongation were calculated for 5 specimens at each condition.

4.2.10 Differential scanning calorimetry (DSC)

The crystallization behavior of composites and matrix polymer was studied with a Differential Scanning Calorimeter (METTLER TOLED) under flowing nitrogen atmosphere. In order to remove the influence of the previous thermal and mechanical history, 12+/-1.0 mg samples were initially heated from 20 ^{o}C to 180 ^{o}C at 10 ^{o}C/min, held at that temperature for 5min, and then cooled to 25 ^{o}C at 10 ^{o}C/min. They were kept for 5 min, heated again to 180 ^{o}C at 10 ^{o}C/min, and cooled to 20 ^{o}C at the same rate.

The crystalinity of the PP matrix in PP-clay nanocomposites was determined by the following equation in the first cooling proess.

$$\chi = (\Delta H_m \times 100) / (f_p \times \Delta H^{o}_f) \quad (\%) \qquad (4)$$

where ΔH_m ($J \cdot g^{-1}$) is the enthalpy of melting of the polymer matrix, f_p is the PP weight fraction in the nanocomposites and ΔH^{o}_f is the enthalpy of melting of pure crystalline PP ($207.1 J \cdot g^{-1}$) [2].

Copyright by Mahidol University

4.2.11 Scanning electron microscopy (SEM)

The particle morphologies of PP clay nanocomposites were observed by scanning electron microscopy (SEM) (HITACHI SEM S-2500) with an operation voltage of 15kV. Fracture surface was prepared by breaking a notched specimen in liquid nitrogen. The specimens were chemically etched by a solution of 0.7 wt% $KMnO_4$ in a 2:1 mixture of H_2SO_4 and H_3PO_4 (85 %) for certain time, then washed by 30 % H_2O_2 aqueous solution and distilled water and dried in the air [53]. Degree of delamination of clay particles was investigated by calculating aspect ratio.

4.2.12 Gas barrier property

Thin films (1mm) of pure PP as well as PP and PP nanocomposites (LC10MA10PP, MC10MA10PP, and HC10MA10PP) were formed. Oxygen permeation meter (ILLINOIS MODEL 8000) at 23 ^oC and 0% RH were used to measure oxygen permeation through these films according to ASTM D3985. An average of ten measurements for each sample were reported.

4.3 Results and discussion

4.3.1 Thermogravimetric analysis (TGA)

The TGA curves of organoclays (LC, MC, and HC) are plotted in figure 4.1. In the first place, it can be seen that all of organoclays slightly lost their weights at a temperature below 200^oC. Each of them was about 1.4, 3.0, and 1.7wt% for LC, MC, and HC, respectively. This is believed to be due to the evaporation of moisture

Copyright by Mahidol University

present on the surface of clay platelets. The amount of water was subtracted from the total weight loss in the calculation.

LC and HC began to loose their weights at 156 and 144°C. Major weight losses of three organoclays occurred in the temperature range of 200-600°C due to decomposition of the interlayer surfactant occurred in this temperature range. [55]

The residual weights for LC and MC at 900°C were 71.3 and 71.7wt%. The residual weight for HC was 49.7wt%, which indicates that the surfactant present in HC is about twice as that of LC and HC by weight. Moreover, we can see that the half weight of HC is composed of the interlayer surfactant.

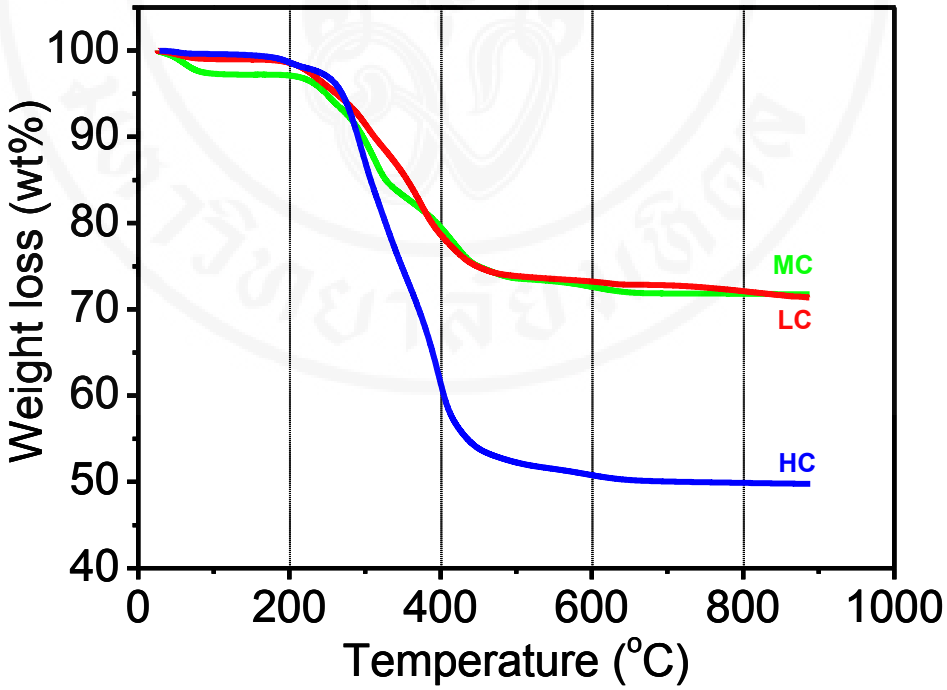

Figure 4.1 TGA curves of organoclays (LC, MC, and HC).

Copyright by Mahidol University

4.3.2 Contact angle measurement and critical surface energy (CSE)

Contat angles from distilled water (W), di-iodomethane (D), glycerol (G),

and benzyl alcohol (B) were measured and the surface energy (SE, γ_S) of LC, MC, and HC was calculated using Owedt's method [35, 36]. LC demonstrated total surface energies of 35.45mN m^{-1} as listed in table 4.2. As expected, the total surface energy decreased with increasing surfactant surface coverage. Total surface energies of LC and HC were relatively close to each other, although that of HC was the lowest. The TGA shows that the HC has the highest amount of the intercalate surfactant. The ratio of the polar to dispersive components is an indicator of contribution from van der Waals interaction and other polar interactions. In order to enhance wettability of rganoclay with polymer, a low ratio such as from 0.01 to 0.05 is better [36], although the values obtained 0.11 to 0.32.

Table 4.2 Dispersive component, polar component, overall surface energy (γ_S), ratio between the polar to dispersive component, and the critical surface tension of LC, MC, and HC.

Organoclay	**Dispersive component ($mN \cdot m^{-1}$)**	**Polar component ($mN \cdot m^{-1}$)**	**Total surface energy ($mN \cdot m^{-1}$)**	**Ratio P / D**	**Critical surface tension ($mN \cdot m^{-1}$)**
LC	27.33	8.12	35.45	0.320	28.79
MC	23.61	6.55	30.15	0.277	23.78
HC	17.99	2.01	20.00	0.111	14.80

Zisman plot and correlation coefficients of each plot on LC, MC, and HC are shown in figure 4.2. The critical surface energies (CSE) of LC, MC, and HC are also listed in table 4.2. The CSE of organoclays was determined by calculating γ_L at the intersection between extrapolation of the plots and cos θ =1. The CSE of

Copyright by Mahidol University

organoclay decreased with increasing surface coverage on clay. The CSE of LC, MC, and HC decreased as surface coverage of clay increases. The obtained values of LC and MC were very close one another, 28.8 and 23.8 $mN \cdot m^{-1}$ for LC and MC. The CSE of HC was 14.8 $mN \cdot m^{-1}$. The trend of CSE of LC, MC, and HC was similar to that of the calculated surface energy. It is reported that surface energy of polypropylene is about 15 $mN \cdot m^{-1}$ [56], so that well-dispersion of LC and MC in PP-g-MA and matrix polymer can be expected.

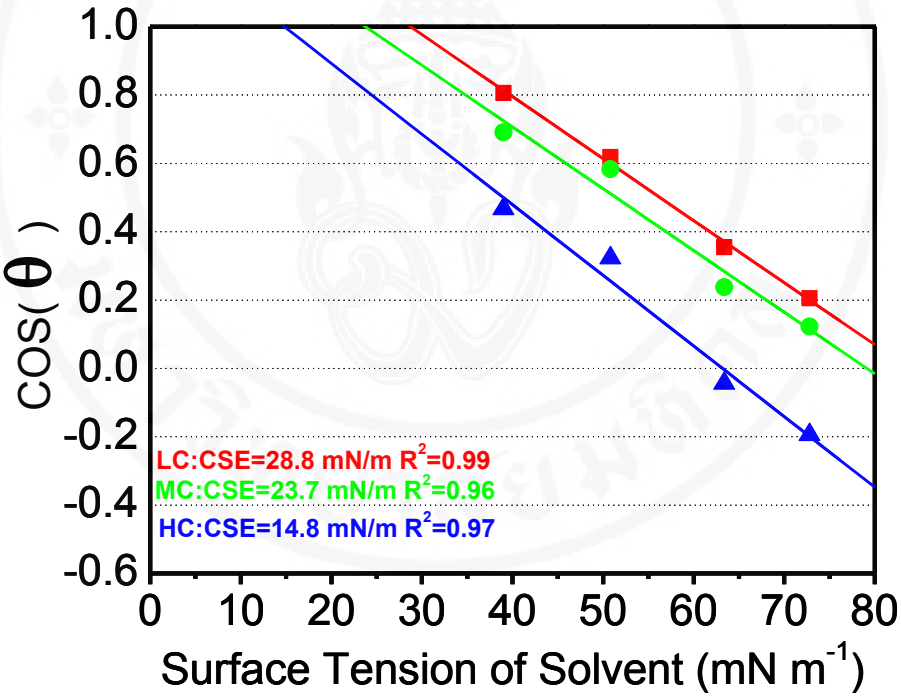

Figure 4.2 Critical surface energy of LC, MC, and HC.

4.3.3 Organoclay and pre-dispersed organoclay

X-ray diffractmetry was performed for the obtained MA-g-PP compatibilizer effect in order to follow intercalation process. The XRD patterns of organoclays, pre-dispersed organoclays, and nanocomposites with 2wt% of organoclay

Copyright by Mahidol University

loading are shown in figure 4.3.

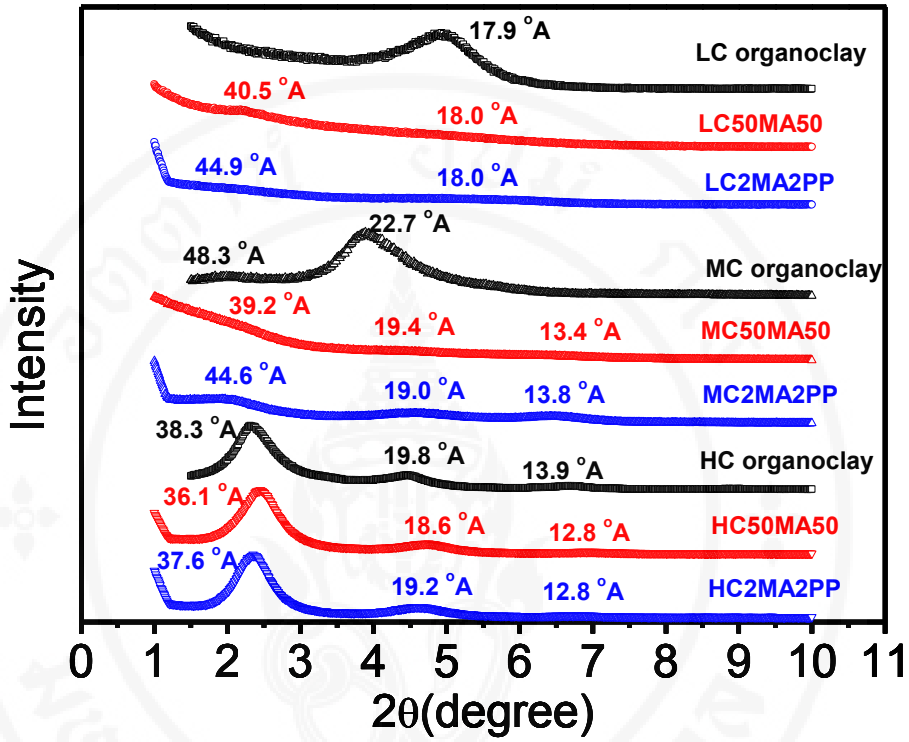

Figure 4.3 X-ray diffractgram of organoclays, pre-dispersed organclays and nanocomposites with 2wt% loading of organoclay loading.

LC showed a sharp interlayer spacing with the peak 4.93° (17.9A°) and was indexed as d_{001} [29, 57, 61]. When LC was compounded with MA-g-PP (LC50MA50), this peak turn into a shoulder at 2.18° (40.5A°, d_{001}) along with a broader peak at 4.92° (18.0A°, d_{002}). The shift of the peak to a lower angle is resulting from intercalation of MA-g-PP molecules into clay interlayer.

MC shows two peak at 1.83° (48.3A°) and a sharp peak at 3.89° (22.7A°). Both peaks were believed to come from two different arrangement of the surfactant in the interlayer due to a layer charge heterogeneity of clay [58]. As a result, two different packing of the organoclay were observed in this case including high surface

Copyright by Mahidol University

coverage and lower surface coverage. By mixing MC with PP-g-MA, MC50MA50 showed a shoulder at 2.12^{o} (41.7^{o}A), and two broad peaks at 4.18^{o} (21.1^{o}A) and 6.36^{o} (13.9^{o}A) corresponding to d_{001}, d_{002}, d_{003} planes, respectively. These peaks represent the higher surface coverage portion of the MC organoclay. The peak due to the lower surface coverage was disappeared due to the exfoliated structure. It was expected that intercalation/exfoliation was achieved in this case [49, 57]. There could be two reasons why the intercalation was achieved at LC and MC. The first reason was that the LC and MC did not have mismatch of surface energy against MA-g-PP based on the results from contact angle measurement. The second reason was that LC and MC had some space for intercalation of MA-g-PP [6].

HC showed a characteristic diffraction pattern, which consist of two sharp peaks at 2.31 ^{o} (38.3 A^{o}) and 4.47 ^{o} (19.8 A^{o}) and one broad peak at 6.7 ^{o} (13.2 A^{o}). They were indexed as d_{001}, d_{002}, and d_{003} planes. When HC was mixed with MA-g-PP, HC50MA50 showed a diffraction pattern with peaks at 2.45º (36.1A^{o}), 4.76º (18.6A^{o}) and 6.89º (12.8A^{o}). There was no difference in diffraction patterns between HC and HC-MA-g-PP, although each peak slightly shifts toward to higher angle values. This indicated that not only no intercalation of MA-g-PP molecules into interlayer of HC organoclay interlayer [57], but also a slight collapse of silicate layers occurred [59]. This could be caused by the degradation of surfactant in the processing or elimination of the interlayer molecules. As expected, HC with low CSE cause by high surface coverage did not indicated intercalation and exfoliation in HC50MA50. The mismatching of surface energy between MC and MA-g-PP does not allow MA-g-PP molecules of intercalating into interlayer [6].

Copyright by Mahidol University

4.3.4 Nanocomposites formation

Master batch were compounded with pure PP by the twin screw extruder before let down into PP clay nanocomposites at different organoclay composition. Figure 4.3 shows the X-ray diffractgram of LC2MA2PP, MC2MA2PP, and HC2MA2PP. A shoulder corresponding to the d_{001} plane on LC2MA2PP appeared at 1.97° (44.9A°), which was shifted to lower angle compared to that on LC50MA50. This could imply improvement of intercalation on LC by compounding with matrix polymer.

MC2MA2PP showed three broader peaks at 1.97° (44.9A°), 4.65 (19.0A°), and 6.41° (13.8A) which were indexed as d_{001}, d_{002}, and d_{003} due to the higher surface coverage portion of the organoclay. The first peak on MC2MA2PP was slightly shifted to lower angle compared to that on MC50MA50 and become a broader peak due to the disintegration of the organoclay stack. Compared to X-ray diffractgrams of nanocomposites with LC and MA-g-PP, broadness of peaks on composites with MC and MA-g-PP was more distinct, which implies particle size of MC in composites is larger than LC.

A diffraction pattern of HC2MA2PP had three peaks ranging from 2^o to 3^o, 4^o to 5^o, and 6.5^o to 7.5^o corresponding to the d_{001}, d_{002} and d_{003} plane, respectively. Each peak did not show any shifts in the position, which indicated that not only intercalation of PP molecule but also the size reduction of HC did not occur, although we can see a slight shift to lower angle at the peak for d_{001}. This could be caused by high coverage of surface surfactant on HC. It was considered that surface of organoclay was highly occupied with surfactant, so that intercalation of PP molecules is interfered [6].

Copyright by Mahidol University

Based on X-ray diffractogram of organoclays, pre-dispersed organoclay, and PP-clay nanocomposites, the possible structures/surface coverage of LC, MC, and HC can be assumed as shown in figure 4.4.

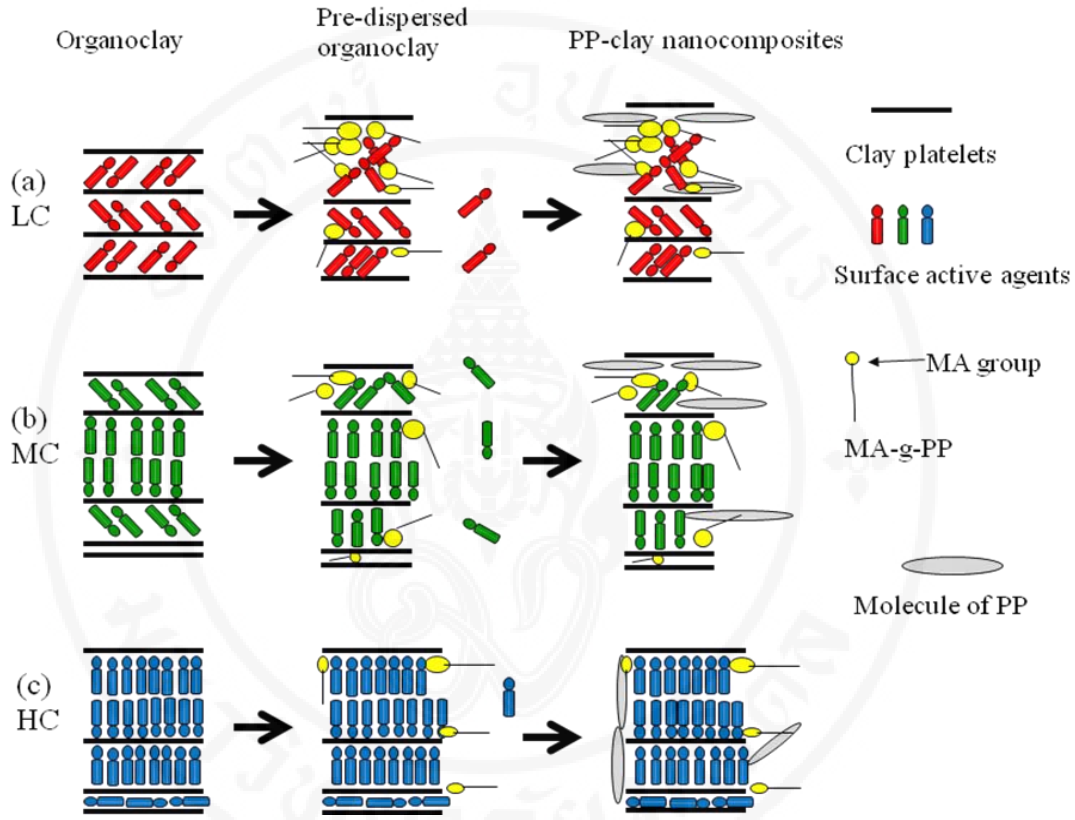

Figure 4.4 Possible structures/surface coverage of LC, MC, and HC.

It was expected that LC changed the structure in compounding PP-clay nanocomposites as shown in figure 4.4(a), because HC showed improved intercalation of MA-g-PP and PP. This was achieved by low surface coverage with homogeneity on LC surface. It was expected that MC changed the structure of clay in compounding PP-clay nanocomposites as shown in figure 4.4(b), because X-ray diffractogram of MC50MA50 and MC2MA2PP indicated three broad peaks for d_{001} d_{002}, and d_{003} plane, respectively. The surface coverage on MC consists of a mixture

Copyright by Mahidol University

of low and high surface coverage. It was expected that HC was highly-closed packed by surfactant molecules shown as figure 4.4(c), because of no intercalation of HC on the X-ray diffractgram. It was expected that HC had at least highly-closed packed mono and double layer, because X-ray diffractgrams of HC, HC50MA50, and HC2MA2PP indicated three sharp peaks for d_{001} d_{002}, and d_{003} plane, respectively.

4.3.5 Tensile test

Tensile testing of dumbbell-shaped specimens (Type-4) was carried out at 50 mm/min of an elongation rate. Tensile strength and elongation for composites and pure PP were illustrated in figure 4.5(a) and (b), respectively.

Tensile strength of pure PP and PP clay nanocomposites were shown in figure 4.5(a). Tensile strength of pure PP was 37.5 MPa. It has been reported that increase in clay content, less than 10wt%, contributes to improvement of tensile strength [61]. However, tensile strengths of PP clay nanocomposites gradually decreased with increasing organoclay loading. Tensile strengths of LC2MA2PP, LC5MA5PP, and LC10MA10PP were 36.46, 34.68, and 31.3 MPa respectively, which were higher than the other composites at every concentration of organoclay loading. It could be considered intercalation/exfoliation of LC was enhanced more than that of MC and HC.

Figure 4.5(b) depicts elongations of pure PP and PP clay nanocomposites. Elongation of pure PP was 7.08%. LC2MA2PP, LC5MA5PP, and LC10MA10PP showed 7.51, 7.36, and 3.67%, respectively. MC2MA2PP, MC5MA5PP, and MC10MA10PP showed 9.65, 6.65, and 3.48%, respectively. Composites with HC showed 7.40, 7.03, and 2.69% at 2, 5, and 10wt% content, respectively. It has been

Copyright by Mahidol University

reported that elongation decreases with increasing MA-g-PP content [61]. Only MC2MA2PP showed higher value of elongation than the other composites with 2wt% of organoclay loading. Elongation of composites with 2wt% of organclay exhibited the values in the range of error bar of HC2MA2PP, which indicated that there was not a considerable difference in exfoliation/intercalation among different degree of surface coverage on clay platelets.

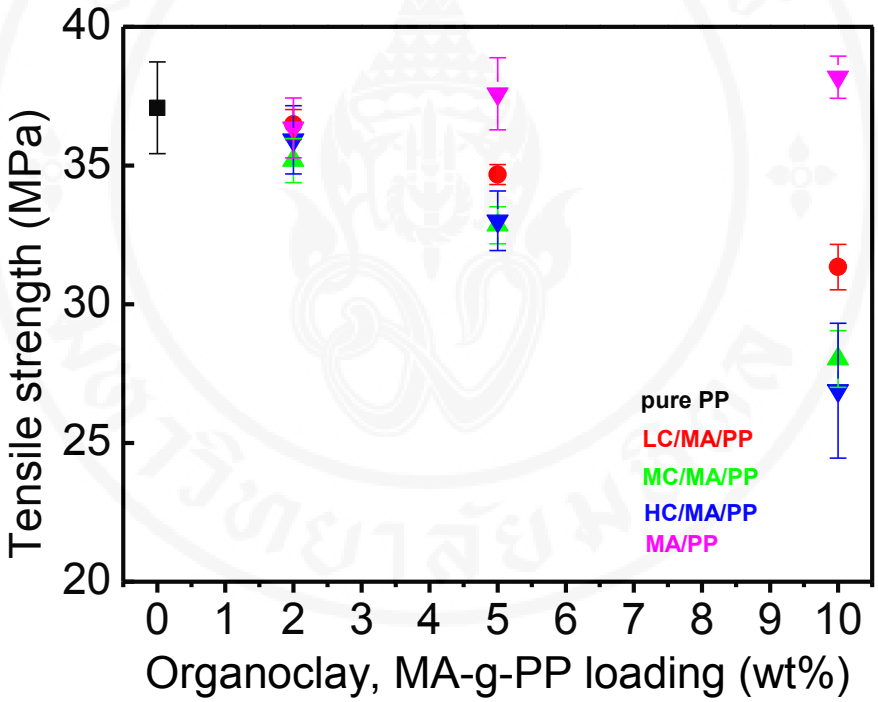

Figure 4.5(a) Tensile strength of polymer-clay nanocomposites and pure PP.

Copyright by Mahidol University

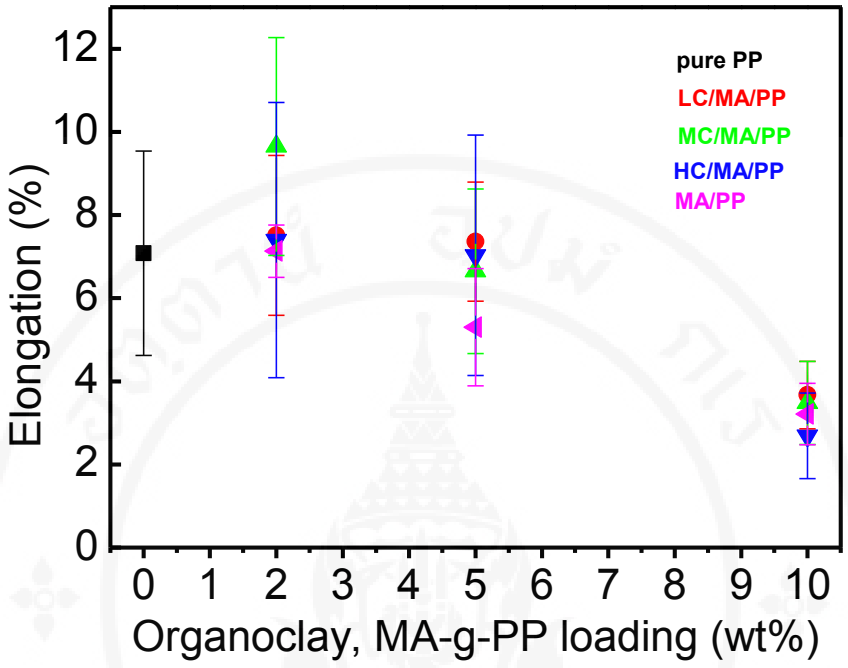

Figure 4.5(b) Elongation of polymer-clay nanocomposites and pure PP.

4.3.6 DSC (differential scanning calorimetry)

The influence of the different types of organoclay and MA-g-PP on melting and cooling behaviors was investigated by DSC. DSC provides the melting and crystallization temperature of pure PP, two-component MA-g-PP/PP composites, and PP clay nanocomposites [62].

Copyright by Mahidol University

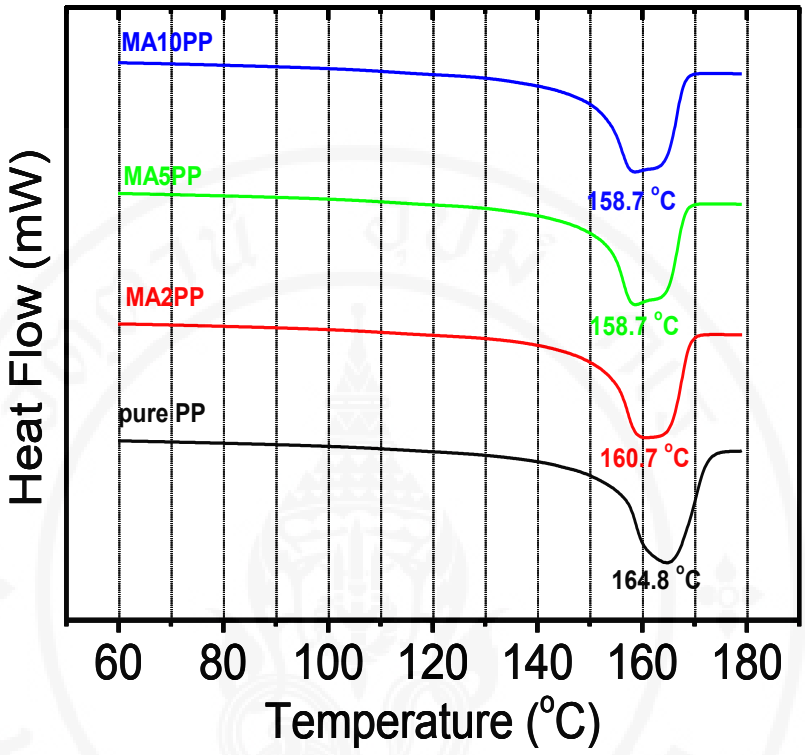

Figure 4.6(a) DSC curves of two-component composites in heating process.

DSC curves of MA2PP, MA5PP, and MA10PP in heating process were shown in figure 4.6(a). Melting peak temperature of pure PP was 164.8 °C. When the MA-g-PP was added, two-component MA-g-PP composites, melting temperature reduced to 160.7, 158.7, and 158.7 °C for MA2PP, MA5PP, and MA10PP, respectively. This behavior results from the presence of low-molecular weight MA-g-PP in the nancomposites. DSC curves for MA2PP, MA5PP, and MA10PP had single peaks, although each of them was broader than pure PP. This indicated that MA-g-PP and PP are molecular miscible. However, melting peak temperature of two-component composites slightly decreased as compared to pure PP owing to lower melting points of MA-g-PP,

Copyright by Mahidol University

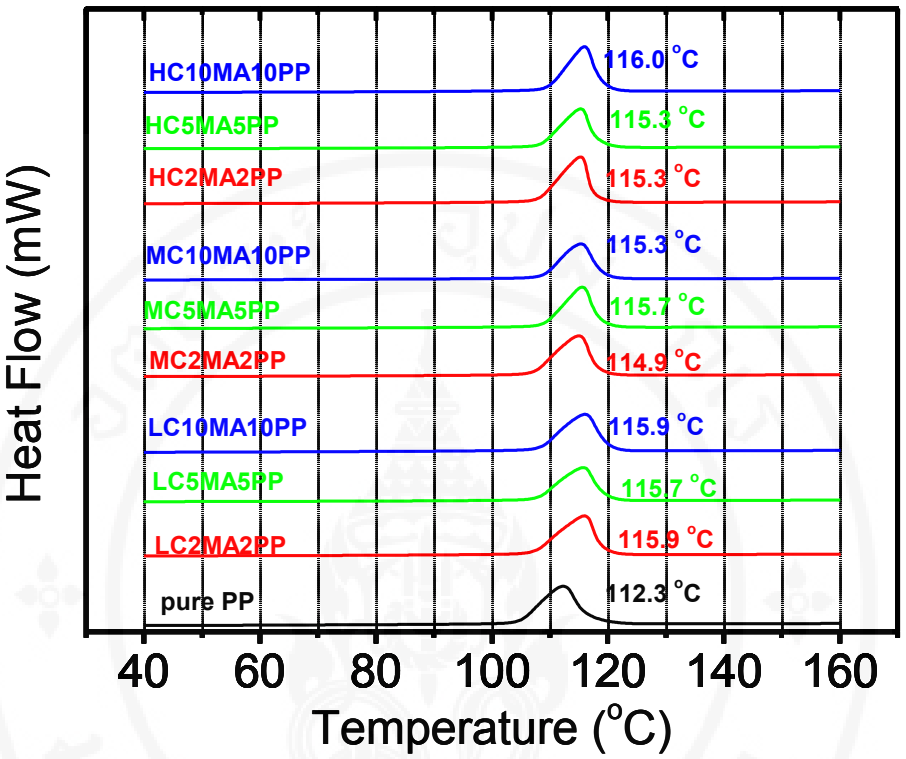

Figure 4.6(b) DSC curves of PP clay nanocomposites in cooling process.

DSC curves of PP clay composites in cooling process were illustrated in figure 4.6(b). All of the prepared PP-clay composites exhibited higher crystallization temperatures than pure PP. This implies that clay particles incorporated into polymer matrix play a role as effective nucleating agents for crystallization [63, 64]. It is reported that increase in amount of clay loading increase crystallization temperature [53]. It is well-known that small amount of well-dispersed organoclay can act as the effective nucleating agents to accelerate the crystallization of PP matrix [65]. No relationship between crystallization temperature with the amount of clay loading and the degree of surface coverage were found in this study.

Copyright by Mahidol University

The crystalinity of the PP matrix in PP-clay nanocomposites in the cooling

process on DSC curves was shown in figure 4.6(c). Pure PP showed 49.7% of crystallinity. By adding 2wt% of clay and MA-g-PP into matrix polymer, PP-clay nanocomposites (LC2MA2PP, MC2MA2PP, and HC2MA2PP) showed 50.1, 50.0, and 49.7%, respectively. With increasing clay and MA-g-PP content, crystallinity of PP-clay nanocomposites was slightly increased. No distinct relationship between crystallinity of the nanocomposite and the degree of surface coverage of organoclay was found. The same trend was reported in literature [6] that the partial exfoliation of organoclay increases the nucleation effect and accelerates the crystallization process while the confined PP segment in the organoclay interlayer in nanocomposites will be restricted.

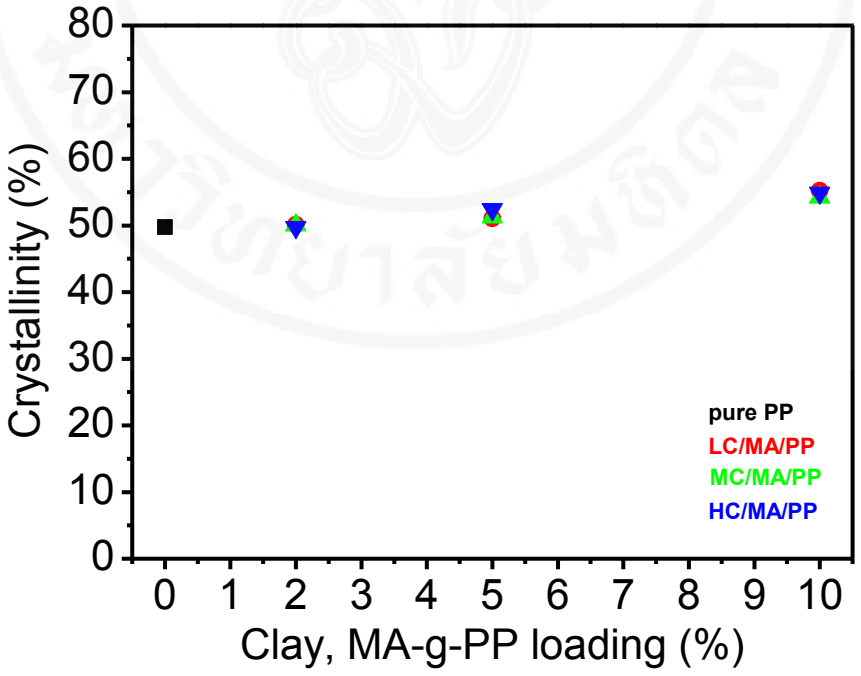

Figure 4.6 (c) Crystallinity of PP-clay nanocomposites.

Copyright by Mahidol University

4.3.7 SEM (scanning electron microscopy)

SEM micrigraphs taken from the etched surface of the PP composites are

shown in figure 4.7. The dark areas indicated matrix polymer, on the other hand, white areas depicted organoclay particles. Aggregations of organoclay particles were clearly visible on the surface for not only campsites with 5wt% organclay lading (HC5MA5PP (figure 4.7(a)), LC5MA5PP (figure 4.7(b)) and MC5MA5PP (figure 4.7(c)), but also 10wt% rganoclay loading (HC10MA10PP (figure 4.7(d)), LC10MA10PP (figure 4.7(e)) and MC10MA10PP (figure 4.7(f)). The length of most of the particles was ranging from 1.0 to 2.0μm. It is found that exfoliation of organoclay particles was obviously far from complete.

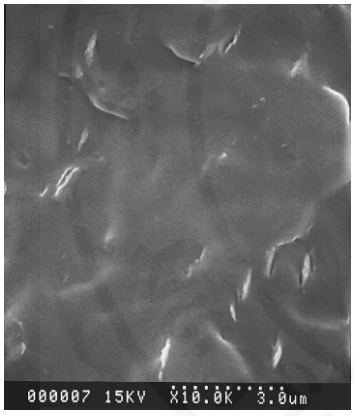

(a) LC5MA5PP

(b) MC5MA5PP

(c) HC5MA5PP

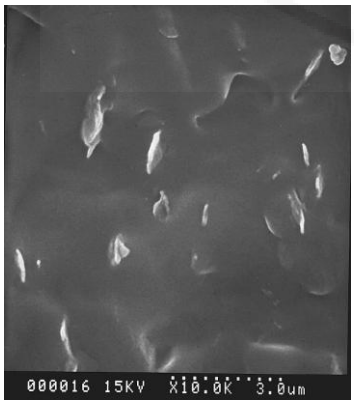

(d) LC10MA10PP

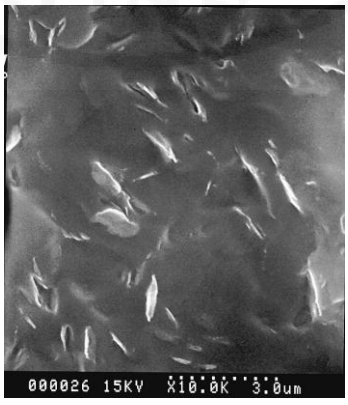

(e) MC10MA10PP

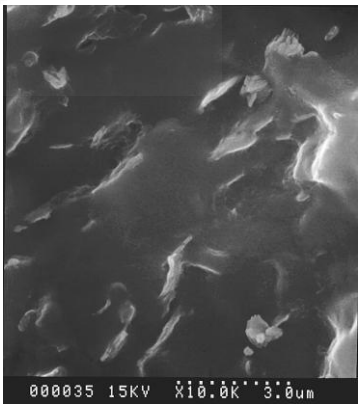

(f) HC10MA10PP

Figure 4.7 SEM micrgraphs of PP clay nanocomposites.

Copyright by Mahidol University

On SEM observation, fifteen particles at each specimen were chosen. Aspect ratio of the clay particles on specimens was calculated. Composites with

10wt% organoclay indicated the aspect ratio of 4.74, 4.75, and 3.60 for LC10MA10PP, MC10MA10PP, and HC10MA10PP, respectively. The high aspect ratio in LC10MA10PP and MC10MA510PP should be reflected in an enhanced gas barrier property. When organoclay loading was reduced to 5wt%, the aspect ratio of LC5MA5PP was increased to 6.17. One of major factors for increased aspect ratio of composites comprising LC can be delamination of clay particles, because the width of LC reduced to 2.83. It was found aspect ratio of MC and HC did not increase because that the reduction of width of MC and HC is smaller than that of LC.

4.3.8 Gas barrier property

Figure 4.8 shows the relative oxygen permeability of PP nanocomposites (LC10MA10PP, MC10MA10PP, and HC10MA10PP). The relative oxygen permeability is the ratio of the oxygen permeation coefficient of nanocomposites to that of pure PP. It is well-known that the gas barrier property depends on the aspect ratio of clay particles [66]. As expected form the calculated aspect ratio of HC particle in SEM, HC10MA10PP film did not show a drastic reduction compared to pure PP, which was about 2 % of reduction. This indicated that gas barrier property for oxygen was not improved in the presence of HC organoclay. LC10MA10PP and MC10MA10PP indicated a reduction in the gas permeation about 12 and 20 %, respectively. It was mentioned in the SEM observation on nanocomposites with 10wt% organoclay loading that the aspect ratios of LC and MC were larger than that of HC. The aspect ratio of MC was slightly larger than that of LC. These results were consistent to the result of relative oxygen permeability of LC10MA10PP and MC10MA10PP.

Copyright by Mahidol University

It is reported that 7 wt% of clay loading leads to 40% reduction of oxygen permeation coefficient [67]. This reduction is almost two times as same as that of MC10MA10PP. This difference in reduction of relative oxygen permeability may be because of aspect ratio of clay particles.

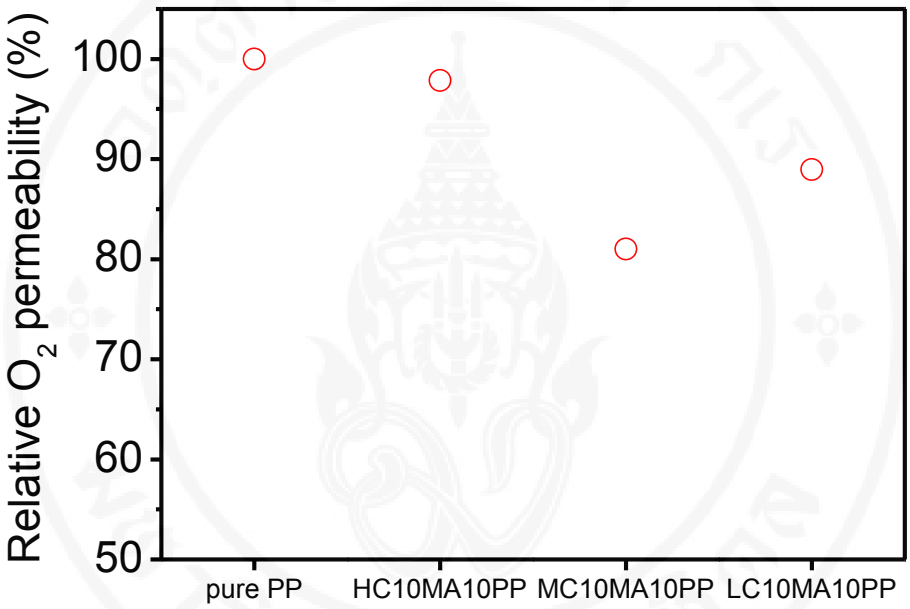

Figure 4.8 Relative oxygen permeability of nanocomposites with 10 wt% of organoclay loading.

4.4 Conclusion

Organoclays with different degree (low, medium, and high) of surface coverage were used in formation of PP-clay nanocomposites twin screw extruder. LC which indicated about 71.3wt% of the residual weight had 35.45 and 28.79 $mN \cdot m^{-1}$ of total surface energy and critical surface tension, respectively. High intercalation on HC was observed in LC50MA50 and LC2MA2PP, although total

Copyright by Mahidol University

surface energy and critical surface tension of LC were higher than those of MC and HC, respectively. It was found that nanocomposites with LC did not show drastic reduction of tensile strength on tensile test, which were comparable to those with MC and HC. LC played a role of nucleating agents for crystallization, but crystallinity was not influenced by organoclay surface coverage but amount of organoclay loading. LC particles which were high aspect ratio observed in PP-clay nanocomposites, which resulted in 88% of relative oxygen permeability at LC10MA10PP. MC shows about 71.7wt% of residual weight and possess 30.15 and 23.78 $mN \cdot m^{-1}$ for the total surface energy and critical surface tension, respectively. It was found that the surface coverage on MC was heterogeneity from MC50MA50 and MC2MA2PP. Nanocomposites with MC indicated similar reduction in tensile strength as those with LC. MC particles had high aspect ratio which indicated 80% of relative oxygen permeability at MC10MA10PP. HC indicated about 49.7wt% of the surfactant content, which resulted in 20.0 and 14.80 $mN \cdot m^{-1}$ of total surface energy and critical surface tension, respectively. HC showed no intercalation of MA-g-PP and PP molecules, which resulted in lowest aspect ratio of the three organoclays. Relative oxygen permeability at HC10MA10PP was almost same as pure PP, which was 98%.

Copyright by Mahidol University

CHAPTER V
HIGH-DENSITY POLYETHYLENE (HDPE) CLAY NANOCOMPOSITES FORMATION BY TWIN SCREW EXTRUDER

5.1 Introduction

HDPE is one of the most widely used thermoplastic in both pure form and as the composites. The inorganic fillers such as CaCO3 [68, 69], mica [69], and clay minerals [1, 8, 62, 70, 71] have long been used in the HDPE to reduce cost and/or improve the mechanical property. HDPE-clay minerals has drawn a lot of attention as the new type of nanocomposites where the clay platelets have high aspect ratio can produce unique synergetic properties such as mechanical, flame retardant and barrier properties. These unique properties arise when the clay platelet is highly dispersed in the polymeric matrix; however, the dispersing of the clay particles in nanoscale is difficult to achieve due to nature of the clay and the HDPE. The clay is hydrophilic while polymer matrix is hydrophobic. Proper dispersing of the organoclay is very important for the preparation polymer-clay nanocomposites. The combination of clay surface modification and proper processing technique was the key for the preparation of polymer-clay nanocomposites [72]. The clay surface modification is often done by treating the clay with surface active agents (surfactant), alkyl ammonium salt, to form an organoclay It was reported that a choice of surface coverage of clay particle, low, medium or high coverage, is very important in the

Copyright by Mahidol University

treatment with surfactant [1, 71]. The clay particles with proper surface coverage of cationic surfactant can be dispersed in matrix polymer [73] and improve the properties such as mechanical properties, gas barrier properties, and flame retardancy.

It is also reported that compatibilizers, such as maleic anhydride modifies polyolefins, or oxidized low molecular weight polyolefin, can be used as a compatibilizer to promote the dispersion of the organoclay in polymeric matrix [8], especially for most of the low polarity polymer. Many types of compatibilizer, including low molecular weight polymer with some polar group on the structure, were used in order to promote intercalation and exfoliation of organoclay particles in the polymeric matrix [7].

The objective of this study is to investigate effects of organoclay surface coverage with low (LC), medium (MC) and high surface coverage (HC) for the preparation of HDPE-clay nanocomposites through the master batch process with oxidized polyethylene (Owax) wax as a compatibilizer. The oxidized polyethylene wax was used in order to promote intercalation into clay intergallery. The organoclay is the grade used in the paint industry which is being marketed at the lower cost. The cost control is one of the most essential factors for economically producing a large quantity of HDPE-clay nanocomposites.

5.2 Experiments

Copyright by Mahidol University

5.2.1 Materials

Three different types of organoclay were investigated, which were hectorite

treated with trialkylaryl ammonium (commercial name: Bentone 27, referred to as LC from low surface coverage), bentonite treated with tetra-alkyl ammonium (commercial name: Bengel 434, referred to as MC from medium surface coverage), and organic derivative of montmorillonite clay (commercial name: Bentone SD-1, referred to as HC from high surface coverage). All the organoclays were manufactured by Elementis Specialties Inc and were used without any further purification. Oxidized polyethylene wax with acid number of 25mgKOH/g (available under the commercial name EO-42, referred to as OWax) were obtained from Q-compound Co., Ltd (Nonthaburi, Thailand), which was used as co-intercalants. High density polyethylene, HDPE (Thai-Zex 7000F, produced by Bangkok Polyethylene Company Limited, MFI: 0.04g/10g), was used as the matrix polymer.

5.2.2 Formation of pre-dispersed organoclay

Pre-dispersed organoclays were prepared by mixing OWax and organoclay at weight ratio of 1:1. Compounding was carried out using a co-rotating twin screw extruder (produced by En Mach Co., Ltd in Thailand L/D=40:1). The process temperature was set at 50°C in the 1st zone and at 140 °C from 2nd to 9th zone in the barrel of the extruder with the screw speed of 180 rpm. The extrusion was quenched with water and dried for more than 24 hours before further processing. Pre-dispersed organoclay composed of 50wt% of organclay and 50wt% of OWax, which was referred to as LC50-OWax50, MC50-OWax50, and HC50-OWax50. The first two letters indicate the type of organoclay used which are low, medium and high surface coverage. The next number represents the amount of the organoclay in the composition. The type of the compatibizer was indicated by next letters which

Copyright by Mahidol University

include Owax and Wax. The last number indicates that amount of the compatibilizer in the total composition.

5.2.3 Formation of HDPE-clay nanocomposites

The master batch having 20wt% of organoclay was prepared by adding pure HDPE into the pre-dispersed organoclay. The preparation was conducted by using a co-rotating twin screw extruder (produced by En Mach Co., Ltd in Thailand L/D=40:1). The processing temperature was set at 100 ^{o}C in the 1st zone and at 230 ^{o}C from the 2nd to 9th zone in the barrel of extruder with the screw speed of 600 rpm. In this paper, master batch having 20wt% of LC was described as LC20-OWax20NC.

Table 5.1 Formulation of the prepared nanocomposites.

	Organoclay			**OWax**	**HDPE**
	LC (wt%)	**MC (wt%)**	**HC (wt%)**	**(wt%)**	**(wt%)**
LC2-OWax2NC	2	-	-	2	96
LC5-OWax5NC	5	-	-	5	90
LC10-OWax10NC	10	-	-	10	80
MC2-OWax2NC	-	2	-	2	96
MC5-OWax5NC	-	5	-	5	90
MC10-OWax10NC	-	10	-	10	80
MC2-OWax2NC	-	-	2	2	96
MC5-OWax5NC	-	-	5	5	90
MC10-OWax10NC	-	-	10	10	80
OWax2-HDPE98	-	-	-	2	98
OWax5-HDPE95	-	-	-	5	95
OWax10-HDPE90	-	-	-	10	90
Pure HDPE	-	-	-	-	100

Copyright by Mahidol University

Polymer clay nancomposites with 2, 5, and 10wt% of organoclay was

compounded by adding pure HDPE into master batch. The process temperature was set at 100°C in the 1st zone and at 230 °C from 2nd to 9th zone in the barrel of the extruder with the screw speed of 600 rpm. In this paper, polymer clay nanocomposites having 2wt% of organoclay was described as LC2-Owax2NC.

Two-component nanocomposites were prepared by directly mixing HDPE with OWax as references. The process temperature was set at 100°C in the 1st zone and at 230 °C from 2nd to 9th zone in the barrel of the extruder with the screw speed of 600 rpm. In this paper, two-component composite with 2wt% of OWax was described as OWax2-HDPE98. All formulation prepared were described in Table 5.1.

5.2.4 X-ray diffractometry (XRD)

The measurement was carried out by using D8 XRD (Bruker-aus Co., Ltd., Germany) using CuKα radiation with the voltage of 40 kV and current of 30 mA. The samples were scanned by using the step scanning at 0.01º/step and integration time of 10sec/step. Pre-dispersed organoclays were grounded with mortal. HDPE-clay nanocomposites were compression-molded into the shape of a disc with 25 mm diameter.

5.2.5 Tensile test

Tensile test of the HDPE-clay nanocomposites and pure HDPE was carried out by using the Series IX Automated Materials Testing System (INSTRON Corporation) with 50cm/min of crosshead speed according to ASTM D638. HDPE-clay nanocomposites were compressed by using a hydraulic pressing (K. V. S Engineering Co., LTD. Patumwan, Thailand) prior to die-cutting into the shape of

Copyright by Mahidol University

type-4. Tensile strength and elongation were calculated for five specimens at each condition.

5.2.6 Differential scanning calorimetry (DSC)

The crystallization behavior of composites and matrix polymer was studied with a differential scanning calorimeter (METTLER TOLED) under flowing nitrogen atmosphere. In order to remove the influence of the previous thermal history, 12+/-1.0 mg samples were initially heated from 20 ^{o}C to 180 ^{o}C at 10 ^{o}C/min, held at that temperature for 5min, and then cooled to 25 ^{o}C at 10 ^{o}C/min. They were kept for 5 min, heated again to 180 ^{o}C at 10 ^{o}C/min, and cooled to 20 ^{o}C at the same rate.

The crystalinity of the PP matrix in PP-clay nanocomposites was determined by the following equation in the cooling proess.

$$\chi = (\Delta H_m \times 100) / (f_p \times \Delta H^{o}_f) \quad (\%) \qquad (4)$$

where ΔH_m ($J \cdot g^{-1}$) is the enthalpy of melting of the polymer matrix, f_p is the HDPE weight fraction in the nanocomposites and ΔH^{o}_f is the enthalpy of melting of pure crystalline HDPE ($293.1 J \cdot g^{-1}$) [24].

5.2.7 Scanning electron microscopy (SEM)

The particle morphologies of HDPE-clay nanocomposites were observed by scanning electron microscopy (SEM) (HITACH SEM S-2500) with an operation voltage of 15kV. Fractured surface for observation was created by breaking a notched specimen quenched with liquid nitrogen. The specimens were etched by a solution of 0.7 wt% $KMnO_4$ in a 2:1 mixture of H_2SO_4 and H_3PO_4 (85 %) for certain time, then washed by 30 % H_2O_2 aqueous solution and distilled water and dried in the

Copyright by Mahidol University

air.

5.3 Results and discussion

5.3.1X-ray diffractometry (XRD)

5.3.1.1 Formation of pre-dispersed organoclay

The organoclay used in this study is commercially avialable organoclay which are marketed for the paint industry. They are marketed at a lower price than the polymer-clay nanocompposite grade. The structural information regarding the organoclay is limited; therefore, the nature of the orgnaoclay was first investigated. The d-spacing of organoclay particles was obtained using Bragg's equation. Diffractgrams of HC, MC, LC, and pre-dispersed organoclays are illustrated in figure 5.1.

Copyright by Mahidol University

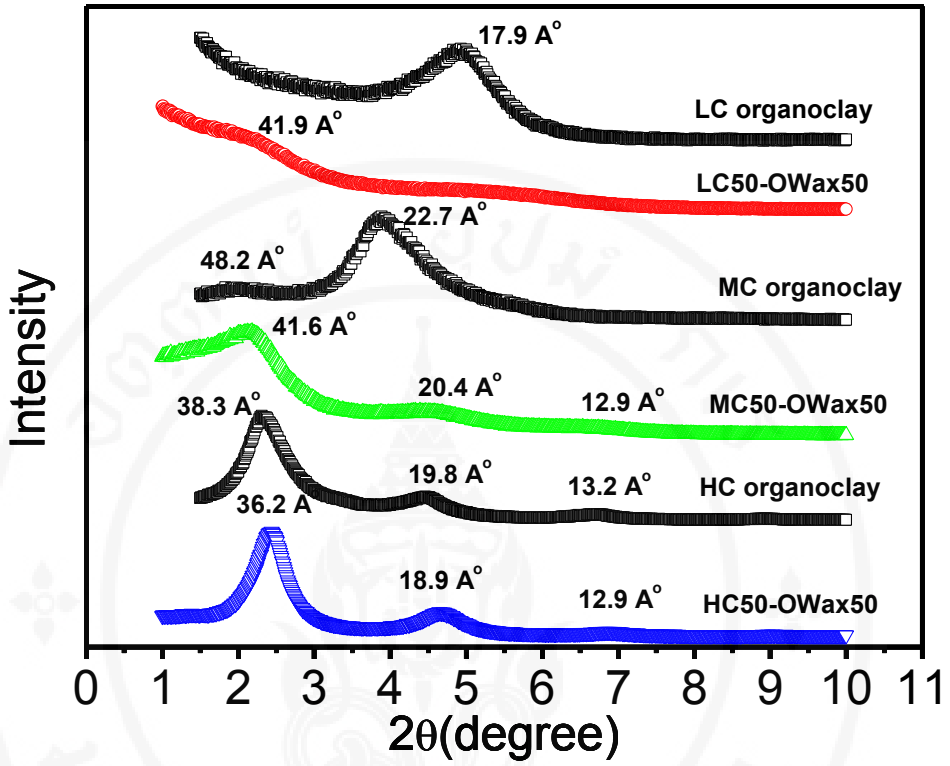

Figure 5.1 X-ray diffractgram of LC, MC, and HC and pre-dispersed organoclay.

HC showed a sharp peak, 2.31° (38.3A°), and two broad peaks, 4.47° (19.8 A°) and 6.7° (13.2 A°). Those peaks corresponded to d_{001}, d_{002}, and d_{003} plane of organoclay. When HC was mixed with OWax, referred to as HC50-OWax50 showed one sharp peak at 2.44° (36.2 A°) and two broad peaks at 4.68° (18.9 A°) and 6.87° (12.9 A°), respectively. No peak shifts to lower angle observed [64], except the boardening of d_{002} and d_{003}. This indicates that no intercalation occurs in the HC50-OWax50, although particle size of HC attributed to high-ordered peaks may become smaller. The peak for d_{001} plane slightly shifted to higher angle, which indicated the collapse of the interelayer due to the thermal degradation induced during the processing [67, 73].

LC shows a sharp peak at 4.93° (17.9 A°). When LC was compounded

Copyright by Mahidol University

with OWax in the extruder, referred to as LC50-OWax50, it showed a broad peak between 4º and 7º along with a shoulder (41.9 A^o) between 2º and 3º. This indicated LC mainly consisted of two types of clay structure. The shoulder between 2º and 3º results from improved intercalation of OWax molecules into LC interlayer. The broad peak between 4º and 7º indicated small LC particles with smaller d-spacing (a majority of d-spacing is about 18 A^o). It was expected that exfoliation did not occur. This may be achieved by synergetic effects between LC organoclay platelets with low surface coverage and OWax molecules with a polarity originated from hydroxyl functional groups such as -COOH or –OH.

MC showed a broad peak at 1.83^o (48.2 A^o) and a sharp peak at 3.89^o (22.7 A^o). Both peaks were indexed as the d001 from two different packing types in the clay interlayer. This may be originated from the layer charge heterogeneity of the clay. The larger d-spacing is exceeding the length of the alkyl ammonium molecule in the interlayer [65] and is believed to be originated from the bilayer packing of the interlayer surfactant. The shorter d-spacing is originated from the lower surface coverage orgnoclay portion that presences in the structure. When MC was mixed with OWax in the twin screw extruder, referred to as MC50-OWax50, the masterbatch of MC organoclay shows a sharp peak at 2.12º (41.6 A^o) and other two broad peaks at 4.33^o and 6.85^o (20.4 A^o, and 12.9 A^o). According to the positions at 2θ, the first, second, and third order peaks indicated d_{001}, d_{002}, and d_{003} plane, respectively. This is believed to be the phase with the high surface coverage where the Owax cannot wet on the surface. The Owax is only wet or intercalate into the lower surface coverage phase, 3.89 º.

Copyright by Mahidol University

5.3.1.2 Nanocomposites formation:

Pre-dispersed organoclays, LC50-OWax50, MC50-OWax50, and HC50-OWax50, were further compounded with HDPE in order to master batches, LC20-OWax20NC, MC20-OWax20NC, and HC20-OWax20NC, respectively. The organoclay content of each master batch was diluted by mixing with HDPE in order to form HDPE–clay nanocomposites.

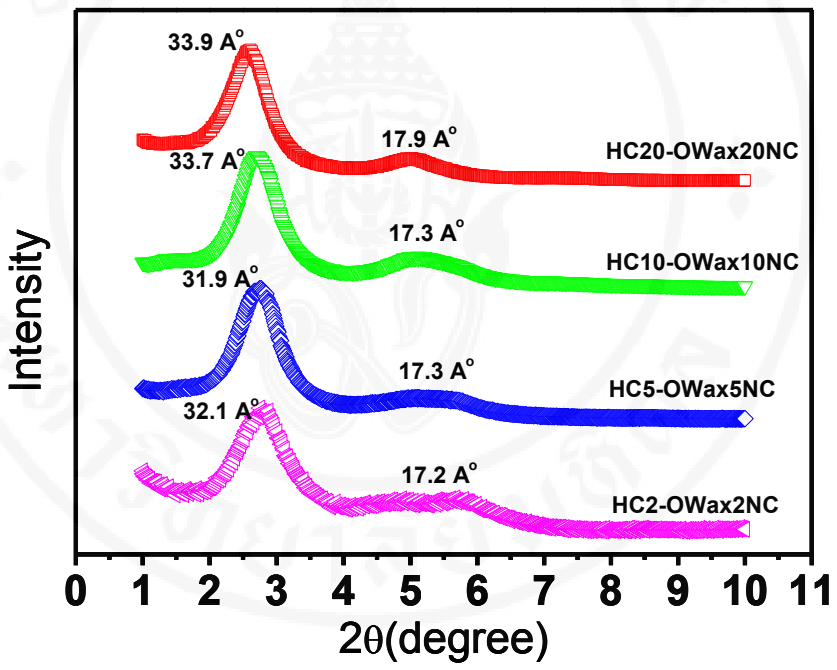

Figure 5.2 X-ray diffractograms of nanocomposites with HC.

Diffractograms of HC20-OWax20NC and nanocomposites compounded with HC are shown in figure 5.2. It was considered that the d_{001} planes were also collapsed where the observed peek was slightly shifted to the higher angle. This indicated that HC was not been intercalated by neither OWax nor HDPE molecules, therefore layered structure of HC in HC20-OWax20NC was no difference from that of as-received HC. The slight collapse of interlayer gallery occurred at each

Copyright by Mahidol University

concentration of HC in composites, this is believed to be due to the degradation of the surfactatn in the interlayer. The second order peaks of NC-OWax-HC became broader than those of HC20-OWax20NC、which implies the size of organoclay stack may get smaller induced by shear force during the processing. Neither intercalation nor exfoliation was observed with HC [6].

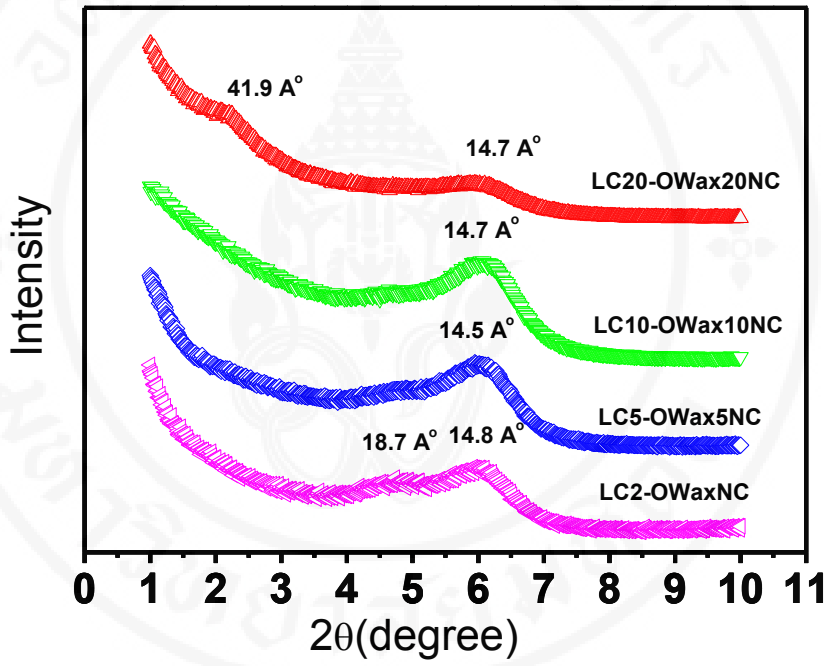

Figure 5.3 X-ray diffractogram of nanoposites with LC.

Diffractgrams of LC20-OWax20NC and nanocomposites compounded with LC are illustrated in figure 5.3. Formation of LC20-OWax20NC showed a slight shoulder (41.9 A^o) between 2^o and 3^o and a broad peak at 6.02^o (14.7 A^o), which was quite similar to as-received LC. This indicated that intercalation into LC was not improved compared to diffractgram of LC50-OWax50 in figure 1.

Copyright by Mahidol University

The first order peak (shoulder) completely disappeared on not only LC2-OWax2NC, but also LC5-OWax5NC and LC10-OWax10NC. This resulted

from the delamination of clay particles with large d-spacing corresponding to the first peak in compounding nanocomposites. It was observed that the third order peaks at 5.96° (14.7 A°) and 6.08° (14.5 A°) remained on LC10-OWax10NC and LC5-OWax5NC, respectively. It could be expected that LC platelets with smaller size were stacked with smaller gallery spacing. However, there still existed the both of second and third order peaks at 4.69° (18.7 A°) and 6.28° (14.8 A°) on LC2-OWax2NC. LC particles with a gallery spacing of 14.8 A° was delaminated and some of the platelets were intercalated. It was not apparently observed the second peaks on LC10-OWax10NC and LC5-OWax5NC, because of higher shear force from volume effect of HDPE.

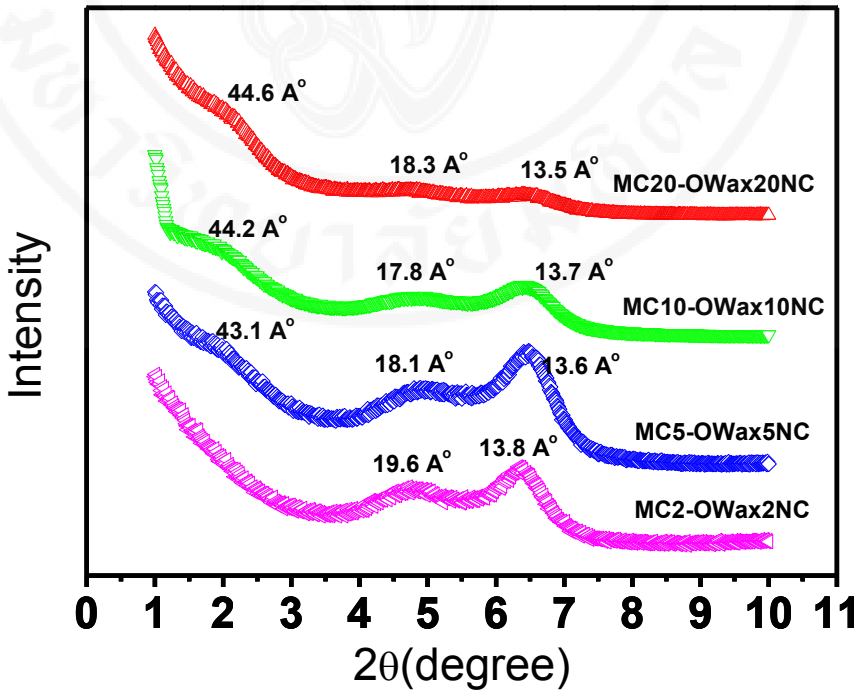

Figure 5.4 X-ray diffractogram of nanocomposites with MC.

Copyright by Mahidol University

Diffractograms of MC20-OWax20NC and nanocomposites made with MC are depicted in figure 5.4. The shoulder at the first order peak at 1.98^{o} (44.6 A^{o}) in MC20-OWax20NC did not disappear completely in MC5-OWax5NC and MC10-OWax10NC. This indicated that delamination of clay platelets on MC5-OWax5NC and MC10-OWax10NC was not improved compared to MC20-OWax20NC. However, formation of MC2-OWax2NC makes the first order peak disappeared, which implies that the d_{001} plane was delaminated. Both of the second and third order peaks at 4.49^{o} (19.6 A^{o}) and 6.41^{o} (13.8 A^{o}) still remained on MC2-OWax2NC. MC5-OWax5NC showed the second and third order peaks at 4.89^{o} (18.1 A^{o}) and 6.48 ^{o} (13.6 A^{o}) respectively. The second and third peak of MC2-OWax2NC and MC5-OWax5NC were more prominent than those of MC10-OWax10NC, which implied there existed smaller gallery spacing and larger organoclay particles on LC5-OWax5NC and LC5-OWax5NC compared to MC10-OWax10NC. It could be also assumed that breakdown and delamination were enhanced by higher viscosity from volume effect of HDPE.

Based on X-ray diffractogram of organoclays, pre-dispersed organoclay, and HDPE-clay nanocomposites, the possible structures/surface coverage of LC, MC, and HC can be assumed as shown in figure 5.5.

It was expected that LC changed the structure in compounding HDPE-clay nanocomposites as shown in figure 5.5(a), because HC showed improved intercalation of OWax. This was achieved by low surface coverage with homogeneity on LC surface. The first order peak (shoulder) completely disappeared on LC2-OWax2NC, LC5-OWax5NC, and LC10-OWax10NC. This may be dur to the delamination of organoclay platelets. It was expected that MC changed the structure of clay in

Copyright by Mahidol University

compounding HDPE-clay nanocomposites as shown in figure 5.5(b), because X-ray diffractogram of MC50-OWax50 indicated three broad peaks for d_{001} d_{002}, and d_{003} plane, respectively. This result gave us assumption that surface coverage on MC composed of a complex of low and high surface coverage. By compounding with HDPE, MC10-OWax10NC showed the first order peak as the shoulder. This indicated a slight intercalation of HDPE into d_{001} plane. It was expected that HC was highly-closed packed by surfactant molecules shown as figure 5.5(c), because of no intercalation of HC on the X-ray diffractgram.

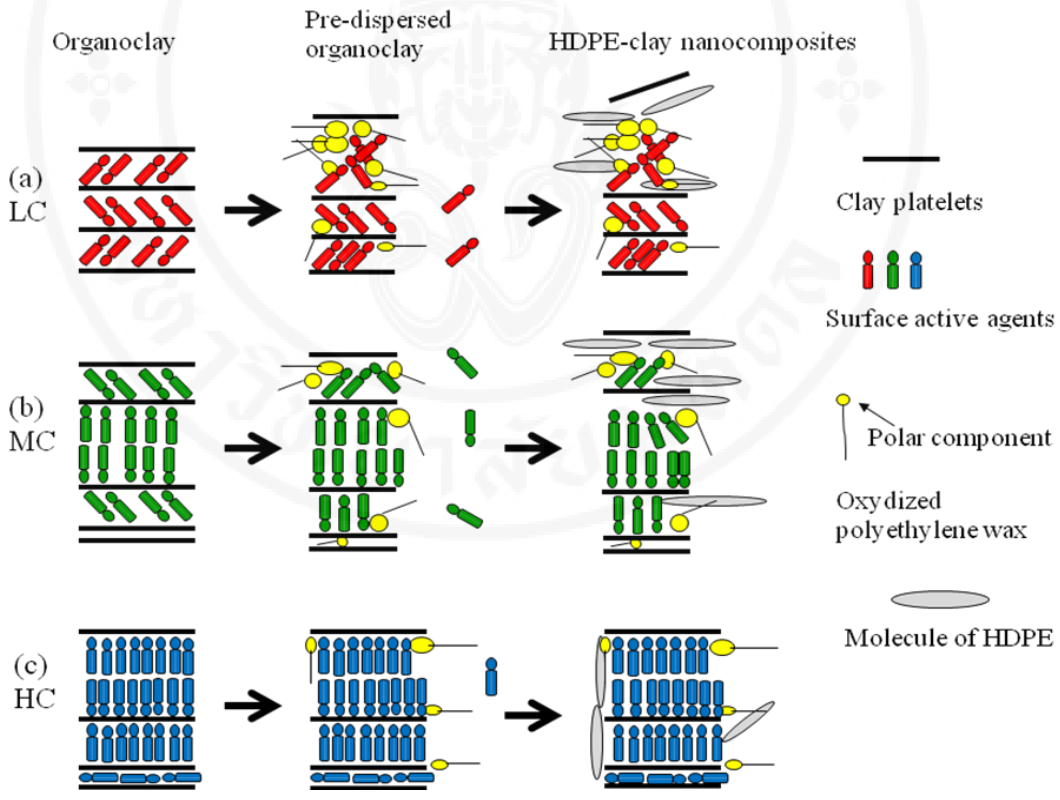

Figure 5.5 Possible structures/surface coverage of LC, MC, and HC.

Copyright by Mahidol University

5.3.2 Differential Scanning Calorimetry (DSC)

The influence of the different types of organoclay and OWax on melting

and cooling process was investigated by DSC. Melting and crystallization temperature can be obtained on heating and cooling proress, respectively.

DSC curves on melting process of two-component OWax-HDPE composites are depicted in figure 5.6. The melting peak temperature of HDPE100 indicated 130.9 ^{o}C. The melting peak temperature on OWax2-HDPE98, OWax5-HDPE95, and OWax10-HDPE90 indicated 129.2, 129.4, and 129.4 ^{o}C, respectively. The peak temperatures were slightly decreased by incorporation of OWax, but single peaks were observed. This indicated OWax and HDPE were molecularly mixed.

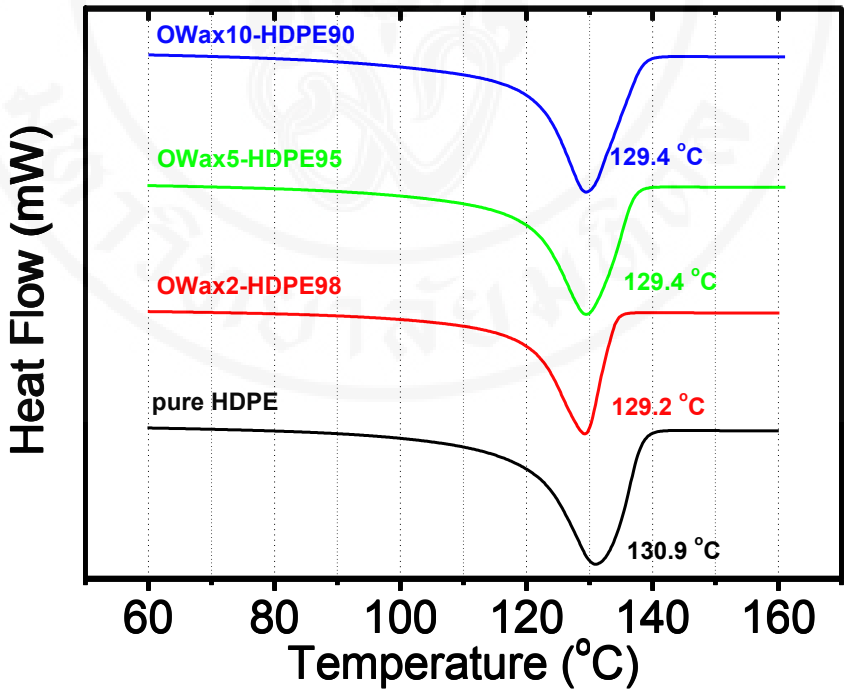

Figure 5.6 DSC curves of melting process on two-component OWax-HDPE composites.

Copyright by Mahidol University

DSC curves on cooling process on HDPE clay nanocomposites were

illustrated in figure 5.7. The crystallization peak temperature of pure HDPE was 116.2 ^{o}C. The crystallization peak temperatures were increased by adding organoclay LC, MC, and HC. This implies that organoclay platelets (particles) play a role of as the nucleating agents. It is reported that increase in amount of clay loading increase crystallization temperature [53]. It was reported that presence of small amount of well-dispersed organoclay can act the effective nucleating agents to accelerate the crystallization of HDPE matrix [65]. It could not be seen that crystallization temperature depends on amount clay loading and the degree of surface coverage on clay surface.

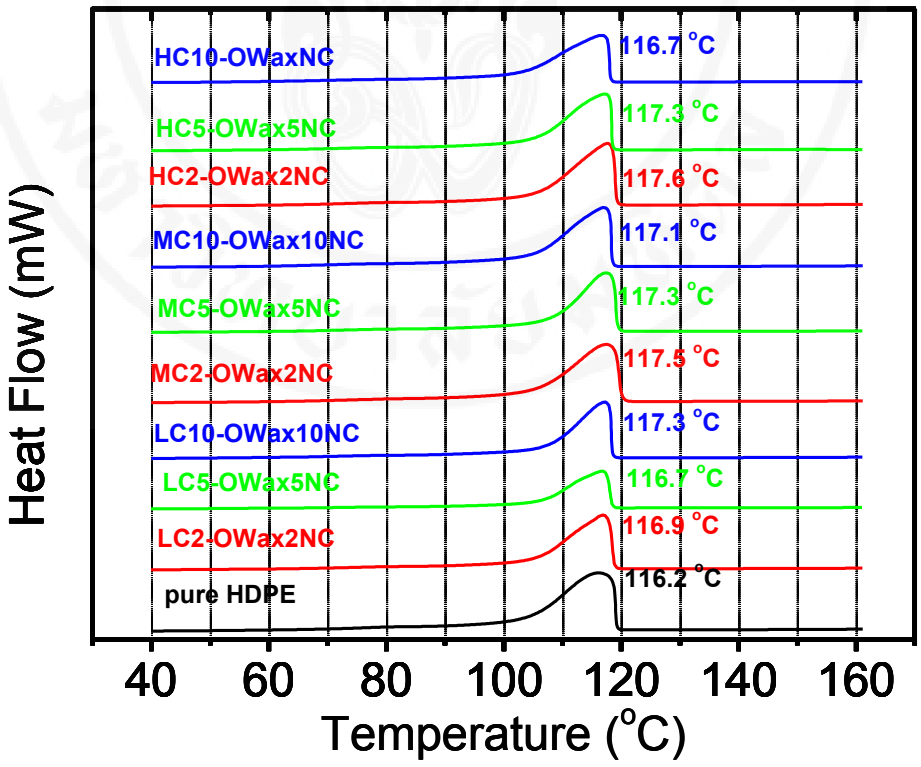

Figure 5.7 DSC curves of cooling process on HDPE clay nanocomposites.

Copyright by Mahidol University

The crystalinity of the HDPE matrix in HDPE-clay nanocomposites in the

cooling process on DSC curves was is shown in figure 5.8. Pure HDPE indicated 69.2% of crystallinity. By adding 2wt% of clay and OWax into matrix polymer, crystallinity of HDPE-clay nanocomposites was 62.0, 69.7, and 68.8% for LC2-OWax2NC, MC2-OWax2NC, and HC2-OWax2NC, respectively. Crystallinity of LC2-OWax2NC is smaller than the others, but it can not be seen that crystallinity depends on surface coverage on clay platelets. With increasing clay and OWax content, crystallinity of HDPE-clay nanocomposites was gradually increased. At 10wt% of organoclay and OWax, all of HDPE-clay nanocomposites indicated the similar amount of crystallinity, 73.2, 74.0, and 73.3% for LC10-OWax10NC, MC10-OWax10NC, and HC10-OWax10NC, respectively. The observed crystallinity of the HDPE matrix does not show any dependence on the degree of surface coverage of organoclay through all of the prepared HDPE-clay nanocomposites. The same trend was reported in the literature [6] wh the partial exfoliation of organoclay increases the nucleation effect and accelerates the crystallization process. The confined PP segment in the organoclay interlayer in nanocomposites will be restricted.

Copyright by Mahidol University

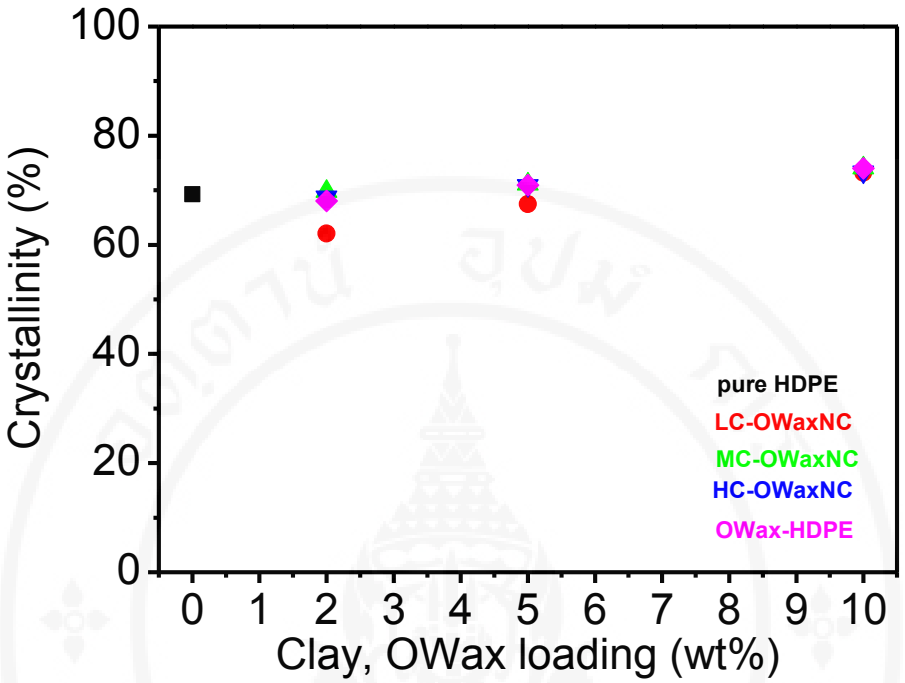

Figure 5.8 Crystallinity of HDPE-clay nanocomposites.

5.3.3 Tensile test

Tensile testing of dumbbell-shaped specimens (Type-4) was carried out at an elongation late 50 mm/min. The tensile strength of composites, pure HDPE, and references were shown in figure 5.9. Tensile strength of HDPE was 28.86 MPa. Two-component OWax-HDPE composites decreased with increasing amount of OWax, and OWax10-HDPE90 indicated 25.21MPa, which was same as LC10-OWax10NC. However, LC2-OWax2NC and LC5-OWax5NC were slightly higher than OWax2-HDPE98 and OWax5-HDPE95, which implied that small amount of loading of LC prevented drastic reduction of tensile strength. MC2-OWax2NC and MC5-OWax5NC showed less reduction of tensile strength than the other systems, OWax-HDPE, LC-OWaxNC, and HC-OWaxNC system, at every concentration of organoclay loading. This implied that MC was a better reinforcing material than the

Copyright by Mahidol University

other organoclays.

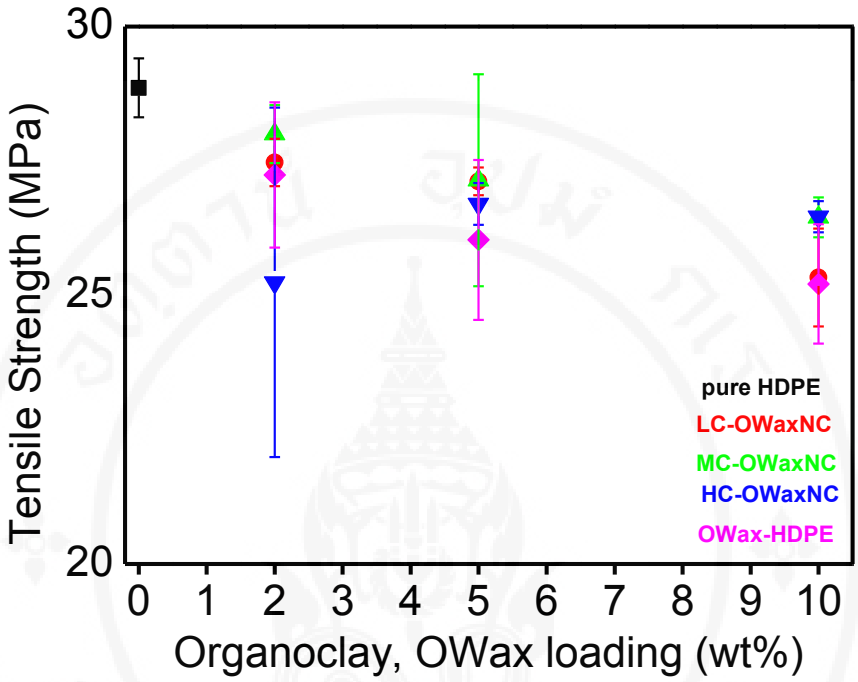

Figure 5.9 Tensile strength of pure HDPE, HDPEclay composites, and two-component OWax-HDPE composites.

Elongation at break of pure HDPE, and two-component OWax-HDPE composites, and HDPE clay nanocomposites were shown in figure 5.10. Pure HDPE showed 749.52% of elongation. LC2-OWax2NC exhibited 238.62% elongation. Incorporation of higher amount of LC and OWax led to reduction of elongation. The softened due to incorporation of OWax was observed due to the presence of the low molecular wax weitht in the polymeric matrix [70]. On MC-OWaxNC system, a drastic reduction of elongation was observed, 15.02, 78.74, and 7.10% at MC2-OWax2NC, MC5-OWax5NC and MC10-OWax10NC, respectively. The tendency of elongation at HC-OWaxNC system, HC2-OWax2NC, HC5-OWax5NC, and HC10-OWax10NC, was same as that of MC-OWaxNC system, which was 9.52,

Copyright by Mahidol University

15.67, and 7.55%, respectively.

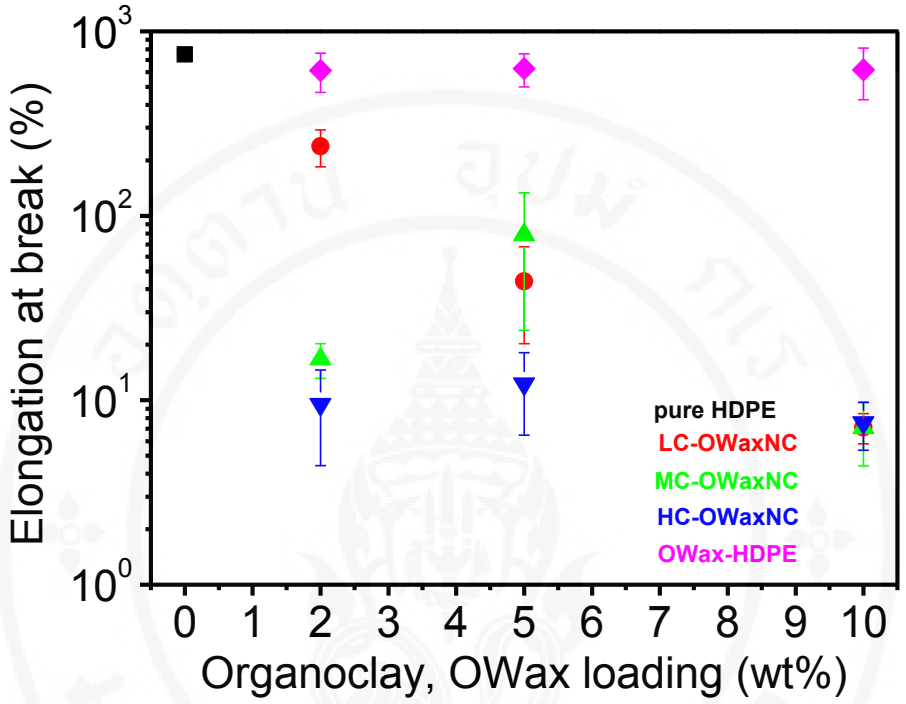

Figure 5.10 Elongation at break of pure HDPE, HDPEclay composites, and two-component OWax-HDPE composites.

5.3.4 Scanning electron microscopy (SEM)

Figure 5.11 shows SEM micrographs of nanocomposites with 5w% and 10w% organoclay loading. The dark area indicated polymer matrix. Apparently organoclay aggregations were observed in all specimens, and the particles were homogeneously dispersed in the matrix polymer. Networks of projection were formed, which surrounded clay particles because the specimens were torn after quenching in liquid nitrogen.

Copyright by Mahidol University

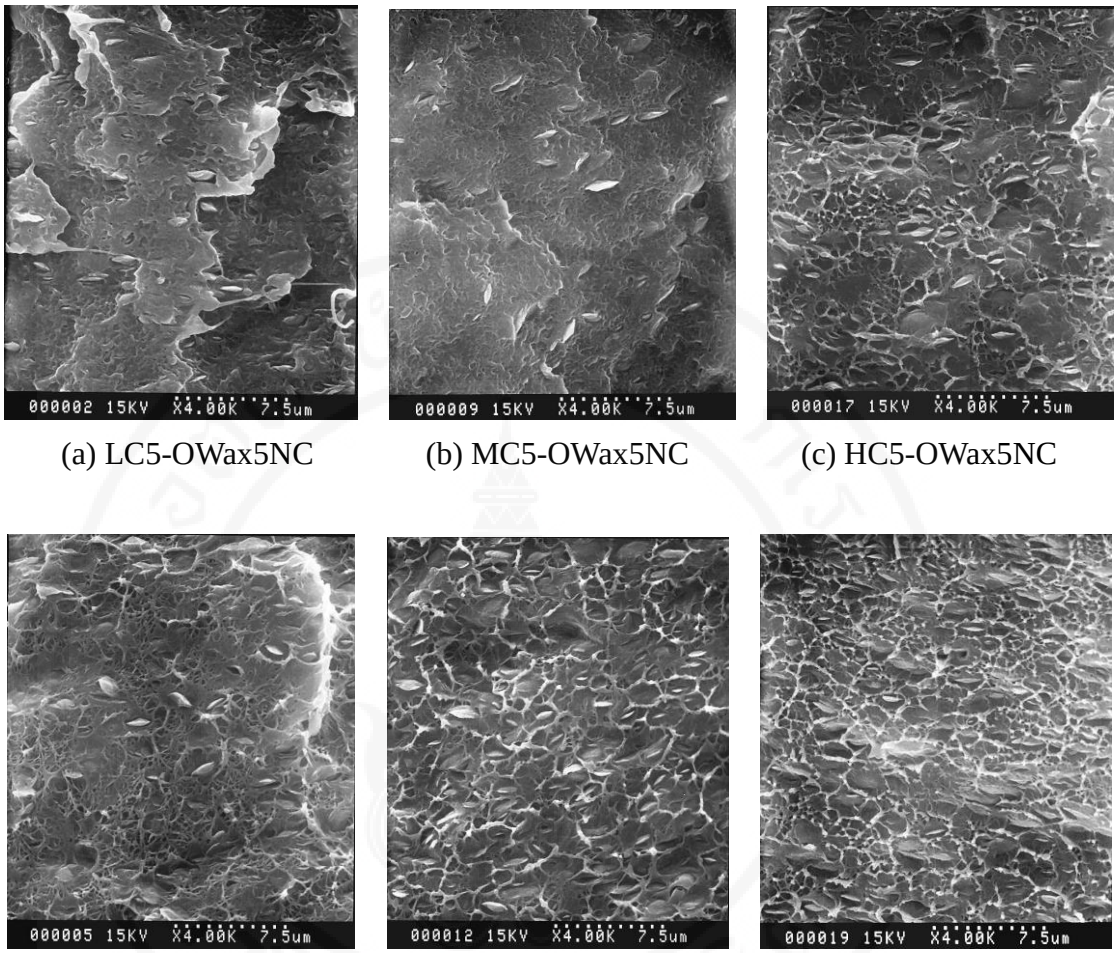

(a) LC5-OWax5NC (b) MC5-OWax5NC (c) HC5-OWax5NC

(d) LC10-OWax10NC (e) MC10-OWax10NC (f) HC10-OWax10NC

Figure 5.11 SEM micrographs of HDPE clay nanocomposites.

The degree of delamination of clay particles were evaluated by aspect ratio. LC5-OWax5NC (figure 5.11(a)), MC5-OWax5NC (figure 5.11(b)), and HC10-OWax10NC (figure 5.11(c)) indicated aspect ratio of 4.55 (+/- 1.53), 4.01 (+/-2.02), and 3.42 (+/-0.7), respectively. This indicated that delamination of clay particles on LC5-Wax5NC was improved, although there was no difference between LC5-OWax5NC and MC5-OWax5NC. However, aspect ratio on composites with 10wt% of organoclay loading were 3.90 (+/-1.18), 3.82 (+/-1.25), and 4.01 (+/-1.05) for LC10-OWax10NC (figure 5.11(d)), MC10-OWax10NC (figure 5.11(e)), and

Copyright by Mahidol University

HC10-OWax10NC (figure 5.11 (f)), respectively. Average value of aspect ratio on HC10-OWax10NC was larger than the others. However, Aspect ratios of LC10-OWax10NC, MC10-OWax10NC, and HC10-OWax10NC can not be thought as a considerable difference, taking into account of error.

5.4 Conclusion

Organoclays with different degree (low, medium, and high) of surface coverage were used in formation of HDPE-clay nanocomposites twin screw extruder. LC showed better intercalation by OWax and HDPE, and it was confirmed that delamination was improved at HDPE-clay nanocomposites with low organoclay and OWax loading on X-ray diffractgram. LC played an effective role of nucleating agents, which resulted in increasing crystallization temperatures. However, crystallinity of matrix polymer in HDPE-clay nanocomposites did not depend on organoclay surface coverage but amount of organoclay loading. Small amount of loading of LC, 2 and 5wt%, prevented drastic reduction of tensile strength. Particles of LC were observed on the fracture surface of LC5-OWax5NC and LC10-OWax10NC on SEM observation. Calculated aspect ratio of the particles on LC5-OWax5NC was 4.55, which was greater than those of MC5-OWax5NC and HC5-OWax5NC. It was found that surface coverage of MC was heterogeneity on X-ray diffractgram. MC also exhibited better intercalation by OWax and HDPE. However, it was found that delamination of MC was more difficult than that of LC. MC2-OWax2NC and MC5-OWax5NC showed less reduction of tensile strength than the other systems. MC also contributed to increase in crystallization temperature,

Copyright by Mahidol University

which implied that MC played an effective role of nucleating agents for HDPE. Particles of MC were found on the fracture surface of MC5-OWax5NC and MC10-OWax10NC. Calculated aspect ratio of the particles on MC5-OWax5NC was 4.01, which was larger than that of HC5-OWax5NC. Both of intercalation and delamination of clay were not observed on HC at all by X-ray diffractgram, although a slight collapse occurred on HC. It was found that HC also increased crystallization temperature on DSC, which implied that HC played an effective role of nucleating agents for HDPE. Particles of HC were also found on the fracture surface. Calculated aspect ratio of the HC particles on HC5-OWax5NC was 3.42.

Copyright by Mahidol University

CHAPTER VI
CONCLUSIONS

The effect of organoclay surface coverage on polymer clay nanocomposites was investigated on the system of PP and HDPE. The variation of the organoclay surface coverage was done by

(1) control the adsorption behavior of surface active agents on clay platelets and organoclay dispersion on the formation of polymer-clay nanocomposites by two roll mill using the home-made organoclay and

(2) using the commercially available organoclay with the different in the surfactant surface coverage on the formation of polymer-clay nanocompsoites with PP and HDPE .

The home-made organoclay was treated with S18 molecules and the formation of the S18 layer on the organoclay was categorized into three states. The first state, where S18 forms a flat-lying monolayer, occurred at low loading concentrations. This state indicated high adsorption efficiency, above 80%, with the surface energy in the range 40.7 – 46.0 mN m^{-1}. Organoclay did not mix with the OWax because of a mismatch between the surface of the organoclay and the melted OWax. The second state was the intermediate state. In this state, the monolayer changed to a double layer formation. OWax interacted only with the portion of the organoclay that was in double layer formation. The third state was the complete double layer formation, involving the formation of the flat-lying double layer and

Copyright by Mahidol University

occurred with high surface coverage. The double layer organoclay was intercalated with OWax and dispersed as smaller particles. These results demonstrated that incomplete intercalation caused heterogeneity in the organoclay and created a non-uniform polymer-clay nanocomposite. Surface energy of the melted OWax matched that of the organoclay, so that delamination of organoclay was enhanced by OWax, resulting in smaller platelets. It was confirmed that both the ultimate strength and toughness of the nanocomposites improved when organoclay was present.

Organoclays with different degree (low, medium, and high) of surface coverage were used in formation of polymer (PP and HDPE)-clay nanocomposites twin screw extruder. LC was intercalated by compatibilizers and matrix polymers because the degree of surface coverage of was lower than those of MC and HC. However, LC and MC indicated high residual weight, which was comparable each other. HC did not show any intercalation by compatibilizers and matrix polymers because organoclay surface coverage on HC was highly-closed packed layers of surfactant. Therefore, HC indicated low residual weight. Organoclay surface coverage of MC was heterogeneity between type of surface coverage of LC and HC, so that MC also indicated better intercalation compatibilizers and matrix polymers. Both of total surface energy and critical surface tension of organoclays (LC, MC and HC) depended on the degree of surface coverage of surfactant. Nanocomposites with smaller amount of LC and MC did not show drastic reduction of tensile strength. Organoclay (LC, MC, and HC) played an effective role of nucleating agents, but crystallinity of matrix polymers did not depend on the degree of surface coverage but amount of organoclay loading. There was a trend that calculated aspect ratio was higher and lower for LC and HC, respectively, which implied that

Copyright by Mahidol University

intercalation/delamination of LC was also improved than that of HC. Relative oxygen permeability on composites with LC was almost same as pure PP.

Copyright by Mahidol University

REFERENCES

[1] M. A. Osman, J. E. P. Rupp, U. W. Suter, Effect of non-ionic surfactantson the exfoliation and properties of polyethylene-layered silicate nanocomposites, *Polymer* **46** (2005) 8202-8209.

[2] F. Perrin-Sarazin, M.-T. Ton-That, M. N. Bureau, J. Denault, Micro- and nano-structure in polypropylene/clay nanocomposites, *Polymer* **46** (2005) 11624-11634.

[3] R. K. Shah, D.R. Paul, Nylon 6 nanocomposites prepared by a melt mixing masterbatch process, *Polymer* **45** (2004) 2991-3000.

[4] www.bccresearch.com

[5] Y. Tang, Y. Hu, L. Song, R. Zong, Z. Gui, Z. Chen, W. Fan *Polymer Degradation and Stability* **82** (2003) 127-131.

[6] J. Li, Minh-Tan Ton-That, S.-J. Tsai, PP-based nanocomposites with various intercalant types and intercalant coverages, "*Polymer Engineering and Science* **46** 8 (2006) 1060-1068.

[7] A. S. Luyt, V. G. Geethamma, Effect of oxidized paraffin wax on the thermal and mechanical properties of linear low-density polyethylene-silicate nanocomposites, *Polymer Testing* **26** (2007) 461-470.

[8] H. S. Mpanza, A. S. Luyt, Comparison of different waxes as processing agents for low-density polyethylene, *Polymer Testing*, **25** (2006) 436-442.

[9] J. R. Araujo, W. R. Waldman, M. A. De Paoli, Thermal properties of high density

Copyright by Mahidol University

polyethylene composites with natural fibres: Coupling agent effect, *Polymer Degradation and Stability* **93** (2008) 1770-1775.

[10] J. Li, M.-T. Ton-That, W. Leelapornpisit, L. A. Utracki, Melt compounding of polypropylene-based nanocomposites, *Polymer Engineering and Science* **47** (2007) 1447-11458.

[11] G. M. Russo, V. Nicolais, L. Di Maio, Montesano, L. Incamato, Rheological and mechanical properties of nylon 6 nanocomposites submitted to reprocessing with single and twin screw extruders, *Polymer Degragation and Stability* **92** (2007) 1925-1933.

[12] E.P. Giannelis, R. Krishnamoorti, E. Manias, Polymer-silica nanocomposites: model systems for confined polymers and polymer brushes, *Adv. Polymer Science* **118** (1999) 108-147.

[13] L. B. de Paiva, A. R. Morales, F. R. V. Diaz, Organoclays: Properties, preparation and applications, *Applied Clay Science* **42** (2008) 8-24.

[14] R. A. Vaia, R.K. Teukolsky, E.P. Gianmmelis Interlayer structure and molecular environment of alkylammonium layered silicates, *Chem. Mater.* **6** (1994) 1017-1022.

[15] E. M. Araujo, R. Barbosa, A. W. B. Rodrigues, T. J. A. Melo, E. N. Ito, Processing and characterization of polyethylene/Brazilian clay nanocomposites, *Materials Science and Engineering A* **445-446** (2007) 141-147.

[16] First Ten Angstroms Application notes Dyne solution Equivalents August 17, 2000.

[17] M. Alexandre, P. Dubois, Polymer-layered silicate nanocomposites: preparation, properties and use of a new class of materials, *Materials Science and*

Copyright by Mahidol University

Engineering **28** (2000) 1-63.

[18] A. Durmus, M. Woo, A. Kasgoz, C. W. Macosk, M. Tsapatsis, Intercalated linear low density polyethylene (LLDPE)/clay nanocomposites prepared with oxidized polyethyleneas a new type compatibilizer: Structural, mechanical and barrier properties, *European Polymer Journal* **43** (2007) 3737-3749.

[19] J.-H. Lee, Daeseng ung, C.-E Hong, K.-Y. Rhee, S.-G. Advani, Properties of polyethylene-layered silicate nanocomposites prepared by melt intercalation with a PP-g-MA compatibilizer, *Composites Science and Technology* **65** (2005) 1996-2002.

[20] X. Liu, Q. Wu, PP/clay nanocomposites prepared by grafting-melt intercalation, *Polymer* **42** (2001) 10013-10019.

[21] Q. Yuan, S. Awate, R.D.K. Misra, Nonisothermal crystallization behavior of polypropylene-clay nanocomposites, *European Polymer Journal* **42** (2006) 1994-2003.

[22] L.E. Nielsen *J Macromol Sci* (Chem) **A1(5)** (1967) 929-942.

[23] K. Yano, A. Usuki, A. Okada, T. Kurauchi, O. Kamigaito *Journal of Polymer Science Part A Polymer Chemistry* **31** (1993) 2493-2498.

[24] L. Minkova, Y. Peneva, E. Tashev, S. Fillippi, M. Pracella, P. Magagnini, Thermal properties and microhardness of HDPE/clay nanocomposites compatibilized by different functionalized polyethylenes, *Polymer Testing* **28** (2009) 528-533.

[25] M.W. Spencer, Lili Cui, Youngjae Yoo, D.R. Paul, *Polymer* **51** (2010) 1056-1070.

[26] B. Xu, Q. Zheng, Y. Song, Y. Shangguan, Calculating barrier properties of polymer/clay nanocomposites: Effects of clay layers, *Polymer* **47** (2006)

Copyright by Mahidol University

2904-2910.

[27] C. Lu, Y.-W. Mai, Influence of aspect ratio on barrier properties of polymer-clay nanocomposite, *Phys. Rev. Lett.* **95** (2005), 88303-88306.

[28] H.R. Dennis, D.L. Hunter, D. Chang, S. Kim, J.L. White, J.W. Cho and D.R. Paul, Effect of melt processing conditions on the extent of exfoliation in organoclay-based nanocomposite, *Polymer* **42** (23), (2001) 9513-9522.

[29] M.A. Osman, M. Ploetzeb, U.W. Suter, Surface treatment of clay minerals - thermal stability, basal-plane spacing and surface coverage, *J. Mater. Chem.***13** (2003) 2359–2366.

[30] M.A. Osman, M. Ernst, B.H. Meier, and U.W. Suter, Structure and molecular dynamics of alkane monolayers self-assembled on mica platelets, *J. Phys. Chem. B* **106** (2002) 653-662.

[31] W. Xie, Z. Gao, K. Liu, W.-P. Pan, R. Vaia, D. Hunter, A. Singh, Thermal characterization of organically modified montmorillonite, *Thermochimica Acta.* **367-368** (2001) 339-350.

[32] N. Hasegawa, H. Okamoto, M. Kato, A. Usuki, Preparation and mechanical properties of polypropylene-clay hybrids based on modified polypropylene and organophilic clay, *J Appl Polym Sci.* **78** (2000) 1918-1922.

[33] M.L. Lopez-Quintanilla, S. Sanchez-Valdes, L.F. Ramos De Valle, F.J. Medellin-Rodriguez FJ., Effect of some compatibilizing agents on clay dispersion of polypropylene-clay nanocomposites, *J Appl Polym Sci.* **100** (2006) 4748-4756.

[34] M. Kawasumi, N. Hasegawa, M. Kato, A. Usuki, A. Okada, *Macromolecules*, **30** (1997) 6333-6338.

Copyright by Mahidol University

[35] D.K. Owens, R.C. Wendt, *J. Appli. Polym. Sci.* **13** (1969) 1741.

[36] D.J. Chaiko, US 2007/0191510 A1

[37] R.J. Good, Contact angle, wetting, and adhesion: a critical review, *Journal of Adhesion Science and Technology* **6** (12) (1992) 1269-1302.

[38] J. Nylund, K. Sundberg, Q. Shen, J.B. Rosenholm, Determination of surface energy and wettability of wood resins, *Colloids and Surfaces A*: Physiochemical and Engineering Aspects, **133** (1998) 261-268.

[39] W.A. Deer, R.A. Howie, J. Zussman, An Introduction to The Rock-Forming Minerals. China : Addison Wesley Longmann Ltd., 1996.

[40] Theng BKG. Bergaya, G. Lagaly, Handbook of Clay Science, Elsevier, 2006.

[41] P.B. Messersmith, E.P. Giannelis, Synthesis and characterization of layered silicate-epoxy nanocomposites, *Chem. Mater.* **6** (1994) 1719-1725.

[42] W. Xie, Z. Gao, W-P Pan, D. Hunter, A. Singh, R. Vaia, Thermal degradation chemistry of alkyl quaternary ammonium montmorillonite, *Chem. Mater.***13** (2001) 2979-2990.

[43] G. Kahr, F.T. Madsen, Determination of the cation exchange capacity and the surface area of bentonite, illite and kaolinite by methylene blue adsorption, *Applied Clay Science* **9** (1995) 327-336.

[44] A. Ulman, An Introduction to Ultrathin Organic Films: From Langmuir-Blodgett to Self-Assembly, Academic Press, 1991.

[45] K. Shinoda, T. Nakagawa, B. Tamamushi, T. Isemura, Colloidal Surfactants. New York: Academic Press, 1963.

[46] I. Novak, I. Krupa, A.S. Luyt, "Improvement of the polarity of polyethylene with oxidized Fischer-Tropsch paraffin wax and its influence on the final

Copyright by Mahidol University

mechanical properties, *J. Appl. Poly. Sci.* **95** (2005) 1164-1168.

[47] D.F. Eckel, M.P. Balogh, P.D. Fasulo, and W.R. Rodgers, Assessing organo-clay dispersion in polymer nanocomposites, *J. Appl Polym. Sci.* **93** (2004) 1110-1117.

[48] J. Gu, D.S. Jia, R.S. Cheng, *Polymer-plastics technology and engineering* **47** (2008) 583-589.

[49] L. Betega de Paiva, A. R. Morles, T. R. Guimaraes, Structural and optical properties of polypropylene-montmorillonite nanocomposites, *Materials Science and Engineering A* **477** (2007) 261-265.

[50] M. Kato, M. Matsushita, K. Fukumori, Development of a new production method for a polypropylene-clay nanocomposite, *Polymer Engineering and Science* **44** (2004) 1205-1211.

[51] K. Cho, F. Li, J. Choi, Crystallization and melting behavior of polypropylene and maleated polypropylene blends, *Polymer* **40** (1999) 1719-1729.

[52] W. Xu, G. Liang, W.Wang, S. Tang, P. He, W.-P Pan, PP-PP-g-MAH-Org-MMT nanocomposites. I. Intercalation behavior and microstructure, *Journal of Applied Polymer Science* **Vol. 88** (2003) 3225-3231.

[53] H. Baniasadi, A. Ramazni S.A., S. Javan Nikkhah *Materials and Design* **31** (2010) 76-84.

[54] J. Hoshino, S. Limpanart, S. Khunthon, T. Osotchan, R. Traiphol, T. Srikhirin, Adsorption of single-strand alkylammonium salts on bentonite, surface properties of the modified clay and polymer nanocomposites formation by two-roll mill, *Materials Chemistry and Physics* **123** (2010) 706-713.

[55] T.Umasankar Patro, Milind V. Mhalgi, D.V. Khakhar, A. Misra, Studies on

Copyright by Mahidol University

poly (vinylidene fluoride)-clay nanocomposites: Effect of different clay modifiers, *Polymer* **49** (2008) 3486-3499.

[56] O.-J. Kwon, S. Tang, S.-W. Myung, N. Lu, H.-S. Choi, Surface characteristics of polypropylene film treated an atmospheric pressure plasma, *Surface & Coating Technology* **192** (2005) 1-10.

[57] J.-H. Park, H.-M. Lee, I.-J. Chin, H.-J. Choi, H.-K. Kim, W.-G. Kang, Intercalated polypropylene/clay nanocomposite and its physical characteristics, *Journal of Physics and Chemistry of Solids* **69** (2008) 1375-1378.

[58] KH Wang, MH Choi, CM Koo, CM Choi, I. Chung, Synthesis and characterization of maleated polyethylene/clay nanocomposites, *Polymer* **42** (2001) 9819-9826.

[59] E. M. Beneti, V. Causin, C. Marega, A. Marigo, G. Ferrara, A. Ferrano, M. Consalvi, F. Fantinel, Morphological and structural characterization of polypropylene based nanocomposites, *Polymer* **46** (2005) 8275-8285.

[60] A. Durmus, A. Kasgoz, C. W. Macosko, Linear low density polyethylene (LLDPE)/clay nanocomposites. Part I: Structural characterization and qualifying clay dispersion by melt rheology, *Polymer* **48** (2007) 4492-4502.

[61] P. Svoboda, C. Zeng, H. Wang, L. J. Lee, D. L. Tomasko, Morphology and mechanical properties of polypropylene/organoclay nanocomposites, *Journal of Applied Polymer Science*, **Vol. 85** (2000) 1562-1570.

[62] Y.-Q. Zhang, J.-H. Lee, H.-J. Jang, C.-W. Nah, Preparing PP/clay nanocomposites using a swelling agent. *Composites*: Part B, **35** (2004) 133-138.

[63] H. Krump, A.S. Luyt, I. Hudec, Effect of different modified clays on the thermal

Copyright by Mahidol University

and physical properties of polypropylene-montmorillonite nanocomposites, *Materials Letters* **60** (2006) 2877-2880.

[64] J. Li, C. Zhou, W. Gang, Study on nonisothermal crystallization of maleic anhydride grafted polypropylene/montmorillonite nanocomposites, *Polymer Testing* **22** (2003) 217-223.

[65] P. H. Nam, P. Maiti, M. Okamoto, T. Kotaka, N. Hasegawa, A. Usuki *Polymer* **42** (2001) 9633-9640.

[66] M. Pannirselvam, A. Genovese, M. C. Jollands, S. N. Bhattacharya, R. A. Shanks, Oxygen barrier property of polypropylene-polyether treated clay nanocomposite, *eXPRESS Polymer Letters* **2** (2008) 429-439.

[67] V. Mittal, Gas permeation and mechanical properties of polypropylene nanocomposites with thermally-stable imidazolium modified clay, *European Polymer Journal* **43** (2007) 3727-3736.

[68] M. Zhang, P.F. Fang, S.P. Fang, B. Wang, S.J. Wang, Study of structural characteristics of HDPE/$CaCO_3$ nanocomposites by positrons, *Radiation Physics and Chemistry* **68** (2003) 565-567.

[69] R. Yang, Y. Liu, J. Yu, K. Wang, Thermal oxidation products and kinetics of polyethylene composites, *Polymer Degradation and Stability* **91** (2006) 1651-1657.

[70] S. K. Swain, A. I. Isayev, Effect of ultrasound on HDPE/clay nanocomposites: Rheology, structure and properties, *Polymer* **48** (2007) 281-289.

[71] Y. Xi, Ray L. Frost, H. He, Modification of the surface of Wyoming montmorillonite by the cationic surfactants alkyl trimethyl, dialkyl dimethyl, and trialkyl methy ammonium bromide, *Journal of Colloid and*

Copyright by Mahidol University

Interface Science **305** (2007) 150-158.

[72] C. Zhao, H. Qin, F. Gong, M. Feng, S. Zhang, M. Yang, Mechanical, thermal and flammabilities of polyethylene/clay nanocomposites, *Polymer Degradation and Stability* **87** (2005) 183-189.

[73] C. O. Rohlmann, M. F. Horst, L. M. Quinzani, M. D. Faila, Comparative analysis of nanocomposites based on plypropylene and different montmorillonites, *European Polymer Journal* **44** (2008) 2749-2760.

[74] H. Zhai, W. Xu, H. Guo, Z. Zhou, S. Shen, Q. Song, Preparation and characterization of PE and PE-g-MAH/montmorillonite nanocomposites, *European Polymer Journal* **40** (2004) 2539-2545.

Copyright by Mahidol University

BIOGRAPHY

NAME	Mr. Jumpei Hosino
DATE OF BIRTH	June 14, 1970
PLACE OF BIRTH	Osaka, Japan
INSTITUTIONS ATTENDED	Muroran Institute of Technology, 1990-1994 Bachelor of Engineering (Materials Science and Engineering) Osaka Prefecture University, 1995-1997 Master's degree of Engineering (Metallurgy and Materials Science) Mahidol University, 2005-2010: Doctor of Philosophy (Materials Science and Engineering)
CURRENT ADDRESS	99, Soi Boonprarop, Ratchaprarop Road, Makkasan, Rajtavee, Bangkok 10400 Thailand
HOME ADDRESS	1-11-7, Sumiyoshi, Sumiyoshi-ku, Osaka, 558-0045 Japan
E-MAIL	junpei_hoshino@hotmail.com

Copyright by Mahidol University